PNNL-13168

Fabrication Technological Development of the Oxide Dispersion Strengthened Alloy MA957 for Fast Reactor Applications

M. L. Hamilton
D. S. Gelles
R. J. Lobsinger*
G. D. Johnson*
W. F. Brown*
M. M. Paxton*
R. J. Puigh*
C. R. Eiholzer
C. Martinez**
and
M. A. Blotter***

February 2000

Work supported in part by
the U.S. Department of Energy
under Contract DE-AC06-76RLO 1830
and in part by the Northwest College
and University Association for Science
under Grant No. DE-FG06-ER-75522

* Originally with Westinghouse Hanford Company
** Originally with General Electric Company
*** Originally with University of Missouri-Rolla

Pacific Northwest Laboratory
Richland, Washington 99352

DISCLAIMER

PNNL-13168

Fabrication Technological Development of the Oxide Dispersion Strengthened Alloy MA957 for Fast Reactor Applications

M. L. Hamilton
D. S. Gelles
R. J. Lobsinger*
G. D. Johnson*
W. F. Brown*
M. M. Paxton*
R. J. Puigh*
C. R. Eiholzer
C. Martinez**
and
M. A. Blotter***

February 2000

Work supported in part by
the U.S. Department of Energy
under Contract DE-AC06-76RLO 1830
and in part by the Northwest College
and University Association for Science
under Grant No. DE-FG06-ER-75522

* Originally with Westinghouse Hanford Company
** Originally with General Electric Company
*** Originally with University of Missouri-Rolla

Pacific Northwest Laboratory
Richland, Washington 99352

CONTENTS

CONTENTS (Cont'd)

LIST OF FIGURES

LIST OF FIGURES (Cont'd)

LIST OF FIGURES (Cont'd)

LIST OF FIGURES (Cont'd)

LIST OF TABLES

I. SUMMARY

A significant amount of effort has been devoted to determining the properties and understanding the behavior of the alloy MA957 to define its potential usefulness as a cladding material in the fast breeder reactor program. The numerous characterization and fabrication studies that were conducted are documented in this report.

The alloy is a ferritic stainless steel developed by International Nickel Company specifically for structural reactor applications. It is strengthened by a very fine, uniformly distributed yttria dispersoid. Its fabrication involves a mechanical alloying process and subsequent extrusion, which ultimately results in a highly elongated grain structure. While the presence of the dispersoid produces a material with excellent strength, the body centered cubic structure inherent to the material coupled with the high aspect ratio that results from processing operations produces some difficulties with ductility. The alloy is very sensitive to variations in a number of processing parameters, and if the high strength is once lost during fabrication, it cannot be recovered. The microstructural evolution of the alloy under irradiation falls into two regimes. Below about 550°C, dislocation development, α' precipitation and void evolution in the matrix are observed, while above about 550°C damage appears to be restricted to cavity formation within oxide particles.

The thermal expansion of the alloy is very similar to that of HT9 up to the temperature where HT9 undergoes a phase transition to austenitic. Pulse magnetic welding of end caps onto MA957 tubing can be accomplished in a manner similar to that in which it is performed on HT9, although the welding parameters appear to be very sensitive to variations in the tubing that result from small changes in fabrication conditions.

The tensile and stress rupture behavior of the alloy are acceptable in the unirradiated condition, being comparable to HT9 below about 700°C and exceeding those of HT9 at higher temperatures. Neither tensile nor rupture strength appear to be degraded by irradiation to fast fluences on the order of 8×10^{22} n/cm^2 in the range of 370 - 760°C, although some loss of ductility has been observed. The impact resistance of the alloy is very poor in the unirradiated condition, and is significantly degraded by irradiation.

II. INTRODUCTION

DOE Program for Advanced Cladding

The U.S. Department of Energy has sponsored several programs to develop improved fuel cladding materials for liquid metal fast breeder reactors since the early 1970s.[1] It was learned that the material of choice, solution annealed 316 stainless steel (SS), underwent an irradiation-induced expansion called swelling that determined the lifetime limits for fueled subassemblies. The lifetime limits could be extended to about 1.5 years by using 316 SS in a 20% cold worked condition (under the auspices of the Reference Core and Structural Materials Program) and to about 3 years with the martensitic stainless steel HT9 (under the auspices of the Alloy Development for Irradiation Performance Program and the National Clad and Duct Materials Development Program). A more advanced class of alloys known as oxide dispersion strengthened ferritic alloys (ODS or DSF) appears to have the potential for up to a 5 year lifetime. This report summarizes the results obtained by the Advanced Cladding Program on MA957, an ODS ferritic alloy.

Description of DSF Alloy

MA957 is a commercially available alloy sold exclusively by Huntington Alloys, a division of the International Nickel Company (INCO) located in Huntington, West Virginia. The alloy is defined in U.S. patent 4,075,010[2] which was granted February 21, 1978, and is produced by a patented process known as mechanical alloying, for which Huntington Alloys controls the rights. Mechanical alloying is a powder metallurgy milling process which distributes alloy ingredients on a very fine scale.

MA957 is a ferritic alloy strengthened by a dispersion of yttrium oxide. The base composition is Fe-14% Cr with additions of 1% Ti and 0.3% Mo (all compositions given in weight percent) and to which is added 0.25% yttrium oxide (Y_2O_3) on a very fine scale. The exceptional high temperature strength of the alloy is due partially, however, to the thermomechanical processing it receives. The alloy must therefore be processed with care to retain these exceptional properties, ensuring that the microstructure of interest is maintained through the fabrication of final product forms.

Summary of INCO Patent

INCO developed the MA957 alloy for cladding applications in liquid metal fast breeder reactors utilizing a process for mechanical alloying, the patents for which they hold. The work on which the patent is based was performed at the INCO's Sterling Forest Laboratory. The patent for the alloy is provided in Appendix A. The data base contained in the patent demonstrates that the alloy that provided the best stress rupture lifetimes at high temperatures had the nominal composition Fe-14Cr-0.9Ti-0.3Mo-0.25Y_2O_3. This alloy has been given the commercial name MA957: "MA" to designate it as a mechanically alloyed product, and "957" to follow MA956, a similar alloy in the 20% chromium

composition range. The mechanical alloying process employs powder metallurgy processes using high energy ball mills or attritors to mechanically redistribute the alloying ingredients throughout each powder particle on a microscopic scale. The mechanically alloyed powders are consolidated by hot extrusion in an evacuated steel can. The resulting wrought bar is hot worked and then cold worked into its final geometry prior to sale and ultimate fabrication into a finished product.

III. COMPOSITION OF MA957

Specifications

Table 1 provides the nominal composition specification for MA957. The alloy is a ferritic steel strengthened at high temperatures by a very fine yttria dispersion. Titanium and molybdenum are added to improve strength, ductility and oxidation resistance.

Commercial Heat Analyses

Numerous chemical overcheck analyses were performed on four heats of the alloy at two different offsite laboratories. The average composition and the composition ranges of the overchecks are also given in Table 1. A complete record of the overcheck analyses is provided in Appendix B.[3] It is evident in Table 1 that the major alloying components (Cr, Ti, Mo and Y_2O_3) are close to their nominal compositions. There is some variability in the amounts of oxygen, manganese and phosphorus, as well as a large amount of aluminum present in the form of alumina stringers. It is believed that these stringers are detrimental to the overall behavior of the alloy. The presence of the aluminum has been attributed to contamination of the ferrochrome powder used to supply the chromium to the alloy. Several percent alumina was apparently present in the powder. It is recommended that further development of the alloy include the elimination of aluminum from the alloy through more stringent limits on the purity of the starting metal powders.

IV. CHARACTERIZATION

Microstructure of MA957

Specimens of MA957 were prepared for examination by optical and transmission electron microscopy (TEM). Optical metallography was performed on sections of various product forms using Villela's etch. Thin foils and precipitate extraction replicas were obtained for TEM from punched and ground 0.12 inch diameter disks using standard electropolishing and replication procedures. TEM examinations were performed on a JEOL 1200EX scanning transmission electron microscope operating at 120 keV.

Table 1.
Composition of MA957

ELEMENT	WEIGHT PERCENTAGE AVERAGE	RANGE	NOMINAL
Cr	13.87	13.49 - 14.19	14
Ti	1.05	0.95 - 1.38	0.9
Mo	0.30	0.28 - 0.32	0.3
$Y(Y_2O_3)$	0.22	0.19 - 0.28	0.25
O	[a]	0.006 - 0.240	-
C	0.014	0.012 - 0.017	-
Mn	[b]	0.05 - 0.12	-
Si	0.04	0.02 - 0.07	-
P	[c]	0.004 - 0.030	-
Ni	0.13	0.10 - 0.15	-
Al	0.10	0.055 - 0.17	-
S	0.006	0.004 - 0.006	-
Fe	Bal.	Bal.	Bal.

[a]Two distinct sets of values were present in the bar stock received from INCO, one with a range of 0.006 to 0.02% oxygen (average of 0.014%) and one with a range of 0.21 to 0.24% oxygen (average of 0.22%).

[b]Two distinct sets of values were present in the bar stock received from INCO, one with a range of 0.05 - 0.06% manganese (average of 0.06%) and one with a range of 0.11 to 0.12% manganese (average of 0.11%).

[c]Two distinct sets of values were present, one at <0.005% phosphorus and one with a range of 0.011 to 0.030% phosphorus (average of 0.017%).

Figures 1 and 2 show examples of the microstructure of MA957 in the as-received bar. Figures 1a and 1b illustrate the transverse and longitudinal structure at low magnification using optical metallography and Figures 1c and 1d illustrate the same regions at higher magnification. The structure is highly anisotropic with equiaxed grains in the transverse direction but with highly elongated grains in the longitudinal or working direction. Figure 1 also reveals many titanium carbide precipitate particles and several alumina stringers. Figure 2 shows the structure at higher magnification using transmission electron microscopy. The grain structure comprises well-defined subgrain boundaries pinned by titanium carbide particles. The subgrains are highly elongated with aspect ratios of about 10 to 1 and widths on the order of 0.5μm. Within the subgrains a moderate dislocation structure is retained, pinned by a high density of fine yttria particles (on the order of 20 Å) which, as will be seen in later figures, are relatively equiaxed and fairly uniformly distributed.

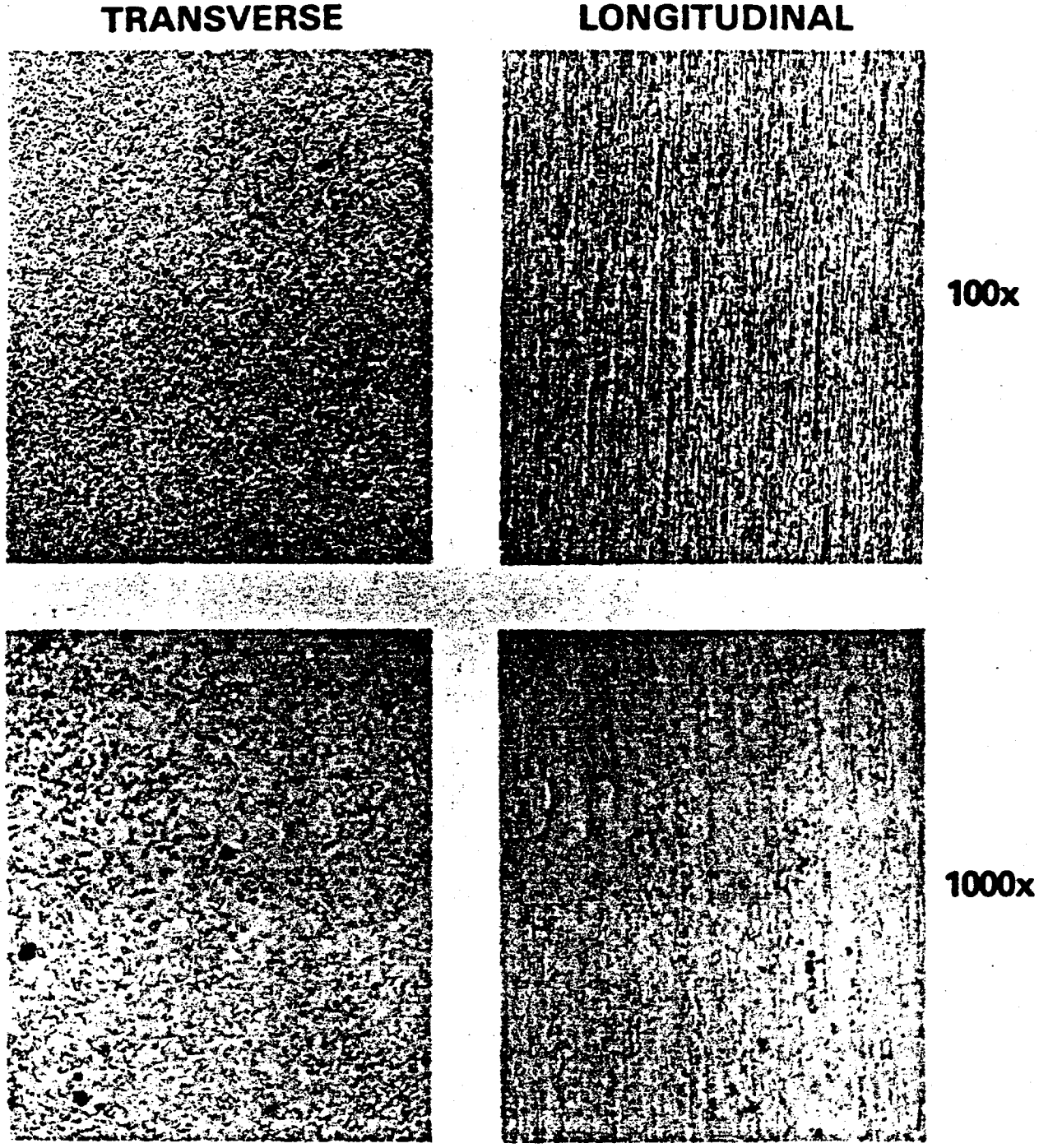

Figure 1. Microstructure of as-received MA957 bar showing optical metallography of transverse and longitudinal sections, respectively, at 100x in (a) and (b) and at 1000x in (c) and (d).

Figure 2. Microstructure of as-received MA957 bar showing a longitudinal section.

Another example of this microstructure is given in Figure 3 for tubing made by Carpenter Technology Corporation (Cartech), showing the subgrain structure at low magnification in Figure 3a and providing an example of the dislocation and precipitate distributions at higher magnification in Figure 3b. The precipitate is imaged as white or dark spots on either side of the dark band on the left hand side of Figure 3b. The large circular feature ~100 nm in diameter that is in the lower part of Figure 3b is a TiO_2 particle; such particles were also present at low densities.

Microstructure of Other ODS Products

The microstructures of three other ODS alloys were compared to that of the Cartech cladding. These included a production run of MA957 tubing produced by Superior Tube Company (STC) for use in the Experimental Breeder Reactor II (EBR-II), MA957 tubing made in Japan by PNC using a proprietary hot drawing process, and tubing made in Belgium by SCK/CEN of the ODS alloy DT2203Y05. The STC tubing was similar to the Cartech tubing, with a subgrain structure 250 to 500 nm in width and an aspect ratio of about 10 to 1. The dislocation structure retained within the subgrains was generally polygonized and evidence for Y_2O_3 particles on the order of 2 nm was present. An example of this microstructure is given in Figure 4. The subgrain structure is shown at low magnification in Figure 4a, the dislocation structure within subgrains is shown in Figure 4b, and evidence for the 2 nm Y_2O_3 is given in Figure 4c.

The PNC tubing made from MA957 also possessed an elongated subgrain structure with subgrain widths on the order of 500 nm. The dislocation structure within subgrains was more polygonized than the STC and Cartech products, presumably because of the higher working temperatures, and evidence for a fine dispersoid on the order of 2 nm in diameter was present. This material contained larger precipitate particles, possibly the complex Y_2TiO_5 oxides that have been identified by PNC, that were coherent and in a specific orientation with the matrix. Since MA957 is a mechanically alloyed product, any precipitate introduced during mechanical alloying should be incoherent and randomly oriented relative to the matrix. In the PNC tubing, however, many precipitate particles were found with the same orientation relationship to the matrix, indicating that those precipitates must have formed during subsequent fabrication operations.

Typical microstructures in the PNC tubing are given in Figure 5. Figure 5a shows the subgrain structure at low magnification. The subgrains were on the order of 500 nm in diameter and were therefore similar in size to the products manufactured in the U.S. Figure 5b shows the dislocation structure at higher magnification. Figure 5c was taken in dark field to show all precipitates in a similar orientation as bright images against a dark background. Both large and small particles appear white, indicating that the white features are in a similar orientation. It is likely that these precipitates were nucleated and grew during fabrication in Japan, rather than originating in the mechanically alloyed and extruded bar, since similar features were not found in U.S. product forms. Fine particles on the order of 2-4 nm in diameter are visible in Figure 5d, suggesting that the original Y_2O_3 dispersoid is still present.

Figure 3. Microstructure of Cartech production lot of cladding at low and high magnifications to illustrate a)the typical subgrain structure and b)the dislocation structure within subgrains and the fine dispersoid.

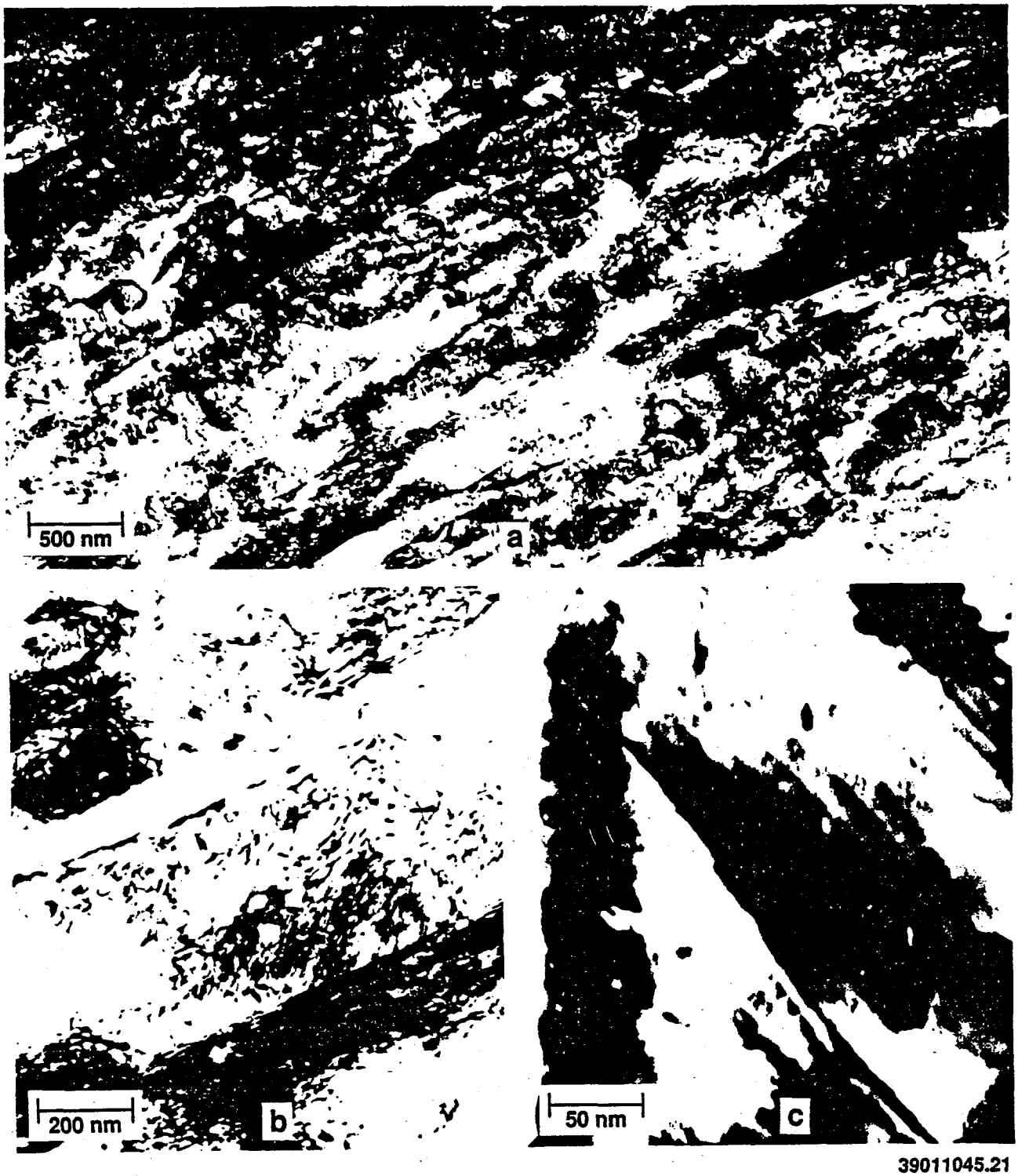

Figure 4. Microstructure of MA957 tubing produced by STC showing typical subgrain structure at low and intermediate magnifications in (a) and (b). The fine dispersoid can be identified in (c) as white spots in the dark bands.

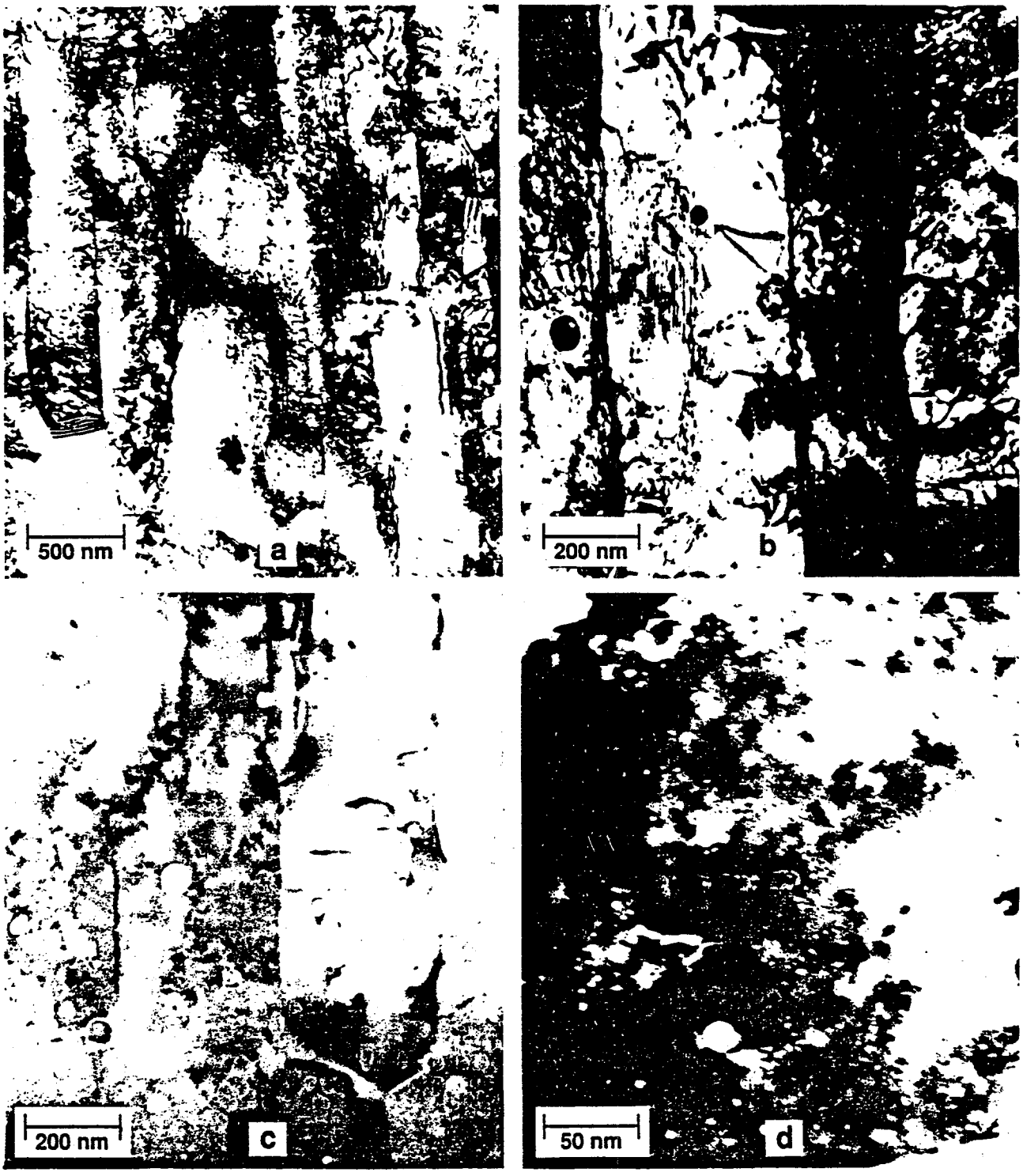

Figure 5. Microstructure of MA957 produced by PNC showing the subgrain structure at low and high magnifications in (a) and (b). Large precipitate particles and the dispersoid are imaged brightly in (c) and (d) in dark field contrast.

In comparison, the structure of the Belgian alloy DT2203Y05 was much coarser, and three microstructurally different regions were identified: recrystallized, recovered and second phase. The dispersoid ranged from 5 nm in diameter to much larger sizes. In recrystallized regions, the dislocation density was low, comprising a few long straight dislocations, but in adjacent regions the dislocation density was quite high, similar to a recovered cold worked structure. Large dark features were distributed throughout the material, the largest in elongated cusp-shaped regions often separating different matrix regions. These features are expected to be chi or Laves phase, rich in molybdenum. A previous investigation of this alloy described it as strengthened by chi phase.

Examples of the DT2203Y05 microstructures are given in Figure 6. The three different regions are shown at low magnification in Figure 6a. A recrystallized region is present in the upper left while a recovered region is present on the right. A dark blocky region typical of chi phase in this material is present at left center. The recovered and recrystallized regions are shown at higher magnification in Figures 6b and c. Evidence for a stable 2 nm dispersoid is visible at the lower right in Figure 6b, but the size distribution in Figure 6c extends to much larger sizes. It would therefore appear that DT2203Y05 has been overly alloyed and that tube fabrication procedures resulted in a very nonuniform microstructure.

Two compositions predominated in the analyses performed on the precipitates in DT2203Y05. They are given in Table 2. One type of precipitate contained

Table 2.
Precipitate Composition in DT2203Y05

COMPOSITION (weight percent)							
Fe	Cr	Ti	Y	Mo	Al	No.	IDENTITY
24-45	3-7	14-22	22-47	-	2-4	3	Y_2TiO_5
75-87	12-14	1-6	-	5-6	-	1	Chi

titanium and molybdenum, while the other contained titanium and yttrium. The latter can tentatively be identified as Y_2TiO_5 (as was observed in the MA957 produced by PNC), while the former is probably related to chi phase. The probable presence of Y_2TiO_5 suggests that the processing of DT2203Y05 was similar to that used by PNC, involving hot working or heat treatment that promoted nucleation and growth of a new phase, Y_2TiO_5, and dissolution of the Y_2O_3 dispersoid.

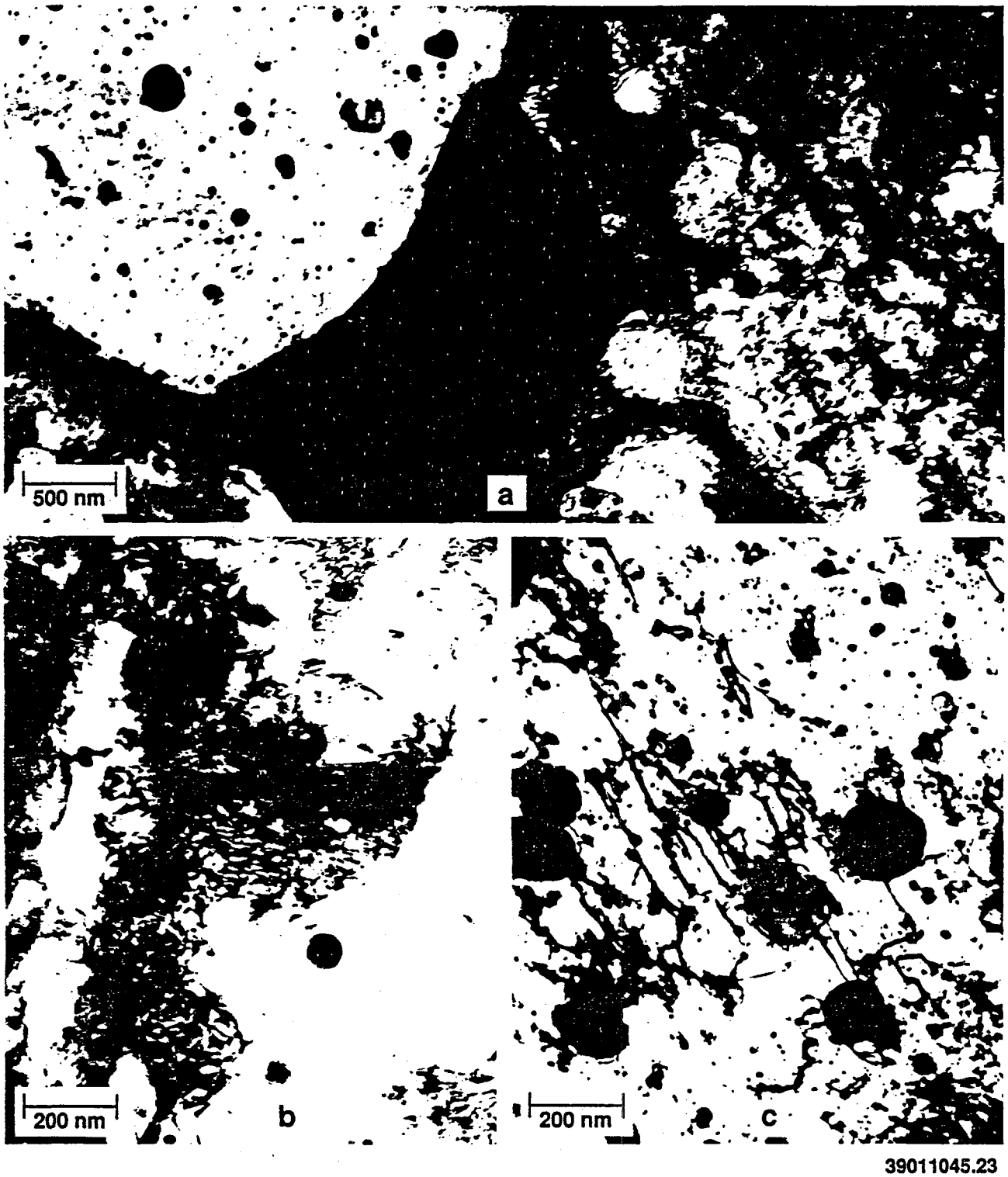

Figure 6. Microstructure of DT2203Y05 produced by SCK/CEN illustrating recovered and recrystallized areas in all three micrographs; blocky precipitation is visible only in (a) at low magnification.

Aging Behavior

The metallurgical stability of MA957 was evaluated after aging for 10,000 hours. Samples of the original bar were aged at temperatures ranging from 490 to 760°C. Optical metallography and hardness measurements were performed at 100, 3000, 6000 and 10,000 hours. Optical microstructures are shown in Figure 7 after about 6000 hours. No change in structure was observed optically. Vicker's microhardness values determined with a 500 gram load are listed in Table 3 and plotted in Figure 8. Hardness remained essentially constant out to 10,000 hours, verifying the stability of the microstructure.

Table 3.
Hardness Data After Aging

AGING TIME (hrs)	VICKER'S MICROHARDNESS (DPH) [500 gm load] AGING TEMPERATURE (°C)			
	490	593	650	760
100	370	352	362	362
1000	NM[a]	NM	NM	NM
3000	362	362	370	352
6000	372	357	357	358
10,000	NM	370	365	NM

[a]NM = not measured.

A slight but consistent hardening occurred after 3000 hours at 490°C relative to aging at higher temperatures. Transmission electron microscopy was therefore performed on the specimens aged at both 490 and 760°C and compared with the as-received condition. The 490°C condition contained precipitates formed during aging that have been identified as α', a chromium-rich, body centered cubic phase known to form in Fe-Cr alloys at low temperatures. Electron micrographs of the structure are shown in Figure 9.

Recrystallization Behavior

A number of recrystallization studies were undertaken in support of the fabrication effort. The first was performed on transverse and longitudinal slices of as-received bar, which were given varying degrees of cold work ranging from 10 to 40% and annealed at temperatures ranging from 700 to 1300°C for periods ranging from 15 minutes to 1 hour. Hardness and the qualitative amount of recrystallization were determined and incorporated into the definition of the optimum processing regime described later in the fabrication section of this report.

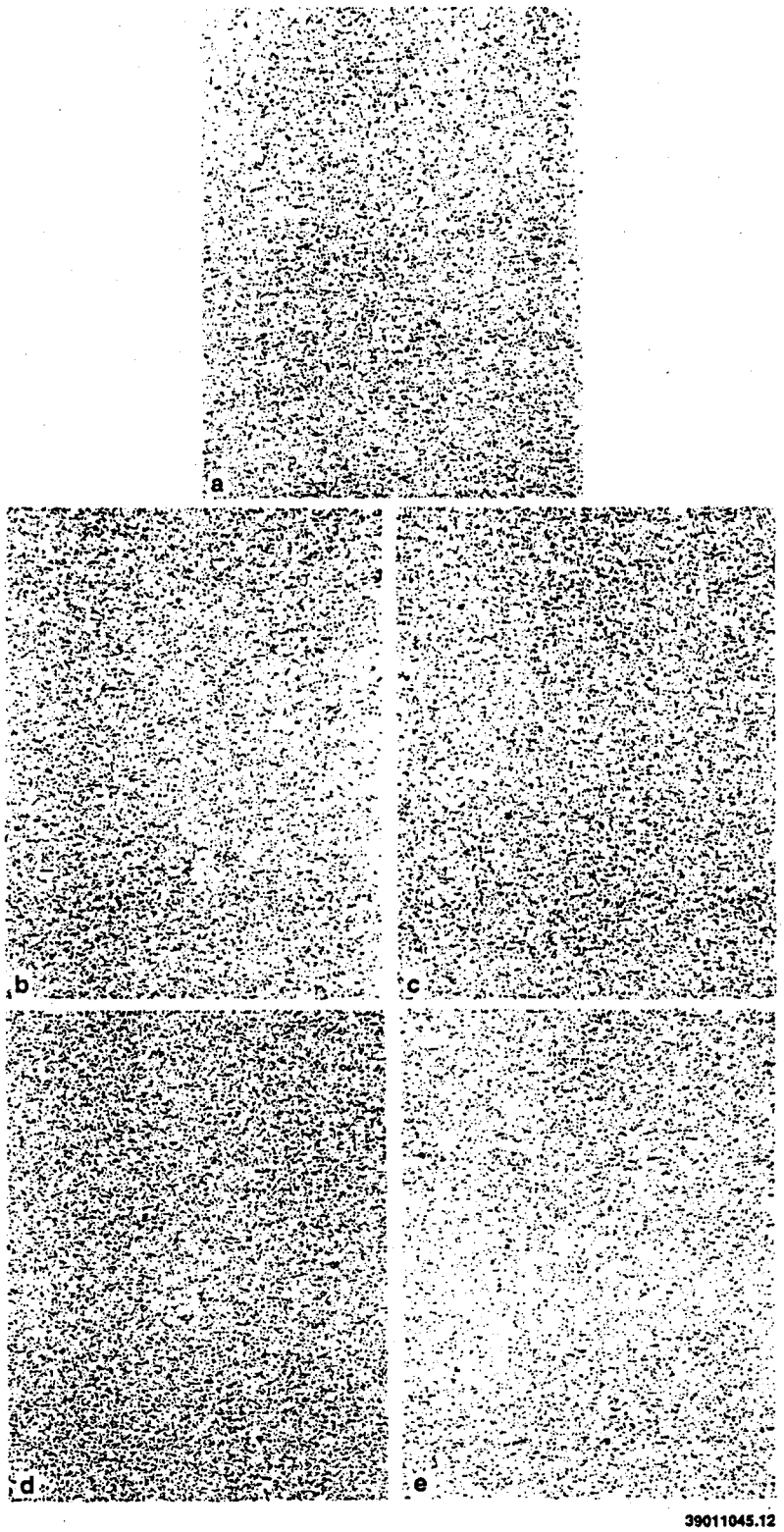

Figure 7. Optical metallography of MA957 a)as-received and after aging 6000 hours at b)490°C, c)593°C, d)650°C, and e)760°C demonstrating identical microstructure (100x).

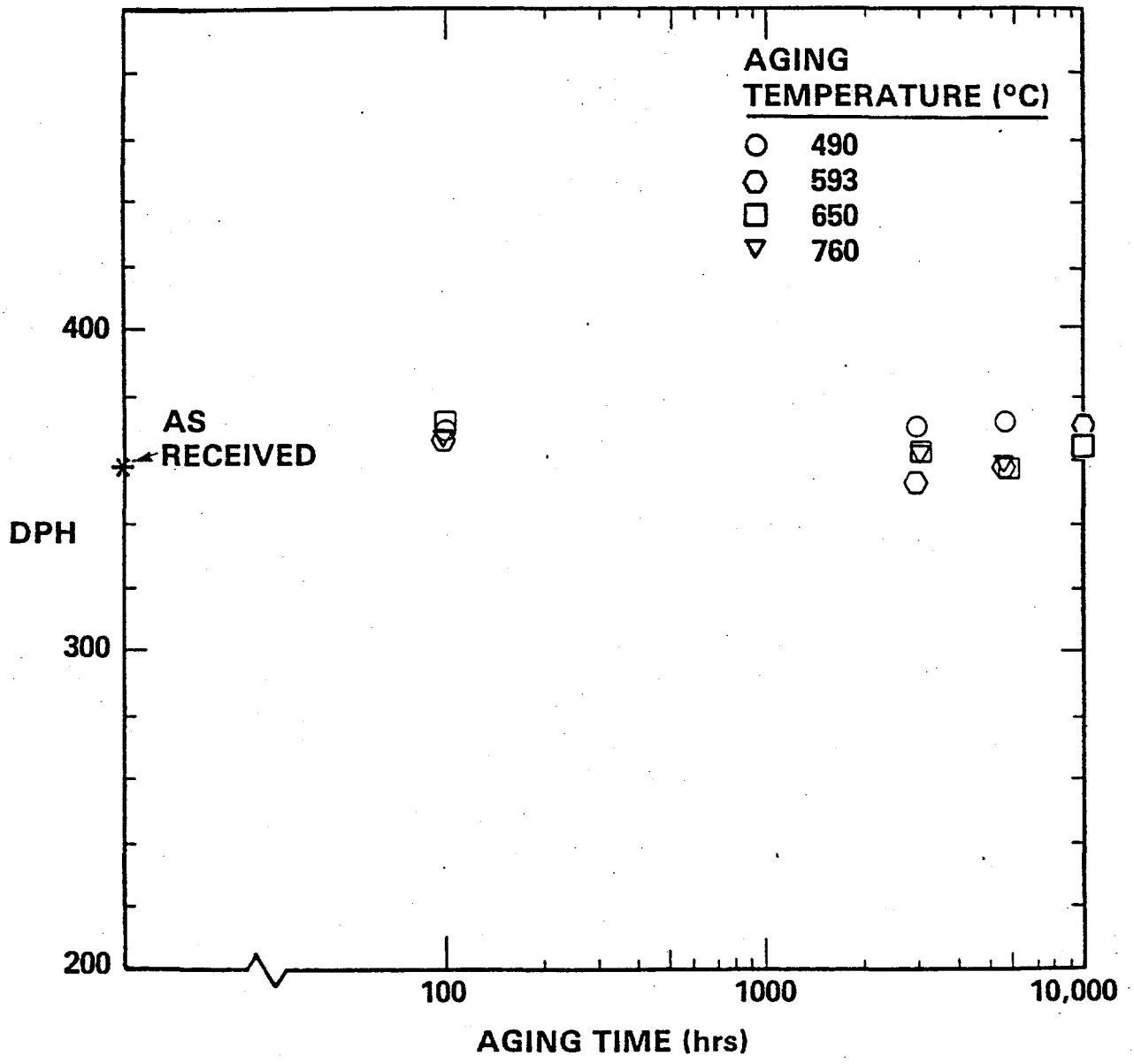

Figure 8. Hardness of MA957 as a function of aging time and temperature.

Specimens diverted from the second Cartech attempt at a pilot lot (referred to as pilot lot 2) were annealed at elevated temperatures for 15 minutes to determine the recrystallization behavior of that particular lot of material. The hardness data are given in Table 4 and plotted in Figure 10. Virtually the entire specimen had recrystallized after exposure to 1300°C, while at the lower temperatures a peak was observed in the fraction of material that

Figure 9. Transmission electron micrographs of MA957 a)as-received and after aging ~5800 hours at b)490°C and c)760°C showing formation of α' at 490°C.

Table 4.
Hardness of Annealed Pilot Lot 2 (Cartech)

ANNEALING TEMPERATURE (°C)	FRACTION RECRYSTALLIZED (%)	AVERAGE HARDNESS (DPH)	
		RECRYS.	UNCRYS.
Control	0.6	367	-
1000	0.4	357	-
1025	12.7	367	312
1050	17.3	349	302
1100	25.7	356	312
1150	40.9	335	300
1200	27.6	328	295
1250	17.4	335	294
1275	5.0	316	-
1300	96.8	-	158
1350	95.1	-	153

recrystallized. Recrystallization did not occur below 1025°C, but when it did occur it was closer to the inner diameter of the tube than the outer diameter. The recrystallization at 1300°C was accompanied by a large drop in hardness, in contrast to the more modest decrease in hardness observed in the partial recrystallization that occurred at lower temperatures. Electron microscopy indicated that the yttria dispersoid had broken down in the completely recrystallized specimens annealed at 1300°C. The incoherent yttria phase was no longer present, and had been replaced by small coherent precipitates containing both yttrium and titanium. This is a plausible explanation for the fact that it is not possible to recover through cold work the strength lost after recrystallization at elevated temperature.

Microhardness values are given in Table 5 for sections of the Cartech production run annealed in argon-filled glass vials at temperatures ranging from 800 to 1300°C. This lot of tubing exhibited better recrystallization behavior than other lots of tubing produced in the U.S. No recrystallization was observed in specimens annealed for 1 hour at temperatures as high as 1300°C, whereas significant recrystallization had occurred in the second pilot lot of Cartech tubing after only 15 minutes at 1300°C (Figure 11).

Significant recrystallization was present in the production run tubing, however, after 8 hours at 1300°C. While the tube did not recrystallize completely, the hardness of the unrecrystallized area dropped to a level almost identical to the hardness of the recrystallized region. The 8 hour anneal at 1300°C also produced a large amount of porosity in the tubing (Figure 12), due most likely to inert gas bubbles retained from the powder consolidation and extrusion. The bubbles appear to be aligned in rows similar to impurity stringers.

Table 5.
Microhardness Data on ODS Tubing After 1 Hour Anneals

ANNEALING TEMPERATURE (°C)	MICROHARDNESS (DPH) [500 gm load] CARTECH PROD. LOT	STC ORT	PNC	SCK/CEN HEAT S54A
800	389	-	-	-
900	383	420	340	242
1000	372	326/411[a]	338	248
1100	359	331	338	247
1200	358	314	318	285
1300	316	278	285	230
1300 (8 hrs)	148/159[a]			

[a]First value is for recrystallized area, second value is for unrecrystallized area.

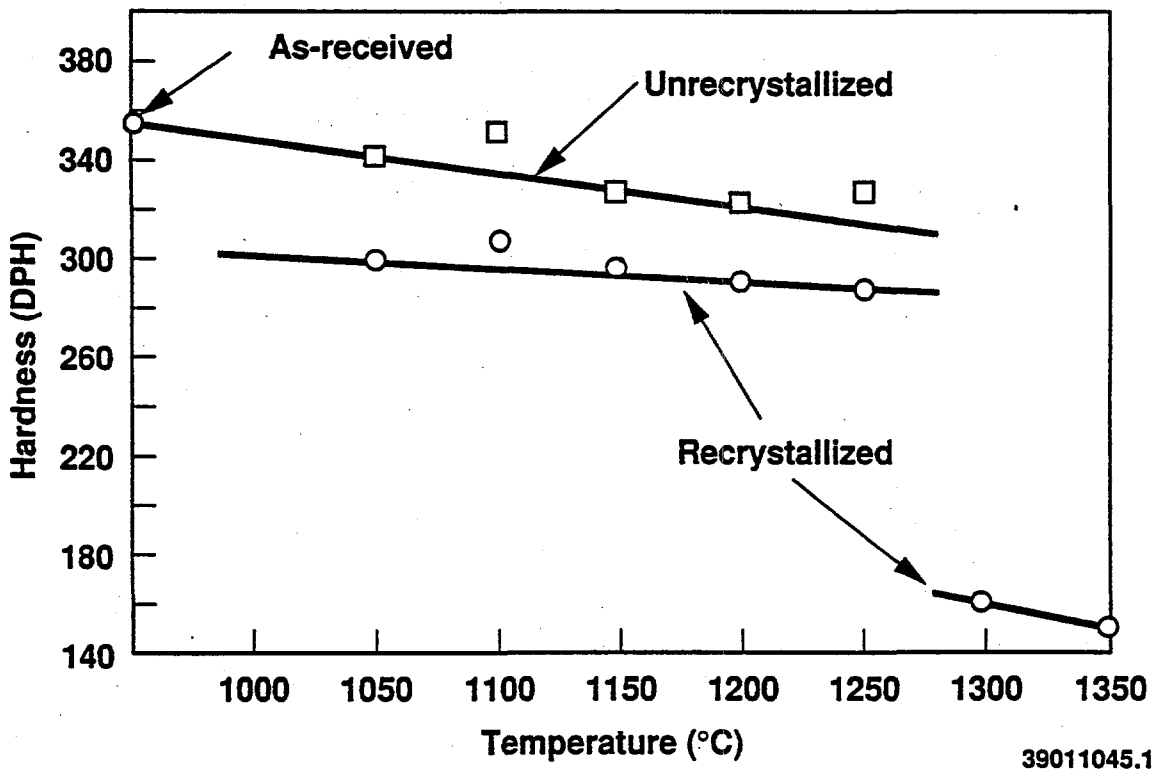

Figure 10. Hardness of recrystallized and unrecrystallized areas following 15 minute annealing treatments.

Table 5 also contains hardness data from a recrystallization study on the tubing produced by STC as well as the Japanese and Belgian ODS tubing. Only one of the three Belgian heats was annealed due to the similarity in their as-received microstructures. The hardness data are shown graphically in Figure 13 with the data on the Cartech production run. While the STC tubing was originally harder than the PNC tubing, it began to recrystallize at 1000°C, dropping in hardness to a level the same as that of the PNC tubing in the unrecrystallized state. The DT2203Y05 tubing was somewhat softer than the MA957 and exhibited no recrystallization or softening after any of the 1 hour treatments. Optical micrographs are given in Figure 14 for the as-received form of the various types of tubing and in Figure 15 for the annealing matrix.

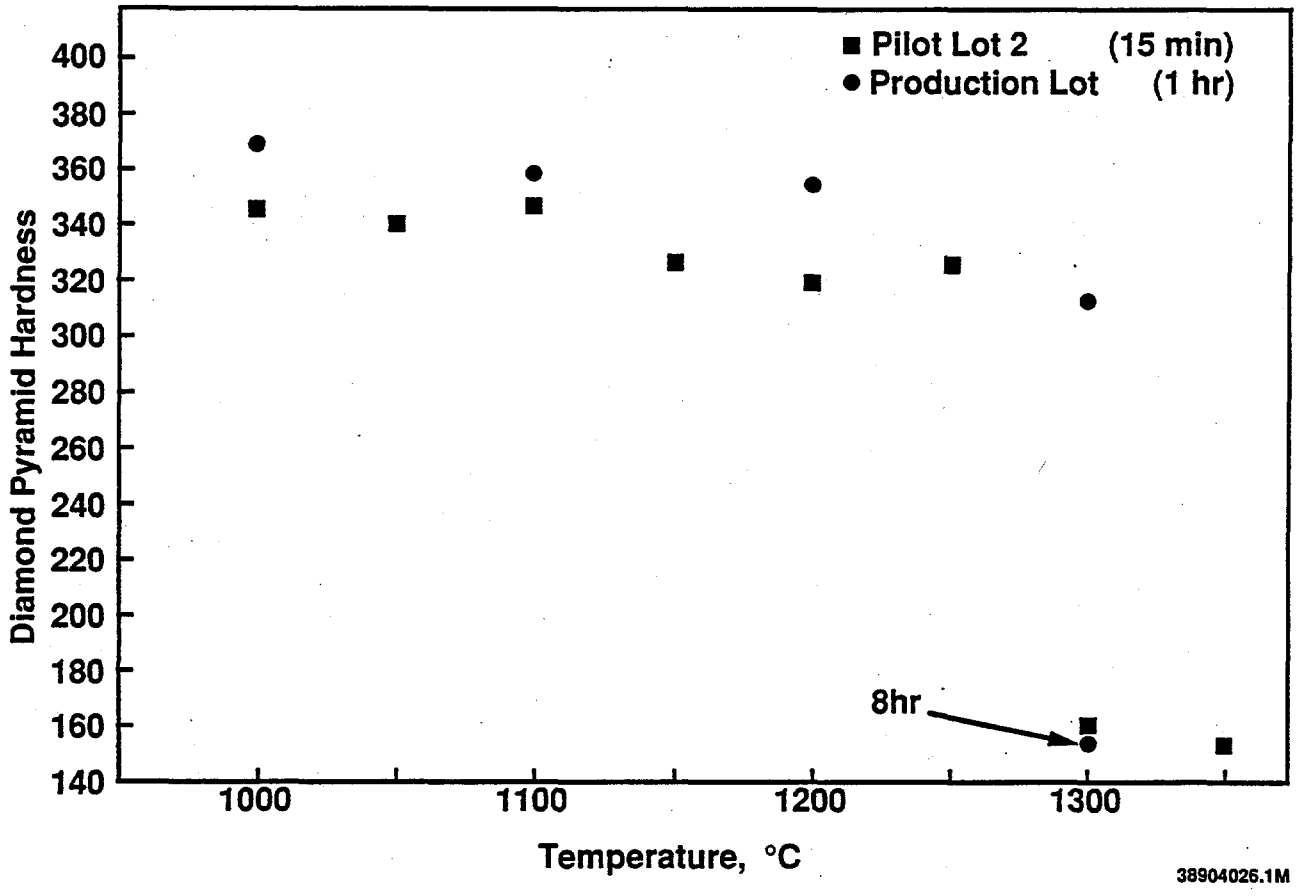

Figure 11. Recrystallization of production lot of MA957.

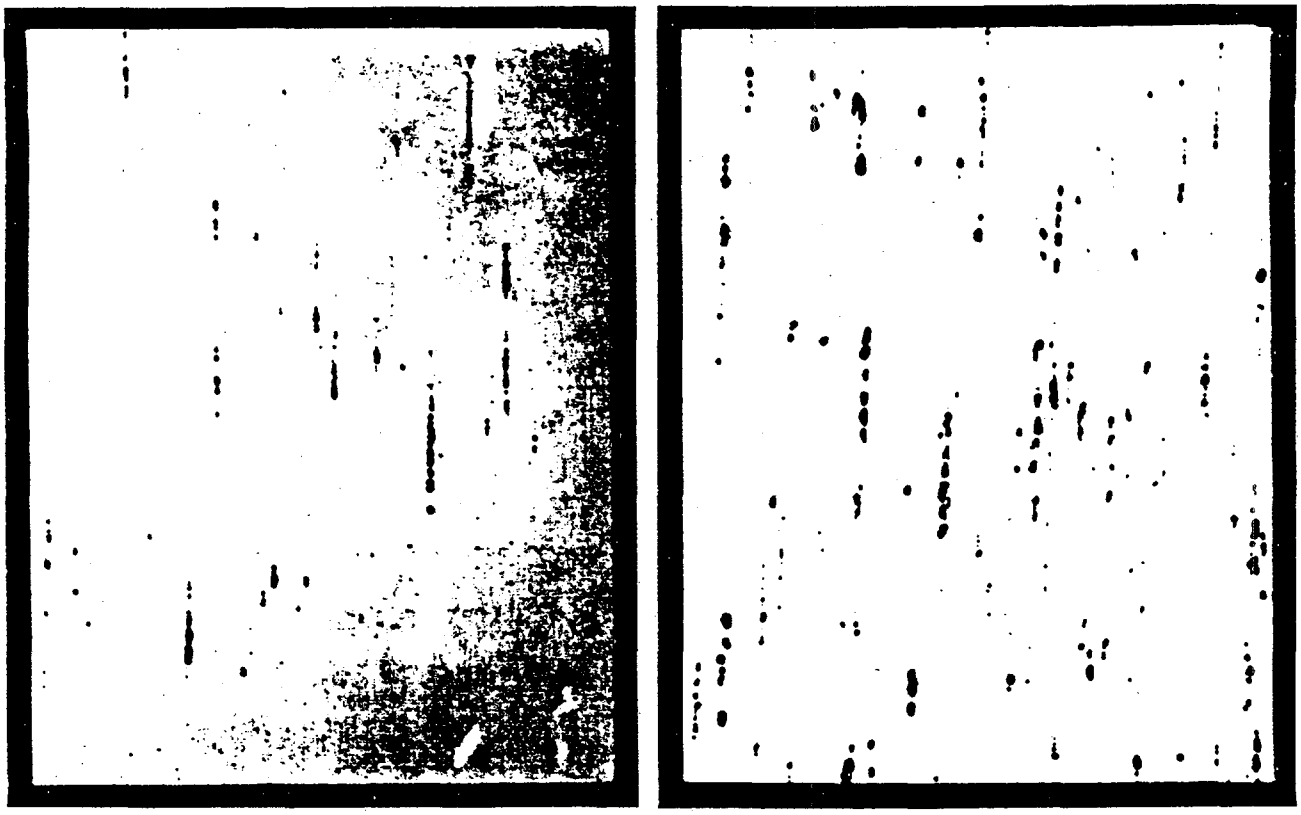

Figure 12. Porosity produced in Cartech tubing during fabrication and after aging.

Non-Destructive Examination

Several types of nondestructive evaluations were performed on as-received bar stock to verify the acceptable condition of the starting material. These included ultrasonic velocity and attenuation, eddy current, radiography, thermoelectric and magnetic field determinations. No flaws were detected in any of these determinations nor were there any unexpected signal degradations which could be attributed to microstructural variabilities.

Thermoelectric Test. A null microvoltmeter was used to measure the thermoelectric emf generated on a bar from heat DBB0114 and compared to an arbitrary reference point on a bar from another heat while heat was applied to the "reference" bar. Readings were taken every 0.5 inch along the length of the bar, and at 0.25 inch increments across the diameter at the ends. The differential measurements ranged from 2.80 - 3.20 μV, within the 2σ limits calculated for these data.

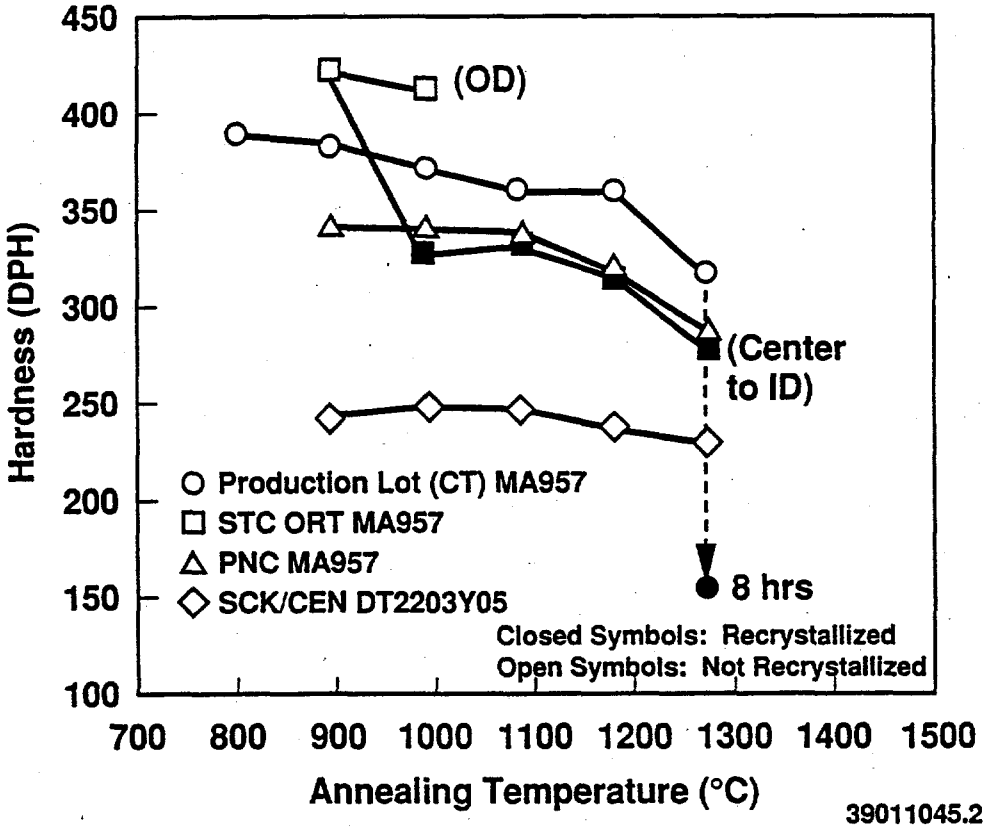

Figure 13. Hardness of several types of MA957 after 1 hour anneals.

Ultrasonic Velocity. Velocity and attenuation data were obtained using contact probes to generate compressional mode waves at a frequency of 5 MHz. Measurements made across the diameter and at one inch intervals along the length were very uniform at a value of 0.2292 inch/μsec. A measurement precision of approximately 0.0004 inch/μsec was established for this method. Additional velocity measurements taken around the bar diameter indicated a change of approximately 3.5% around the bar, suggesting a preferential grain orientation.

Eddy Current. Because the alloy is ferromagnetic, magnetic permeability variations obliterated any useful conductivity data. Equipment to perform magnetic saturation testing was unavailable.

Radiography. Radiography was performed in one view to determine if any gross segregation or regions of extensive fine porosity existed. A long film-focal distance was used with DR film for high resolution and contrast. No discrete discontinuities were observed.

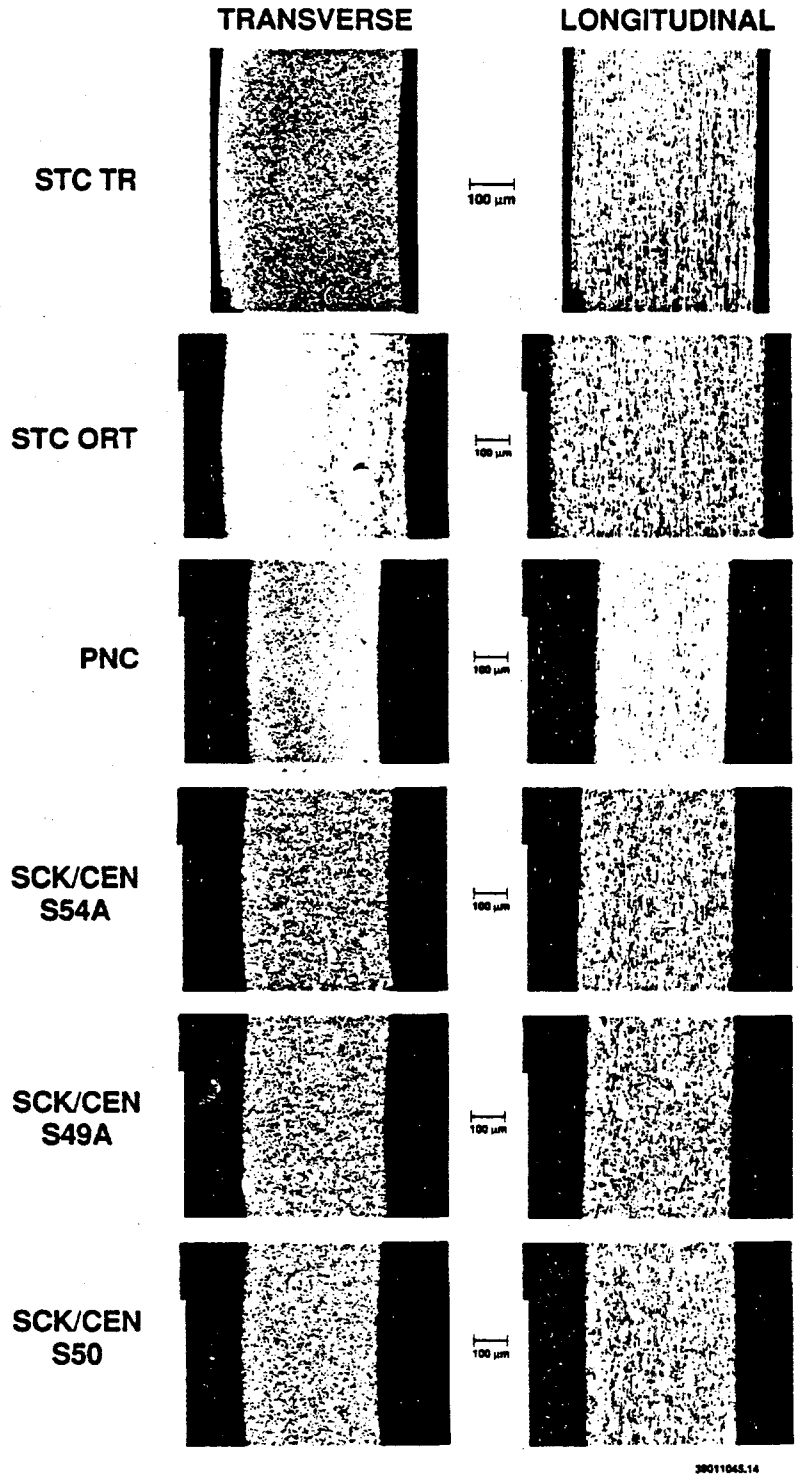

Figure 14. As-received microstructures of various types of ODS tubing.

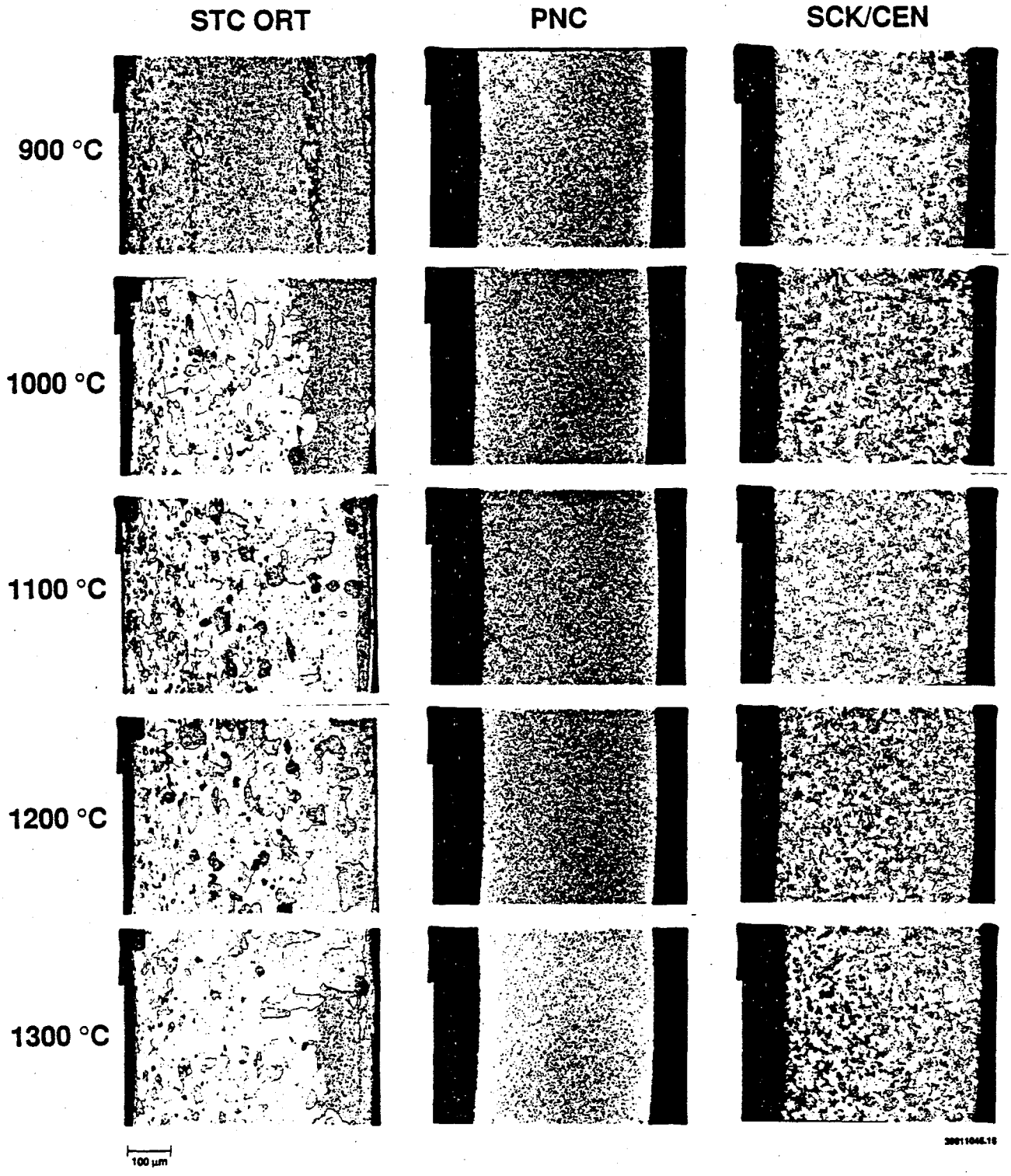

Figure 15. Microstructures of MA957 produced by STC, PNC and SCK/CEN (heat S54A) after 1 hour anneals.

Thermal Expansion

Thermal expansion data were obtained on two samples in flowing helium at 0.04°C/s and the following polynomial expression was fit to the data:

$$TE = K + AT + BT^2 + CT^3$$

where TE is thermal expansion in in./in., K = -5.86435E-4, A = 1.267276E-5, B = -2.201613E-9, C = 3.618884E-12, and T is the temperature in °C. The data and equation are shown in Figure 16. The equation is compared to the average thermal expansion of HT9 in Figure 17. The two are virtually identical until about 850°C, where HT9 undergoes a phase transformation back to austenite. The similarity in thermal expansion of HT9 and MA957 supports the use of HT9 end caps in the pulse magnetic welding of MA957 tubing.

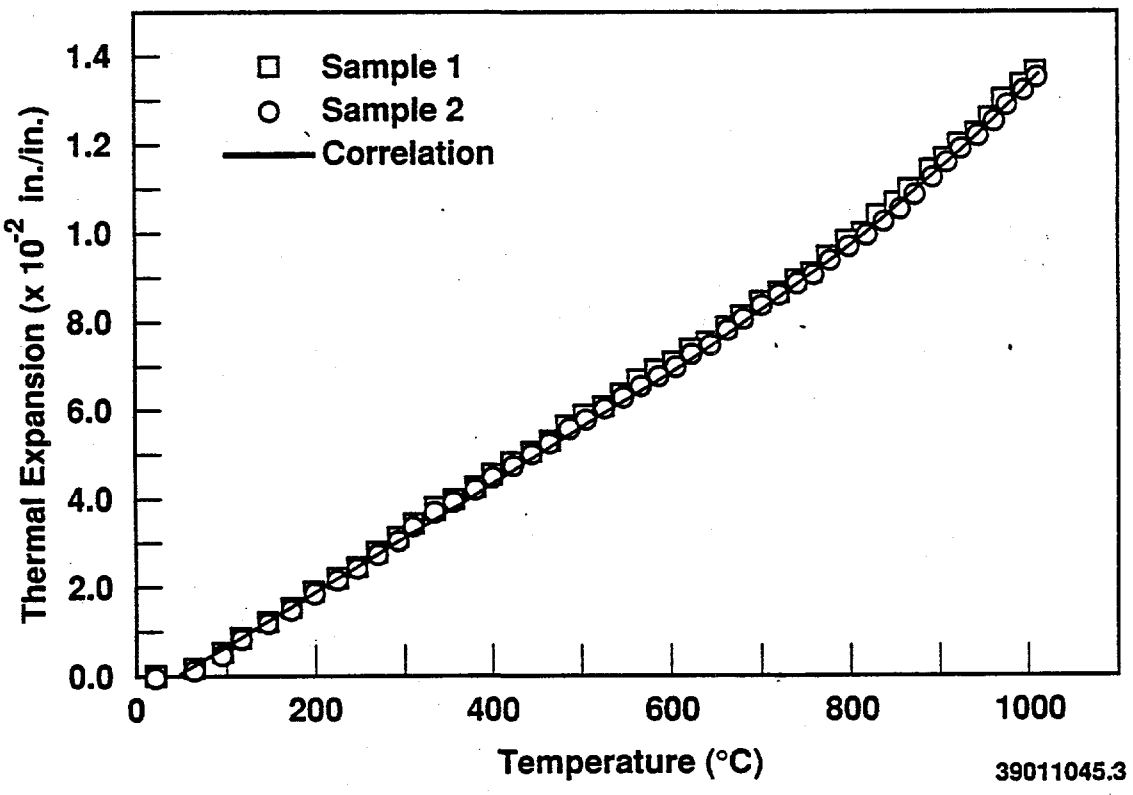

Figure 16. Data and correlation for thermal expansion of MA957.

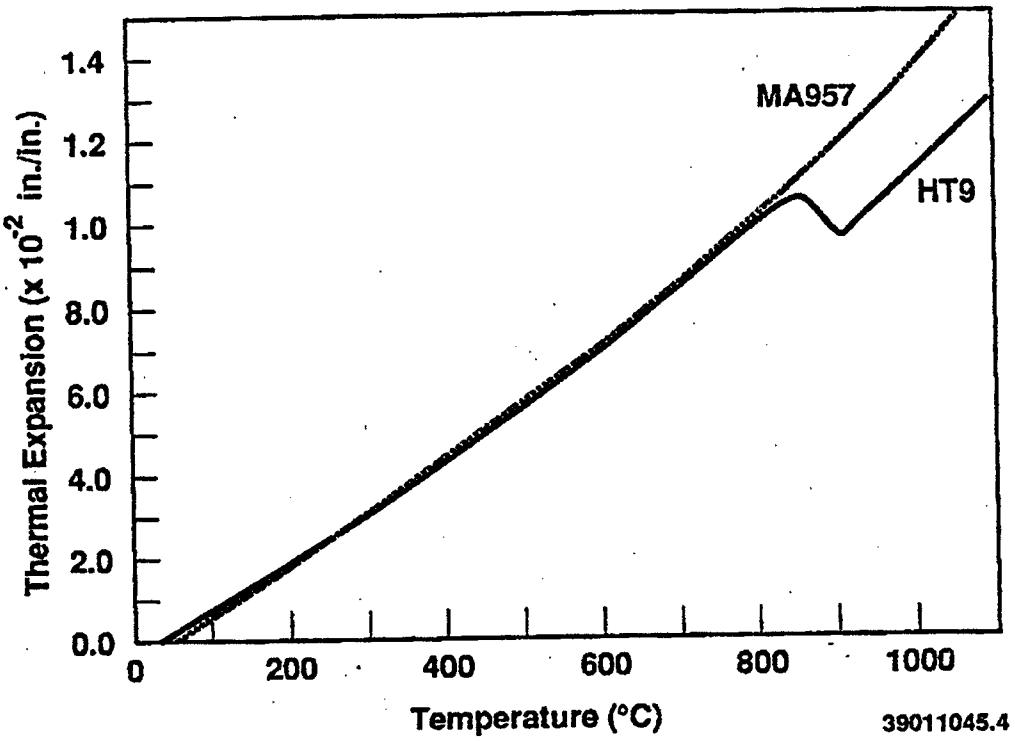

Figure 17. Comparison between thermal expansion of MA957 and HT9.

V. FABRICATION DEVELOPMENT

Processing Issues

Two factors controlled the selection of the final fabrication path: the need to minimize the cost of fabrication and the need to maintain the as-received microstructure. Minimizing the cost of fabrication required that the number of reductions be minimized, hence the largest possible reductions were required. The need to maintain the existing microstructure limited the temperature at which interpass anneals could be performed. The interaction between these two factors was explored at Westinghouse Hanford Company (WHC) as part of the onsite fabrication development effort.[4-6]

It was demonstrated that the working behavior of the alloy was highly anisotropic, with better ductility in transverse orientations than in longitudinal orientations (orientations are given with respect to the working direction and the direction of grain elongation). This is illustrated in Figure 18, which shows the change in hardness as a function of the reduction in thickness after cold rolling flat slices of the as-received bar cut in the two orientations. The maximum reduction level obtained prior to cracking is

shown by vertical lines at roughly 30 and 75% reduction for longitudinal and transverse sections, respectively.

Figure 18 demonstrates that longitudinal and transverse working produced similar increases in hardness, although the longitudinal section failed at a lower reduction than the transverse section. The differences in deformation limit with orientation were not, therefore, due to differences in work hardening but were due rather to strain limits which were orientation dependent. On the basis of numerous observations similar to those shown in Figure 18, the longitudinal reductions of the tube hollows required to produce tubing were limited to about 15 or 20%.

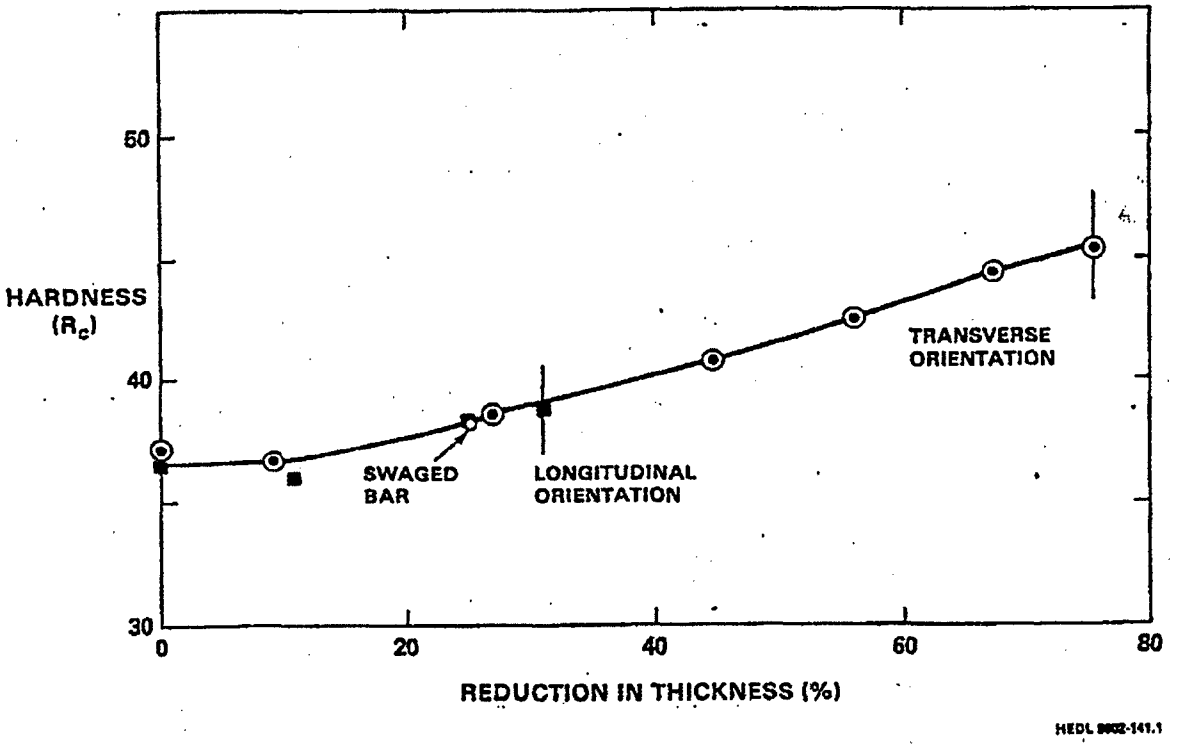

Figure 18. The effect of cold rolling on the hardness of MA957 as a function of thickness reduction.

Continued reduction of sheet or tubing requires interpass anneals to relieve the stresses induced by working. These thermal annealing treatments must also, however, be chosen with care. The higher the stress relief temperature, the more recovery occurs and the larger the subsequent reductions can be. Laboratory experiments and tube drawing tests demonstrated that INCO's

recommended annealing temperature of about 800°C was too low, causing insufficient recovery of the microstructure and subsequent cracking with additional processing. The tendency for recrystallization during thermal annealing must also be avoided, however, since the highly elongated subgrain structure apparently cannot be regenerated by subsequent cold work once it has been eliminated, putting an upper limit on the annealing temperature.

The final processing window determined for successful fabrication is shown in Figure 19, which shows that both cracking and recrystallization could be avoided if cold work levels were held to about 15% and annealing temperatures were around 1000°C. This window was determined by laboratory experiment and verified by tube drawing tests, which demonstrated that only minor recrystallization was observed.

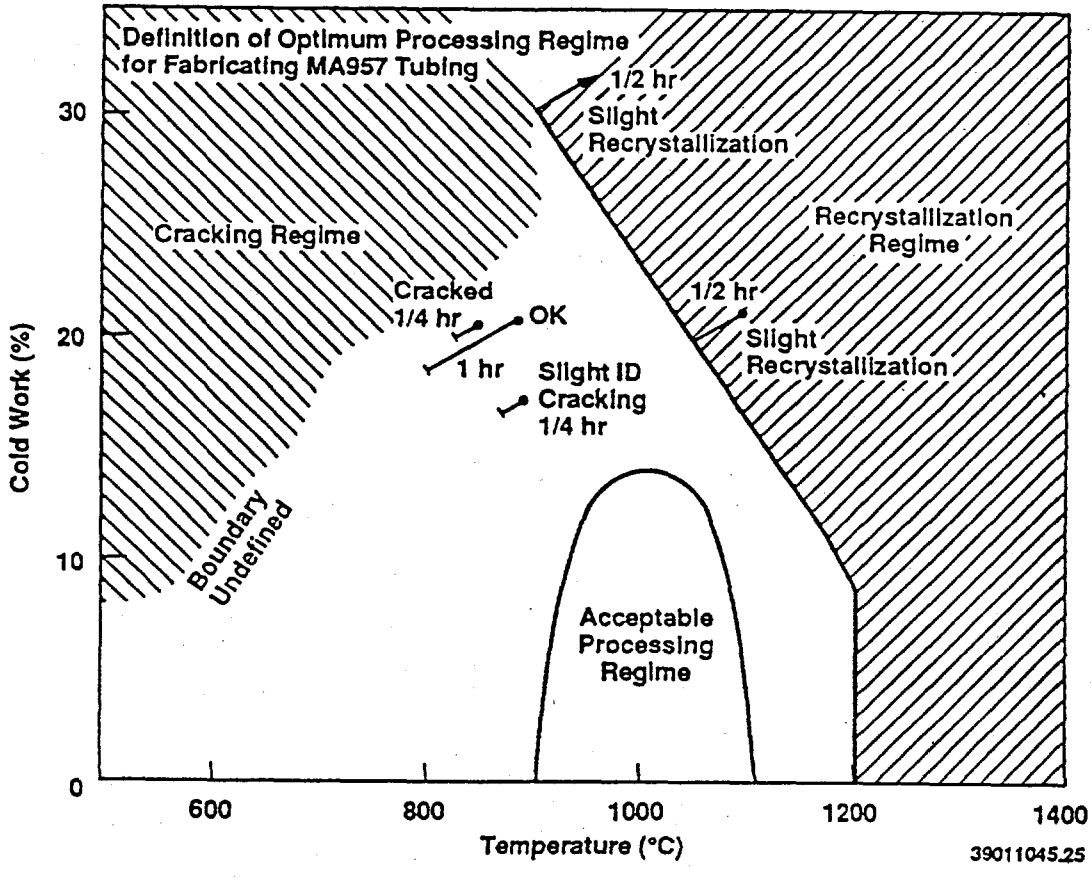

Figure 19. Definition of the optimum processing regime for fabrication of MA957 tubing.

Fabrication Development Efforts at WHC

Rod and tubing were produced at WHC to provide specimens for mechanical properties testing as well as to provide early input that would assist qualified cladding suppliers in producing commercial quantities of fuel and blanket cladding.[3]

A bar of MA957 was successfully swaged from one inch in diameter to 0.260 inches in diameter using an interpass anneal at 1050°C, according to the reduction schedule given in Table C1 (Appendix C). The hardness decreased significantly during reduction as a result of secondary recrystallization. Reduction of a tube hollow (Table C2) which had been partially processed at 1050°C and exhibited secondary recrystallization was continued with a drop in annealing temperature to 800°C on INCO's recommendation. The tube hollow cracked after three anneals at 800°C, indicating that the optimum stress relief temperature was between 1050 and 800°C.

On the basis of this experience, additional fabrication of rod and tubing was initiated at WHC using 15% reductions and 825°C anneals as a precursor to the commercial fabrication effort. A second bar was successfully swaged from one inch in diameter to 0.265 inches in diameter (Table C3). The annealing temperature was increased to 875°C after the first three reductions due to increases in hardness. The first pressurized tube specimens for MOTA irradiation were fabricated by drilling out the interior of this rod.

Another batch of tubing was subsequently made at WHC by rod drawing from a starting size of 0.9 x 0.485 inches to a final size of 0.230 x 0.200 inches (Table C4). All reductions were approximately 15%, and all anneals were at about 1000°C. The initial hardness of the tube hollow, 314 DPH (R_C 31.5), increased as high as 375 DPH (R_C 38) after an anneal about 50% of the way through the reduction process and gradually decreased to 364 and 346 DPH (R_C 37 and 35) after the anneal associated with the final reduction. The latter two hardness values are associated with unrecrystallized and recrystallized regions, respectively, that appeared after the final anneal. Stress rupture tests were performed on samples sectioned from this batch of tubing.

Fabrication Development Efforts with Commercial Vendors[3]

Vendor Fabrication: Superior Tube Company (STC)

A fabrication development contract was placed with STC in Collegeville, Pennsylvania, for the fabrication of 0.270 x 0.226 inch cladding from bar stock provided by WHC. STC selected a reduction sequence using rod drawing followed by two-roll derodding. Initial cold pointing operations resulted in cracking of the point. This was resolved by heating the nose and pointing at red heat, a technique with which WHC also had success. Significant increases in hardness were produced using an annealing temperature of 875°C, selected initially on the basis of prior WHC efforts. Increasing the annealing temperature to 900°C did not ameliorate the problem. After ten draws,

hardness had increased from about 34 to about 42 on the Rockwell C scale, with no recrystallization observed.

The lot was divided into two pieces and the processing temperature of the second lot was increased to 1000°C to increase the probability of success. Fabrication continued on both lots to completion and metallographic examination of both lots revealed a similar structure and hardness. Eight feet of finished tubing (four in each lot) required 17 rod draws and one plug draw. The plug draw was performed last to ensure that dimensional tolerances were met.

Another lot of tubing was later produced at STC for use in the ORT experiment in EBR-II. The fabrication schedule was essentially identical to that used in the developmental STC heat produced using 1000°C interpass anneals.

Vendor Fabrication: Carpenter Technology Corporation (Cartech)

A similar fabrication development contract was placed with Cartech in El Cajon, California. A follow-on effort was included for production quantities of fuel and blanket cladding originally intended for use in the DSF-1 experiment in the Fast Flux Test Facility. Cartech initially elected to use plug draws rather than rod draws in the belief that this would be a more conservative approach. They felt that the only means they had of derodding the tube hollows after a rod draw was to use a straightener, which it was believed would crack the tubing. The combination of the plug draws and the 875°C annealing temperature created serious fabrication difficulties, however, including the breaking off of the point and the appearance of significant transverse cracks. Increasing the annealing temperature to 900 and then to 925°C did not produce the desired softening of the material, the hardness of which had increased to R_C 42. After machining away the cracks on both the inner and outer diameters, a successful rod draw was completed, but the tube split full length during the derodding operation.

A portion of the bar stock was diverted from the intended production lot of cladding for use in Cartech's second unsuccessful attempt to plug draw tubing. Two lots were run at WHC's request at annealing temperatures of 1000 and 1100°C in order to bracket a probable range of feasibility. Cartech declined to consider rod draws on the basis of equipment limitations and the earlier derodding experience. The fabrication effort on the lot annealed at the lower temperature was stopped after cracking problems appeared. The fabrication effort on the lot annealed at the upper temperature exhibited a new problem: recrystallization softened the tubing sufficiently that the necessarily high drawing forces induced local yielding as the tubes were being drawn, producing a series of convolutions on the tube surfaces. Warm working at a temperature below about 150°C did not alleviate the problem, as the elevated temperature caused the lubricant to break down, resulting in significant plug chatter.

It had become evident that the microstructure and therefore the fabrication of MA957 was very sensitive to the combination of drawing method and annealing temperature, since rod draws followed by 900°C anneals were successful at STC while plug draws followed by 1000°C anneals failed at Cartech. The failure of

plug drawing was attributed by WHC to the sensitivity of the alloy to the large tensile loads produced by this method, exacerbated by the non-optimum die angles used by the vendor. Cartech therefore initiated a die angle optimization effort to reduce the draw pressure and established the cold working capability of the alloy by measuring the springback of bar drawn through a range of reduction sequences. The third tubing fabrication effort was approved on the basis of these studies.

Preparation of the additional bars for the third run revealed that excessive eccentricity was sustained during the gun drilling of the production bars supplied by INCO, a problem which had not existed earlier. Neither heat-to-heat variations nor residual stresses accounted for the difficulties, nor was the problem solved by using alternate tool designs. There was some evidence that the hardness of the bars varied along their length, affecting the gun drilling operation. Comparative work with 316 stainless steel demonstrated that the basic gun drilling process was acceptable and that the difficulty lay with the alloy itself. Additional work on the gun drilling problem continued during the third run, culminating in the establishment by Cartech of satisfactory proprietary parameters for the gun drilling operation.

The third run evaluated the viability of both rod and plug drawing in the initial reduction operations. Interpass anneals were performed at 1000°C for both rod and plug drawn material. Both the rod and plug draw operations were performed using the optimized die angles established by the vendor, which successfully reduced the required draw forces. Plug draws, however, were discontinued after the third draw when the rod holding the plug broke. Although the lower die angle reduced the draw bench pressures and the strain hardening of the tubing, it also increased the frictional forces within the die, leading to the rod failure. No unexpected problems appeared during rod drawing operations. Derodding was performed using multiple passes with flattening rolls to thin the wall in numerous locations around the circumference of the tubing, thereby expanding the tubing off the mandrel. A crack induced during a pointing operation propagated a short distance during an intermediate draw; this problem was eliminated in subsequent draws by performing a dye penetrant examination after each pointing operation and removing any cracks before proceeding.

The successful completion of the rod draw portion of the third run finished the pilot process required to establish the reference fabrication parameters for the production of fuel and blanket cladding. It required 23 rod draws and a final plug draw to convert the tube hollow to finished 0.270 x 0.226 inch tubing. The hardness of the tubing during the third run is shown in Figure 20 as a function of reduction pass number; it stabilized at a Rockwell C value of about 40.5. Twenty to thirty percent of the microstructure appears to have recrystallized, but this is not expected to have a significant effect on the behavior of the cladding in the operating regime of interest. Stress rupture tests were performed to verify this expectation. Figure 21 illustrates the microstructure of the tubing produced by WHC, STC and Cartech relative to as-received bar stock.

Cartech successfully completed the third pilot lot of MA957 tubing, producing five lengths of 0.270 x 0.226 inch tubing totalling 357 inches. The final

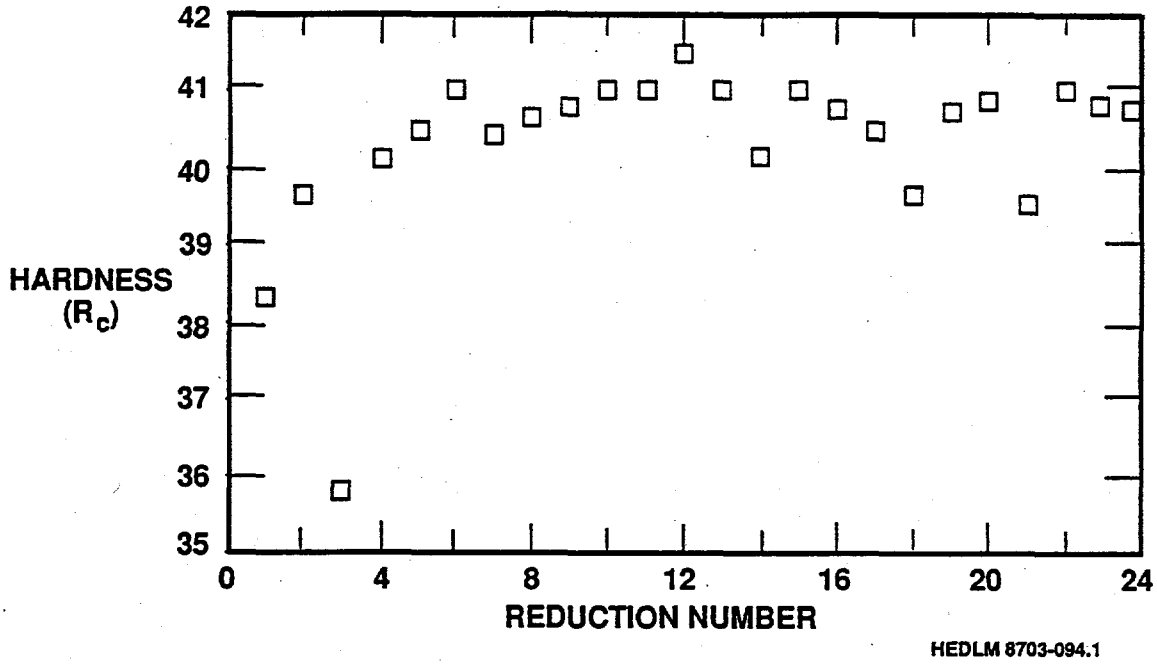

Figure 20. Hardness of tubing produced at Cartech during third pilot run.

thermomechanical treatment comprised a 5% plug draw followed by a 1000°C anneal for 15 minutes.

Changes based on an evaluation of the third pilot run were introduced into the fabrication process prior to the initiation of the production run. In an effort to minimize the localized cold working produced during the derodding operations, the Cartech was directed to minimize the deformation produced in the tubing by the use of the flattening rolls. In addition, use of shaped rolls was required to distribute the stresses as much as possible. To detect any cracking that might occur during the derodding process, increased monitoring was required during fabrication: 100% red dye inspection of the points and fluorescent inspection of 3 tubes per lot were required prior to annealing after every draw. As a final preventive measure, all tubes were to be conditioned by sanding prior to each anneal.

One hundred tube hollows were initially committed for the production run. Another 20 were added later to provide a theoretical yield of 341 tubes. These tube hollows were processed without difficulty through 21 draws as one lot, producing 309 full length tubes. At the final size, it was determined that a straightening operation was required to enable an ultrasonic inspection to take place. Because of the potential for cracking with the straightening operation, two tubes were selected to pilot the operation. The parameters developed on these pilot tubes were then used on the 51 full length tubes that exhibited the worst bow. Fluorescent and ultrasonic inspections were performed on the tubes from this "partial production."

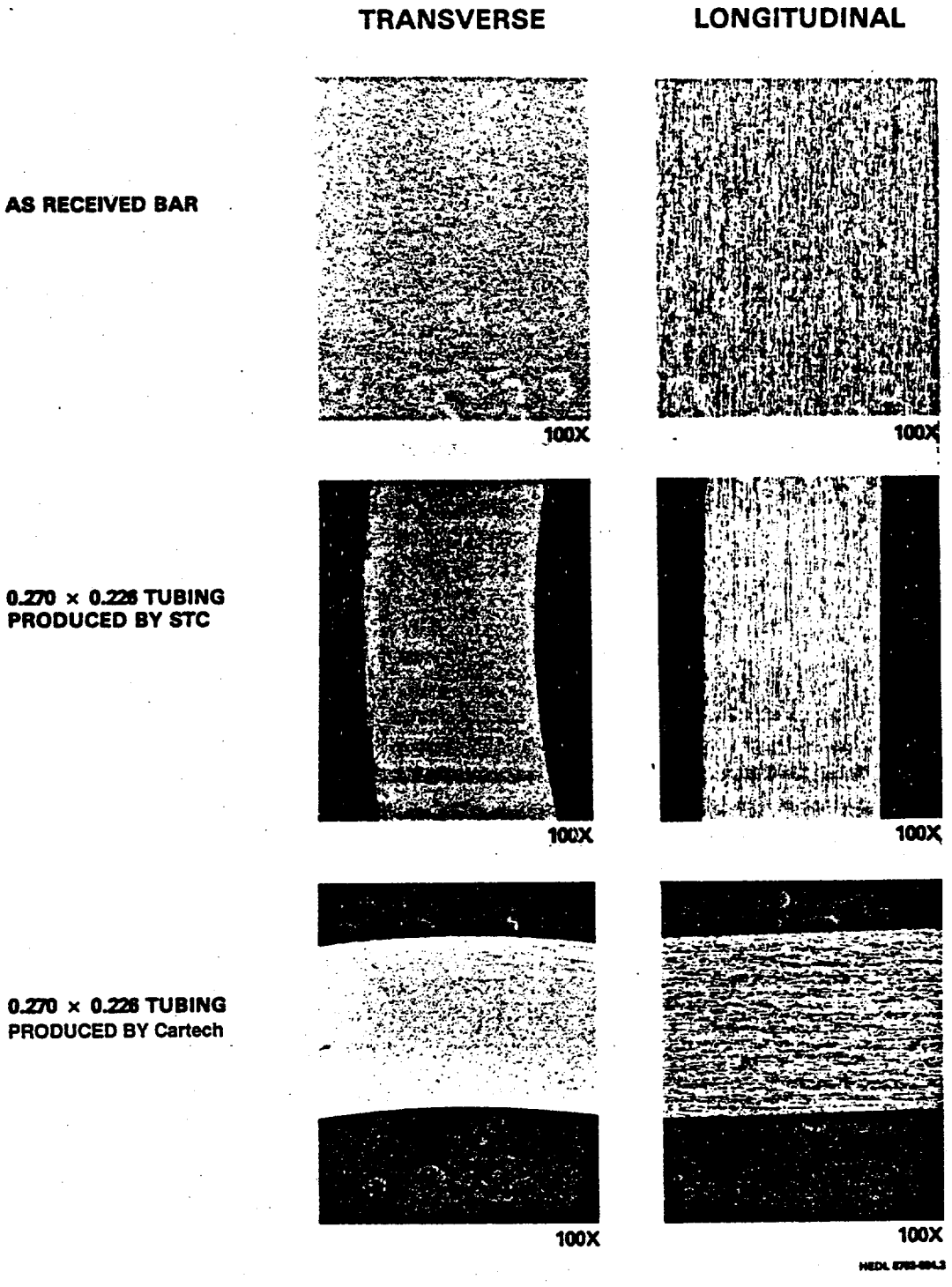

Figure 21. Microstructure of as-received bar stock and the tubing produced by WHC, STC and Cartech.

All of these straightened tubes exhibited ultrasonic indications in excess of that produced by a 0.001 inch notch standard, and all but two exhibited indications in excess of that produced by a 0.002 inch notch standard. Straightening did not appear to be a factor in the formation of these ultrasonic indications, however, as metallographic examination revealed they had existed during one or more annealing cycles. The remaining production tubes were then straightened and inspected ultrasonically, yielding a total of 258 tubes, all rejected at the 0.002 inch defect level. Typical ultrasonic test traces and defects are shown in Figures 22 and 23. In Figure 22, 0.002 inch indications correspond to 36 and 30 divisions in the transverse (top) and longitudinal (bottom) channels, respectively. Figure 23 demonstrates that cracks propagated along recrystallized regions at roughly 45° to the tube wall. Details of the ultrasonic inspection are provided in the following paragraphs.

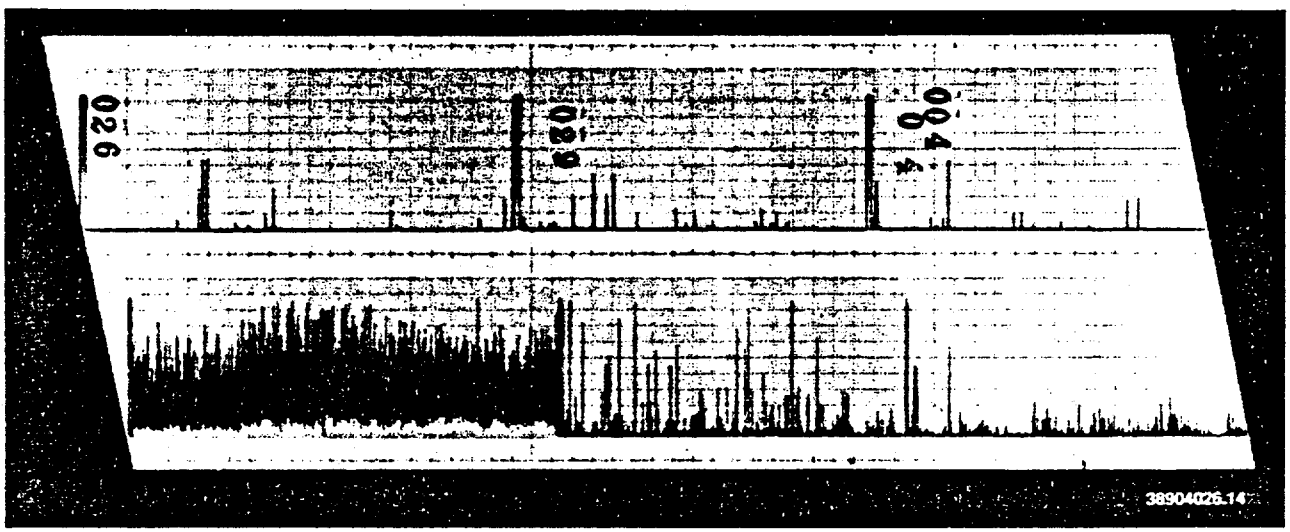

Figure 22. Samples of ultrasonic test traces from partial production lot. Upper trace is for transverse scan, lower trace is for longitudinal scan.

The MA957 tubes from the partial and full production lots were fabricated in accordance with the requirements of ASTM A771. Ultrasonic examination was performed in accordance with ASTM E213 and the following supplemental requirements:

1. The procedure was restricted to the detection of discontinuities by ultrasonic pulse echo shear waves or refracted longitudinal waves using immersion techniques and spherically focused 10 MHz transducers.

2. The ultrasonic inspection was performed using a calibration standard comprising a tube section that contained three notches of a particular

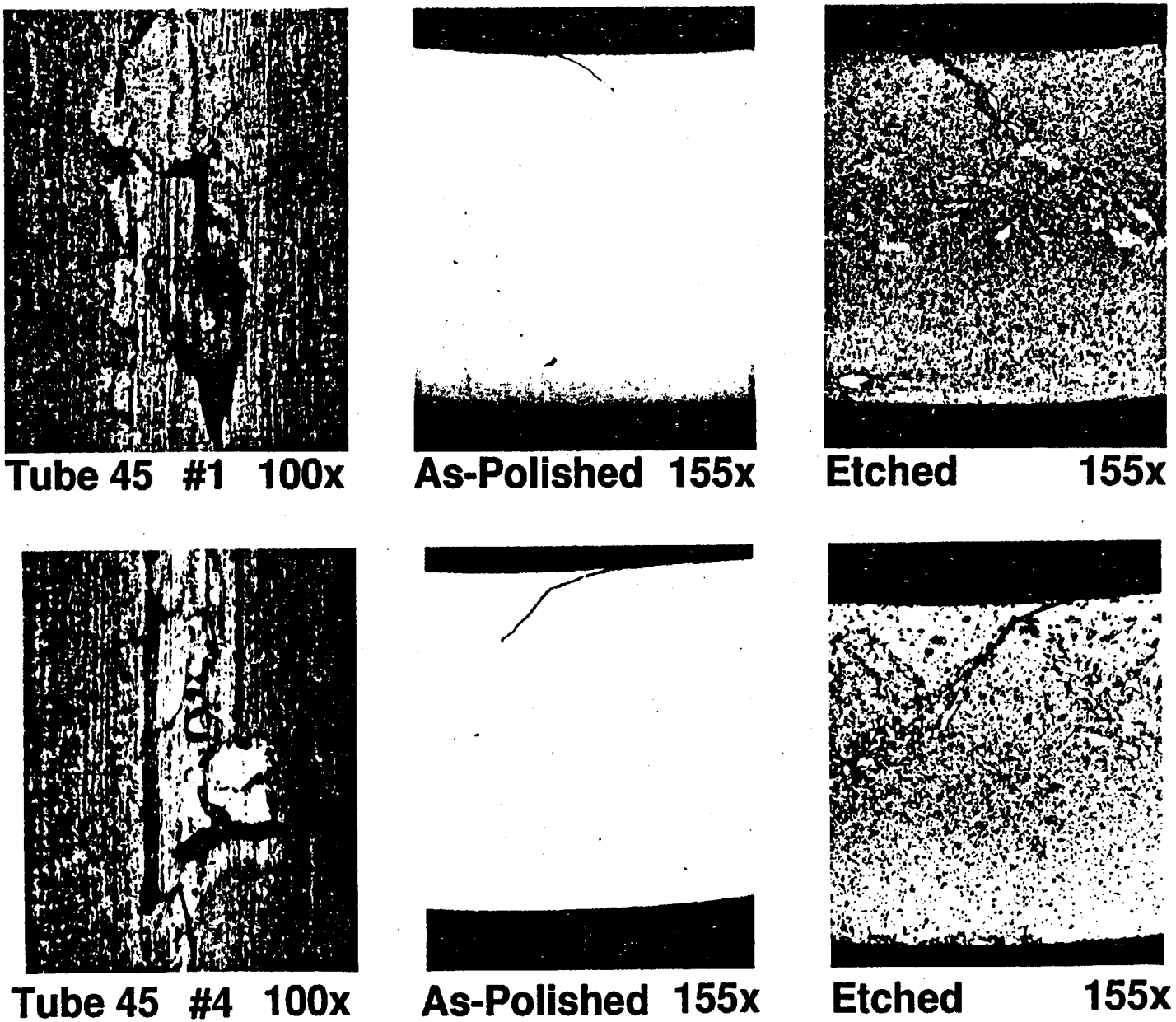

Figure 23. Examples of defects in the partial production lot.

type (ID or OD) and orientation (axial or circumferential), fabricated with nominal depths of 0.0007, 0.0010 and 0.0015 inches. In addition, an alternate notch standard fabricated with nominal depths of 0.0015, 0.0020 and 0.0025 inches was used to determine if relaxation of the defect criteria would increase the yield of acceptable tubes.

3. Calibration of the test system was established using statistical control such that the rejection of the reference defect (0.0010 inch or 0.0020 inch) was assured at the 95% confidence level.

4. After calibration, the response of the test system to each applicable reference notch group was measured at least twice immediately prior to the production examination, once every hour during production examination, and twice immediately following the production examination or prior to any equipment shutdown.

Various types of testing were performed on sections from the production run of tubing produced by Cartech. Specimens were obtained from regions exhibiting a minimum number of ultrasonic indications unless they are referred to as 'defected', in which case they were purposefully taken from tube sections exhibiting the largest indications.

Alternate Fabrication Process Development

Numerous passes are required to fabricate tubing from MA957, because the amount of deformation that can be achieved using conventional drawing operations is limited to small reductions in area per pass. This limitation results in many draws and incurs high fabrication costs. To circumvent this problem, alternate processing methods were evaluated to assess the potential for minimizing fabrication costs. Since the difficulty with conventional drawing methods is primarily a result of the limited tensile ductility of the alloy, particularly at temperatures close to the ductile-brittle transition temperature, the most promising alternatives involve the application of compressive rather than tensile stress states during tube reduction.

Vendor Investigations: Superior Tube Company

Initial development efforts at STC using compressive reduction techniques (pilgering) suggested that this approach might be successful. As a result, a development contract was placed with STC to obtain further information using this type of compressive working of MA957. A similar contract could not be placed with Cartech since this vendor did not have the equipment necessary for this type of process. The goal of the program was to achieve area reductions in the range of 40 - 50% by increasing the percentage of wall reduction in the cold working schedule. Other benefits included 1)starting with a heavier wall thickness, thereby losing less of the expensive starting material to gun drilling, 2)working the wall thickness in preference to the diameter, thereby decreasing the aspect ratio of the grains and hopefully improving the circumferential creep and rupture properties, and 3)removing the need for a

pointing operation, thereby improving material yields and further decreasing the cost.

After drilling the 1 inch diameter bar to generate a tube hollow with a 0.187 inch thick wall, the reduction sequence was to proceed with 26, 30, 42, 46 and 49% compressive reductions followed by three plug draws to the finished size. The stress relieving anneals between reductions were to be performed at 1000°C for 20 minutes. The finished tubing would therefore require only eight passes, rather than the more than 20 passes required using only tensile processing techniques.

The first pilgered tube reduction was completed successfully, although only a 19% reduction was achieved and the wall thickness (0.167 inch) was larger than planned due to die wear. The second reduction was commensurately larger, 39%, and resulted in a 0.123 inch thick wall. The threads on the mandrel fractured during the third reduction, to a 0.625 inch outer diameter (42%). After the mandrel was removed from the tube hollow, it was observed that it had deformed during loading even though it had been hardened to R_C 56. A second attempt with another mandrel produced similar results. It was presumed that the MA957 alloy at R_C 39 was too hard for the mandrels to perform satisfactorily at this small size. The reduction process continued using rod drawing to overcome this problem, striving to simulate compressive working by selecting die and mandrel sets that would favor wall reduction over diametral reduction.

Approximately 9 feet of tubing for material property studies was ultimately produced after six rod draws, at approximately 30% reduction in area per draw, and two plug draws, at 19% reduction per draw. Although the compressive tube reduction route was not completely successful at the smaller sizes, the original goal of working the wall thickness in preference to the diameter was maintained. The fabrication process had been compressed from 18 total draws in the previous STC contract to two pilgered tube reductions, six rod draws, and two plug draws. Additional work in this area appears to be worthwhile and could lead to a significant improvement in the cost of fabrication. Additional work is required, however, to fully evaluate the effects of the processing on material behavior as well as ultrasonic inspection.

Other Investigations: University of Missouri-Rolla

An additional study is ongoing at the University of Missouri, where the use of hydrostatic extrusion is being investigated as a means of fabricating MA957 tubing. This process uses hydraulic pressure during extrusion and allows extrusion into elevated pressure chambers. It was expected that extrusion into elevated receiver pressures might be more successful at preventing cracking than extrusion into air in a material such as MA957, which has very limited ductility.

The initial effort focused on the extrusion of rods rather than tubing to determine the sensitivity of the material to various equipment-related parameters such as choice of lubricant, die angle, required pressure, rate of extrusion, etc. The rods used were obtained from the WHC fabrication development effort described earlier. Investigation of reduction ratios was

obtained by extruding rods containing steps separated by tapered landings to conserve material.

The rod annealed at 1050°C was successfully extruded up to an area reduction of 40% using a pressure-to-1/2 receiver pressure arrangement before reaching the capacity of the press. A 47% percent reduction was achieved before the same limit was reached by extruding into air (i.e., into atmospheric receiver pressure). The rod annealed at 875°C achieved 45 and 48% area reductions, respectively, under the same conditions before reaching the limit of the press. No cracking was observed in either rod, and x-ray radiography revealed no internal defects. Optical metallography will be performed to examine the resulting microstructure. It is anticipated that higher reduction levels can be achieved, since the limiting factor was the capacity of the press. To verify this, steps will be machined into the extruded rods to allow a further pass through the press.

Tube reduction efforts to date have achieved some limited success. Due to the limited die sizes available and the small amount of starting material available, the only variable investigated to date has been the type of mandrel used. The use of fixed and semi-floating constant diameter rods as mandrels was not successful due to the yielding of the mandrels that occurred in both cases. High tensile loads resulted from the friction between the tube and the mandrel, and the acceleration in the tube as it exited the die. This caused the tube and mandrel to deform significantly (and the tool steel mandrel to fracture) in a circumferentially ridged pattern along the length of the tube.

Difficulties with the positioning of a tapered mandrel relative to the billet and the die make the use of such a mandrel impractical. The mandrel effectively acts as a plug if it is located too close to the die, while a hydraulic seal is not maintained if the mandrel is located too far away.

The use of a deformable mandrel was highly successful in extruding mild steel and D57, another ferritic stainless steel that is difficult to cold work in tension. A 57% area reduction was achieved in these alloys with the dies available. The deformable mandrel was created by using talcum powder inside a tube hollow machined from a rod. The tube hollow was sealed by a solid point machined on one end and a steel plug inserted into the other end. MA957 billets subjected to the same 57% reduction cracked axially and around the circumference at the point on the billet where it was released from the die. The limited number of dies available to date precluded extrusion to a smaller area reduction, although future efforts with the deformable mandrel will investigate this area.

Other efforts in the future will investigate the use of a recently designed, fully floating, constant diameter mandrel as well as a modified tapered mandrel. It is fully expected, on the basis of the reductions achieved in MA957 rod, that large reductions are also achievable in MA957 tubing once the pressure-to-pressure extrusion process is optimized.

Foreign ODS Tubing Fabrication

Very little is known about the proprietary processes used to produce the MA957 tubing in Japan for PNC or the DT2203Y05 tubing in Belgium for SCK/CEN. The Japanese process utilized several hot working processes at temperatures ranging from 400 to 800°C.

Pulsed Magnetic Welding Studies

The oxide dispersion added to strengthen the alloy makes MA957 a very difficult alloy to weld by traditional fusion methods. The melting process gives rise to a significant amount of porosity and slag as the dispersion is removed from the weld metal, leaving the remaining base metal in a much weaker condition. Pulsed magnetic welding (PMW) has long been used on ferritic HT9 tubing, and was therefore selected as the technique most likely to be easily adapted for use on MA957 tubing.[3]

MA956 is an ODS alloy similar to MA957 that was used for welding feasibility studies before the MA957 tubing became available. While it was not possible to establish a welding parameter envelop or develop a qualified welding procedure for MA957, the work that was completed was sufficient to demonstrate the feasibility of PMW on both MA956 and MA957 tubing. The limited amounts available of either dispersion strengthened alloy permitted the variation of only one welding parameter, voltage. The results of weld tests on the developmental tubing produced at STC are summarized in Appendix C. As shown in Figure 24, good solid state welds were achieved between MA956 or MA957 tubing and HT9 end caps.

The same end cap design and material (HT9) were employed as were used to weld HT9 cladding. It was demonstrated that this end cap design, with a double angled (8/12°) taper in the plug, or a design with a single 10° taper, produced higher quality bonds than were achieved with end caps having a single, lower (7°) angle, the use of which led to gross cracking in the end plug. Higher energy levels were required to produce successful welds with the dispersion strengthened steels than are used on austenitic stainless steels or HT9. The application of these energy levels, however, frequently caused centerline cracking in the HT9 end plug. Decreasing the applied energy to a level that eliminated the cracking produced unacceptable welds. Applying a high strength heat treatment, 1100°C/15m/AC + 675°C/2h/AC, to end caps previously heat treated in the standard treatment, 1100°C/15m/AC + 780°C/2h/AC, was not successful in eliminating the centerline cracking as it had been in HT9.

One of the difficulties encountered developing a qualified PMW procedure was the variability in the MA957 tubing that was produced. While good welds could be produced in each case, success was not achieved reproducibly due to variations in the cladding. For example, the bands of recrystallized material in some of the tubing deformed or fractured more easily than the unrecrystallized areas. These areas therefore responded differently to both the flaring and the welding processes (flaring the end of the cladding slightly is done to allow funnel loading of the fuel pellets without

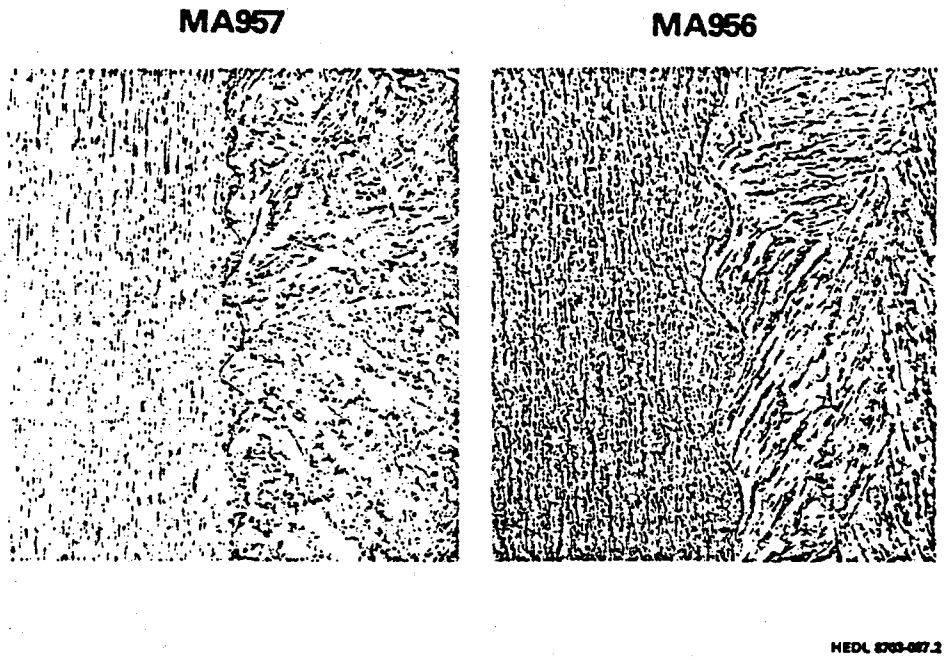

Figure 24. Sound welds in MA956 and MA957.

contamination of the inner cladding diameter, thereby eliminating a decontamination operation prior to welding). Thus some lots of tubing were flared successfully, while others fractured during the flaring operation or yielded nonuniform bonds. Some good weld results were obtained, however, on tubing which had been flared successfully. In addition, the surface condition of the inner wall was highly variable both between and within batches of tubing, necessitating the use of 600 grit paper to remove the oxide, which interfered with the development of a good bond.

It was demonstrated that successful welds could be produced with 3/8 and 3/4 inch long driver sleeves that had wall thicknesses of 0.021 inch. Thinner sleeves (0.015 inch) produced unsatisfactory welds, while thicker sleeves (0.025 inch) exhibited incipient melting at the sleeve end.

VI. MECHANICAL PROPERTIES OF UNIRRADIATED MA957

Tensile Properties

Vendor data supplied with the initial 1 inch diameter bar are shown in Figures 25 and 26 for heat DBB0111 with a comparison to AISI 316, HT9 and another ODS alloy, DT3503Y005.[4] It is evident that a significant improvement in strength was obtained with the addition of a dispersoid, although ductility decreased significantly. Figure 25 also demonstrates that an ~20% increase in yield strength was observed relative to the as-received bar in the MA957 rod drawn at WHC using an interpass anneal of 875°C. The data are given in Table 6. The increase in strength was accompanied by a concurrent loss in ductility, shown in Figure 26, from values ranging from 20 - 35% to values on the order of only 10%. The test traces on this rod revealed that the material exhibits very little work hardening, a fact which undoubtedly contributes to the difficulty of fabrication.

Table 6.
Tensile Data on Unirradiated MA957

$\dot{\epsilon} = 4.1 \times 10^{-4}$ sec^{-1}

PRODUCT FORM	TEST TEMPERATURE (°C)	YIELD STRENGTH (MPa)	ULTIMATE STRENGTH (MPa)	UNIFORM ELONGATION (%)	TOTAL ELONGATION (%)
WHC Rod (875°C anneal)	22	1236	1377	7.1	11.7
	205	1157	1259	4.4	8.4
	500	871	916	2.6	12.1
	700	402	424	2.1	10.4
WHC Rod (1050°C anneal)	22	1158	1433	6.8	11.4
	700	357	370	1.5	9.8
	22[a]	1138	1264	5.0	9.7
	22[b]	1118	1250	5.4	10.2
Production Run Tubing	100	-	-	-	-
	450[c]	432	921	18.3	25.1
	600	261	539	7.8	27.7
	750	155	316	5.9	12.4

[a]Rod heat treated additionally 15 minutes at 1100°C.
[b]Rod heat treated additionally 15 minutes at 1150°C.
[c]Possibly invalid data.

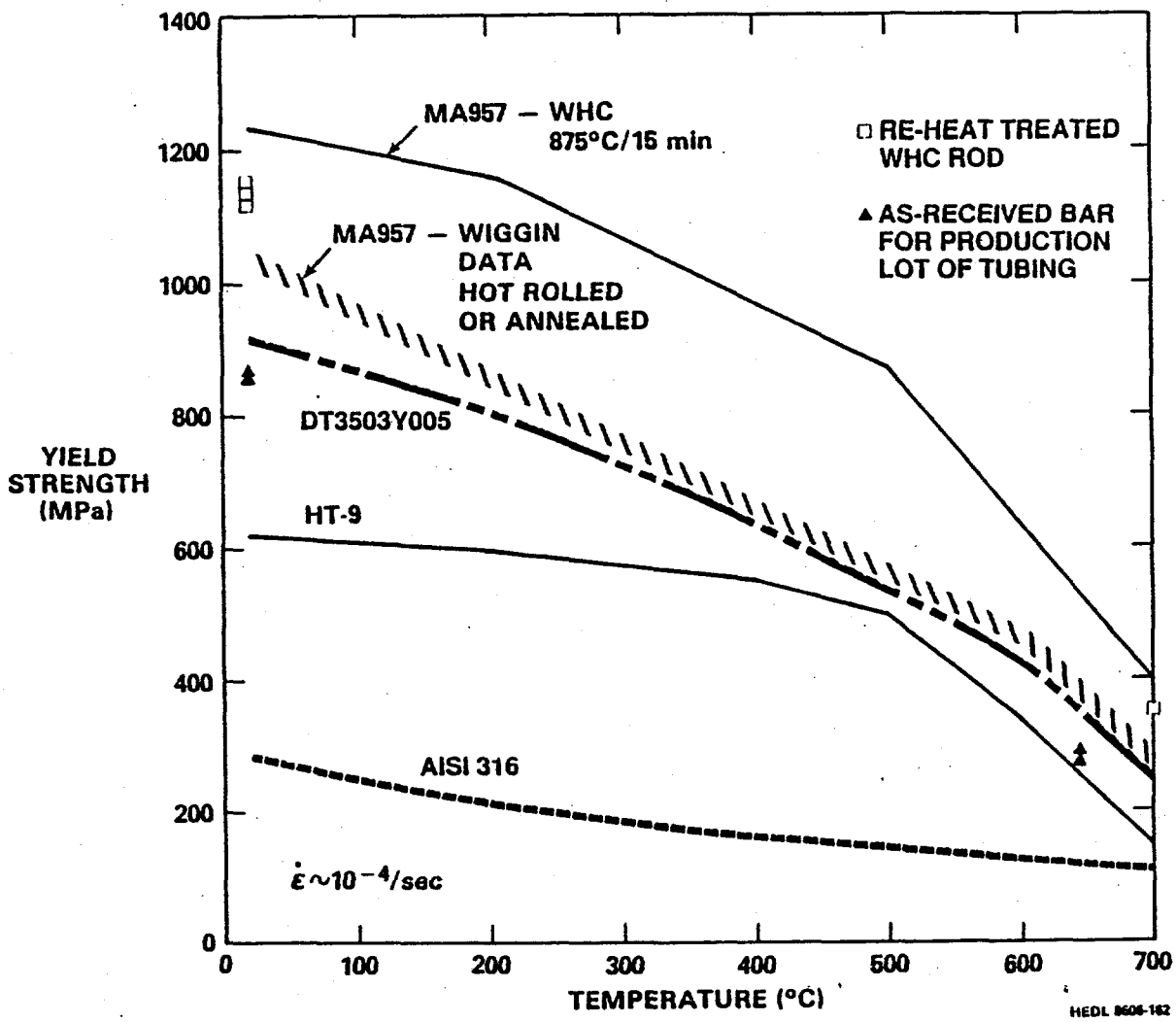

Figure 25. Yield strength of MA957.

Additional tensile tests were performed on the rod drawn at WHC using an interpass anneal of 1050°C and on specimens from this rod which were annealed at 1100 and 1150°C and exhibited some recrystallization. The data are listed in Table 6. As shown in Figures 25 and 26, the yield strength in these partially recrystallized specimens was intermediate to the properties of the as-received bar and the rod annealed at 875°C, while the ductility was the same as was observed in the 875°C rod.

Figures 25 and 26 also show the vendor data for the as-received bars from which Cartech fabricated the production run of tubing. The decrease in strength observed relative to the original as-received bars occurred because the newer heats were extruded and hot worked at 1120°C, 50°C above the temperature at which these operations were performed on the first heat, to

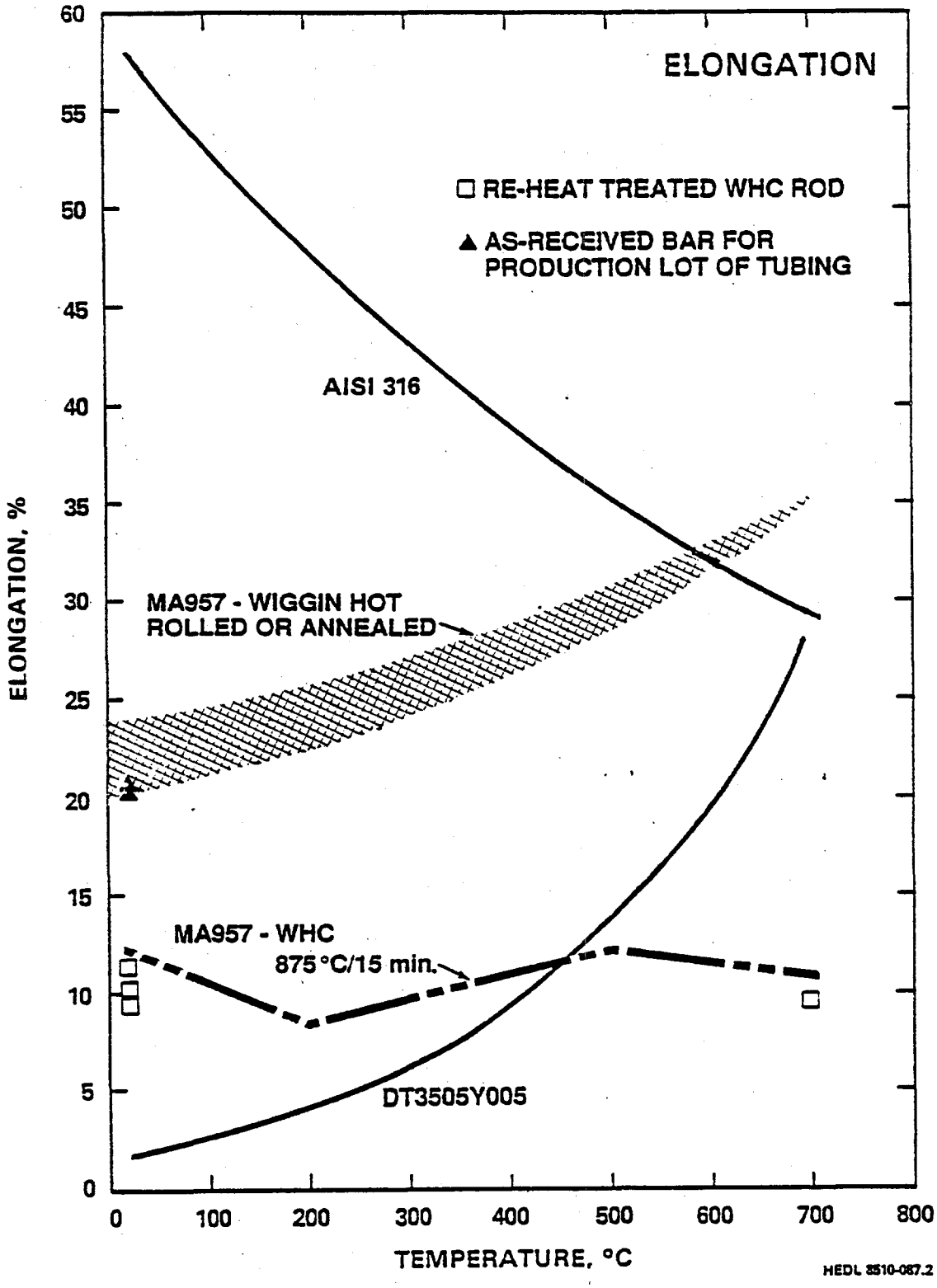

Figure 26. Ductility of MA957.

alleviate the sticking problems encountered previously. The reduction in strength was not associated with differences in composition or mechanical alloying between the heats.

Tensile tests were performed on sections of the production lot tubing having a gauge length of 1.5 inches. The data are given in Table 6 and shown in Figures 27 and 28 in comparison to data generated on other product forms of

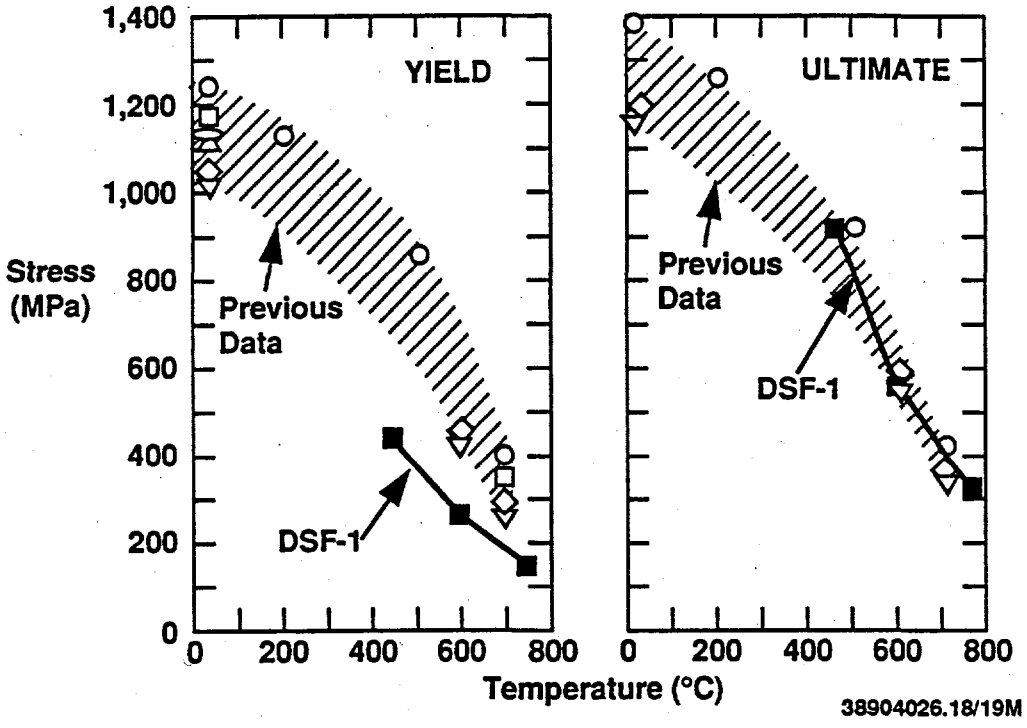

Figure 27. Yield strength (a) and ultimate strength (b) of production lot (DSF-1 experiment) of MA957.

MA957. The specimen tested at 100°C pulled out of the test fixture, providing no data at all. The trace for the specimen tested at 450°C exhibited a large amount of slippage in the test fixture. Analysis of the trace required significant adjustment to compensate for the slippage. There is therefore some question as to the validity of the data obtained on this specimen, particularly the yield strength. While the yield strength (Figure 27a) of the production lot appeared to be somewhat lower than was observed in other product forms, the ultimate strength (Figure 27b) and the total elongation (Figure 28) were consistent with previous data. The slightly lower yield strength therefore probably reflects a somewhat more effective interpass anneal than was previously achieved.

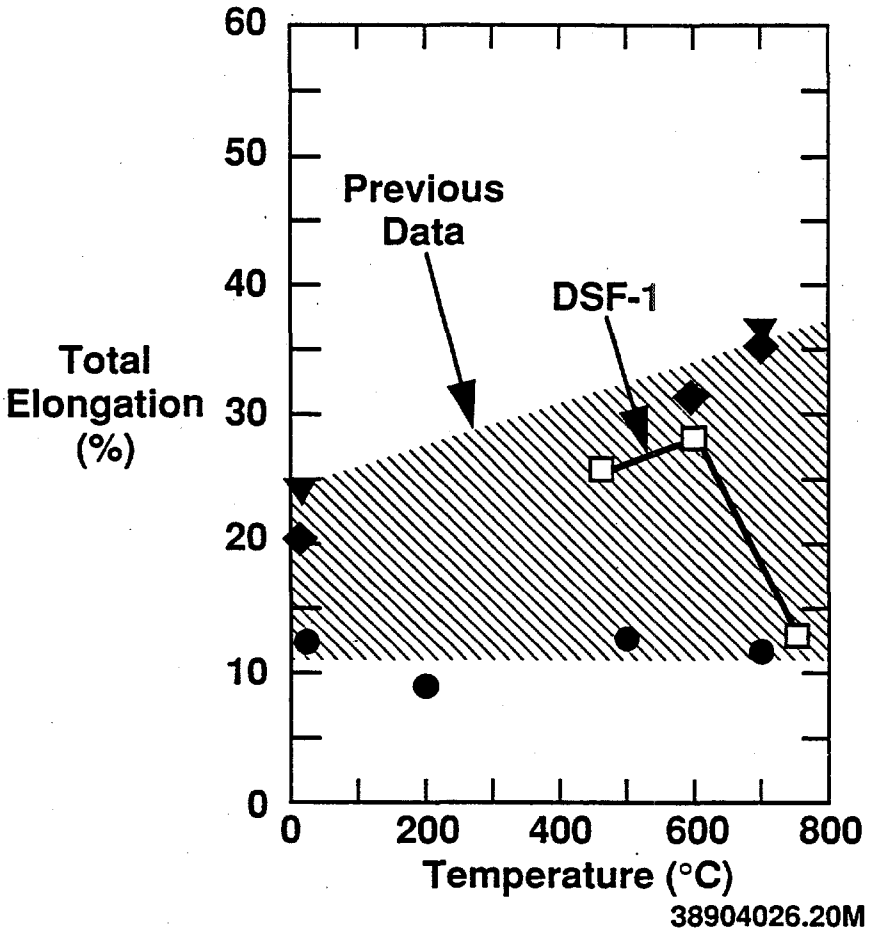

Figure 28. Ductility of production lot (DSF-1 experiment) of MA957.

Stress Rupture Behavior

Uniaxial Tests. Uniaxial stress rupture tests were performed at Koon-Hall Testing Corporation in Albany, Oregon, on rod stock of MA957 fabricated at WHC (see Table C3 in Appendix C). The initial tests were performed on material annealed at 875°C under conditions selected on the basis of the data provided in the INCO patent. The data are shown in Table 7 and Figure 29. Tests that reached 3000 hours without failure were discontinued. Uniaxial stress rupture tests were also performed on the second rod fabricated at WHC, for which the annealing temperature was increased to 1050°C. There was only sufficient time in the fiscal year for these tests to reach 1000 hours. The increase in annealing temperature produced a decrease in rupture life, although the behavior of the alloy was still significantly better than that of HT9.

Table 7.
Uniaxial Rupture Data on MA957 Rod

ANNEALING TEMPERATURE (°C)	UNIAXIAL STRESS (MPa)	TEST TEMPERATURE (°C)	RUPTURE LIFE (hrs)	MAXIMUM STRAIN (%)
875/30	360	650	>2832[a]	1.2
	345	650	>3015[a]	1.1
	320	650	786.1[b]	1.9
	270	650	>1105[a]	1.1
	350	704	136.2	NA
	>280	704	>3000[a]	0.6
	240	704	>426[a]	0.6
	185	760	>381[a]	0.6
1050/15	360	650	316.1	NA
	340	650	>840[a]	0.95
	350	704	1.7	NA
	280	704	>835[a]	0.45
	250	704	>830[a]	0.71

[a]Terminated.
[b]Failed at internal defect.

The data from the uniaxial tests indicated that MA957 was exceptionally strong, with a very strong dependence of rupture life on stress. Uniaxially the alloy appears to be at least as strong as the improved austenitic alloy D9I at temperatures ranging from 650 to 760°C. It is believed that the curve of stress versus rupture life will remain flat out to very long times instead of exhibiting the curvature typical of alloys strengthened by precipitation or cold work.

Biaxial Tests. Biaxial stress rupture tests were performed on a number of different types of MA957 tubing. This was accomplished by heating cladding specimens to elevated temperatures and applying gas (argon) loading at constant pressure. Failure times were determined from timers triggered by solenoid valves actuated by the pressure pulses associated with the release of the argon gas on rupture.

A limited number of biaxial stress rupture tests were performed at 650°C on tubing fabricated at WHC. The data are listed in Table 8 and shown graphically in Figure 30 in comparison with the uniaxial data discussed in the previous section. Despite the paucity of data, it is evident from this figure

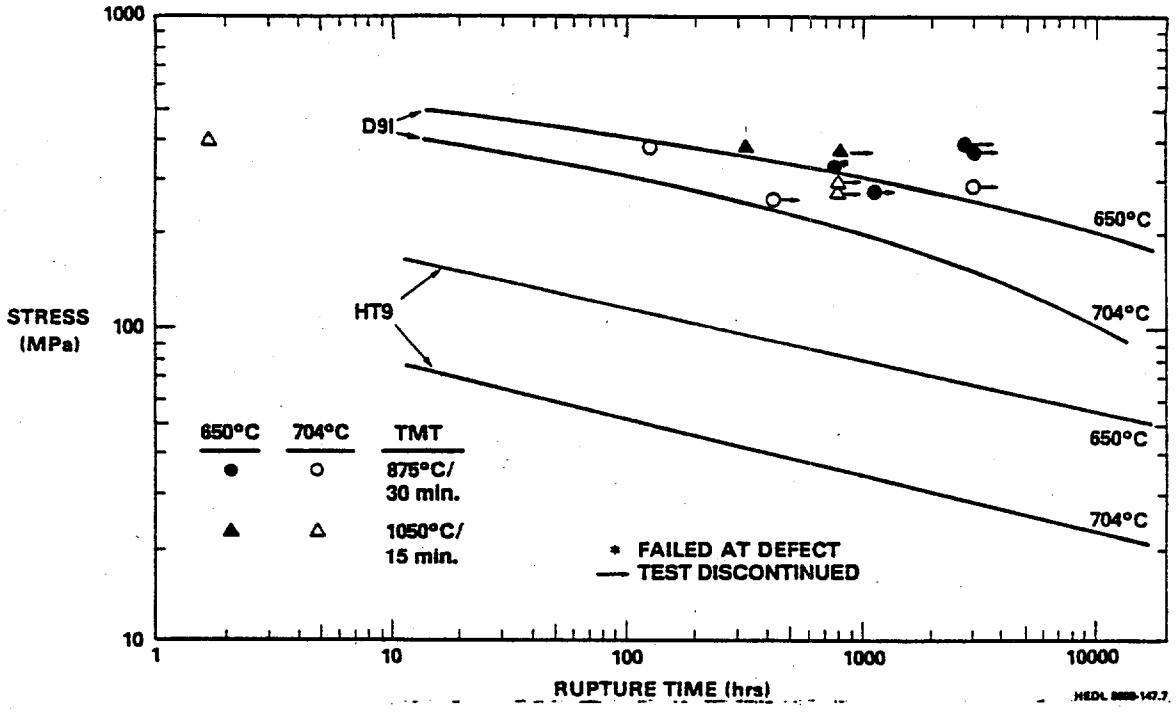

Figure 29. Uniaxial stress rupture data on MA957.

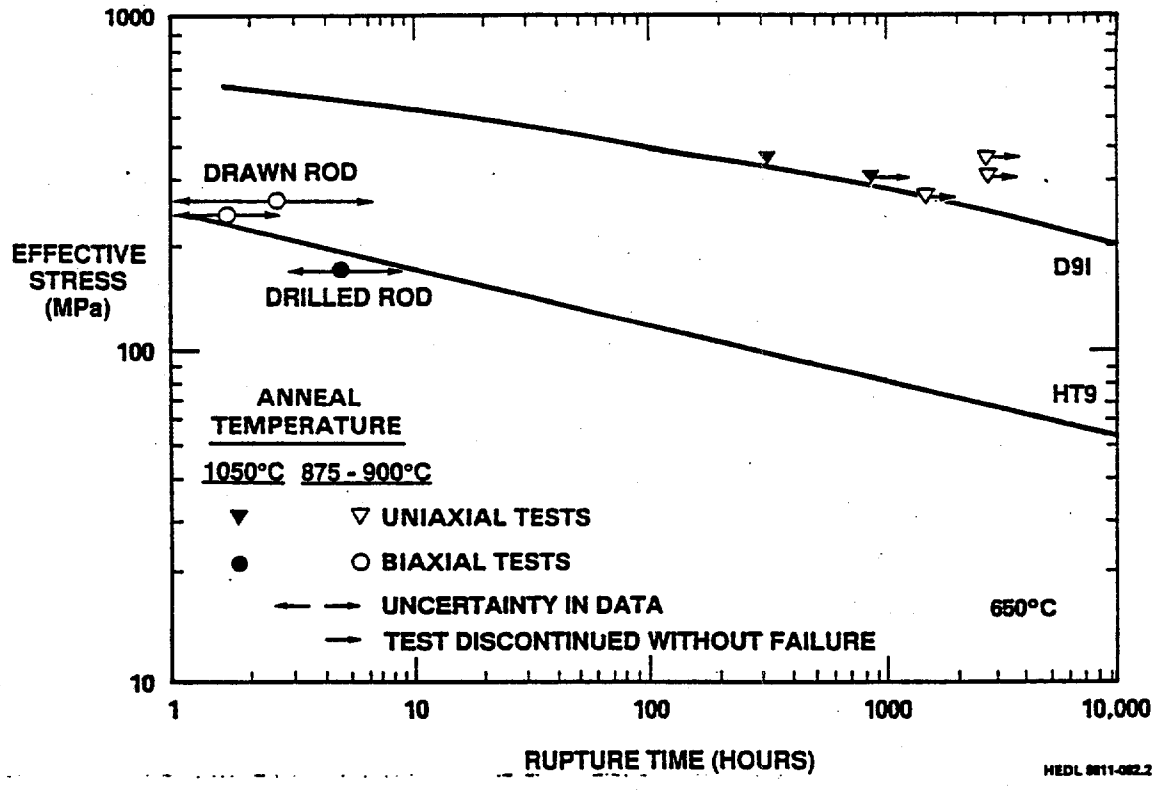

Figure 30. Comparison between uniaxial and biaxial stress rupture data on MA957.

Table 8.
Biaxial Stress Rupture Data on MA957 Tubing

CLADDING SIZE	SPECIMEN ID	TEMPERATURE (°C)	HOOP STRESS (MPa)	RUPTURE LIFE (hrs)
WHC Drawn Tubing (900°C Anneal)				
0.250 x 0.215	-	650	416	FOL[b]
	-	650	398	FOL[b]
	-	650	312 (270)[a]	1-7
	-	650	277 (240)[a]	1-3
WHC Drilled Rod (1050°C Anneal)				
0.230 x 0.200	-	650	170 (147)[a]	3-9
Developmental Lot (STC) - 900°C Anneal				
0.270 x 0.226	1	593	232	WF[c]
	13	650	150	38.9
	3	650	119	WF[c]
	19	650	100	502.7
	16	704	105	12.1 ± 7.7
	22	704	67	294.6
	5	704	52	7155.1
	17	760	57	79.5
	23	760	40	287.1
	7	760	22	23897.3
	9	800	52	25.5
	11	850	21.9	3626.5 ± 12.0
Developmental Lot (STC) - 1000°C Anneal				
0.270 x 0.226	2	593	232	WF[c]
	14	650	150	10.4
	4	650	119	WF[c]
	20	650	100	319.8
	15	704	105	12.1 ± 7.7
	21	704	67	WF[c]
	6	704	52	9375.1
	18	760	57	WF[c]
	24	760	40	471.9
	8	760	22	26583.6 ± 3.9
	10	800	52	18.5
	12	850	21.9	3194.5 ± 35.9

Table 8 (cont.)
Stress Rupture Data on MA957 Tubing

CLADDING SIZE	SPECIMEN ID	TEMPERATURE (°C)	HOOP STRESS (MPa)	RUPTURE LIFE (hrs)
Pilot Lot (Cartech)				
0.270 x 0.226	25	650	110	490.4
	26	650	100	554.7
	27	650	83	718.3 ± 20.4
	28	650	70	>16200[d]
	29	704	75	236.2
	30	704	67	429.9
	31	704	60	521.5
	32	704	53	3316.0
	33	760	50	212.8
	34	760	40	1038.7 ± 36.6
	35	760	34	5615.6 ± 12.0
	36	760	31	4418.9
	37	800	36	237.7
	38	800	32	943.5 ± 11.9
	39	800	30	973.2 ± 36.6
	40	800	28	2311.4
Production Lot (Cartech) - 'Undefected'				
0.270 x 0.226	41	650	120	78.9 ± 32.3
	42	650	105	131.4
	43	650	93	1394.8
	44	650	88	1938.9
	45	704	79	263.6 ± 42.7
	46	704	68	508.1
	47	704	62	1281.6 ± 3.5
	48	704	58	2027.2
Production Lot (Cartech) - 'Defected'				
0.270 x 0.226	49	650	120	78.9 ± 32.3
	50	650	105	585.8
	51	650	93	1113.6
	52	650	88	1761.6
	53	704	79	259.2 ± 42.7
	54	704	68	888.6
	55	704	62	807.4
	56	704	58	1277.3

Table 8 (cont.)
Stress Rupture Data on MA957 Tubing

CLADDING SIZE	SPECIMEN ID	TEMPERATURE (°C)	HOOP STRESS (MPa)	RUPTURE LIFE (hrs)
STC - ORT Lot				
0.2953 x 0.2638	57	650	120	147.1
	58	650	104	263.8
	63	650	89	1948.9
	64	650	77	6143.8
	59	704	79	189.0
	60	704	69	2301.0
	65	704	59	5625.2
	66	704	51	>9600[d]
	61	760	54	745.0
	62	760	47	1419.1
	67	760	40	>9400[d]
	68	760	35	6706.8
PNC MA957				
0.2953 x 0.2638	69	650	120	22.5 ± 12
	75	650	104	67.9 ± 30
	70	650	89	193.5 ± 12
	76	650	77	357.0
	71	704	79	88.6 ± 12
	77	704	69	159.7
	72	704	59	231.6
	78	704	51	>2700[d]
	73	760	54	92.8 ± 12
	79	760	47	862.7 ± 12
	74	760	40	1032.9 ± 30
	80	760	35	>2500[d]

Table 8 (cont.)
Stress Rupture Data on MA957 Tubing

CLADDING SIZE	SPECIMEN ID	TEMPERATURE (°C)	HOOP STRESS (MPa)	RUPTURE LIFE (hrs)
STC - Tube Reduction Lot				
0.268 x 0.223	81	650	120	1455.1 ± 8
	82	650	104	427.1 ± 10
	83	650	89	1196.3 ± 3
	84	650	77	>2800[d]
	85	704	79	434.8
	86	704	69	822.4
	87	704	59	2347.0
	88	704	51	>2600[d]
	89	760	54	245.8 ± 12
	90	760	47	628.7
	91	760	40	413.9
	92	760	35	>2700[d]

[a]Effective stress given in parentheses for comparison with uniaxial data.
[b]FOL = failed on loading.
[c]WF = weld failure.
[d]Ongoing.

that the alloy is significantly stronger uniaxially than biaxially. This is due to the elongated nature of the grain structure and is commonly observed in such microstructures.

Table 8 also lists the biaxial stress rupture data obtained on the developmental tubing (annealed at 900 or 1000°C) produced by STC and the pilot lot of tubing produced by Cartech. These data are plotted in Figure 31. Stress rupture tests on the developmental lots of tubing produced by STC demonstrated that MA957 had reasonable high temperature strength, with a rupture life that was at least an order of magnitude stronger than HT9 at 704 and 760°C and that was somewhat inferior to HT9 at lower temperatures. No dependence on annealing temperature was observed. Similar results were obtained on the pilot lot of tubing produced by Cartech.

The data in Figure 31 were fit by regression to equations based on the Dorn Parameter, the Larson-Miller Parameter, and an equation of state approach. The best fit was obtained with the equation based on the Dorn Parameter given on the next page. Figure 31 includes a plot of the Dorn Parameter equation at the temperatures for which data exist:

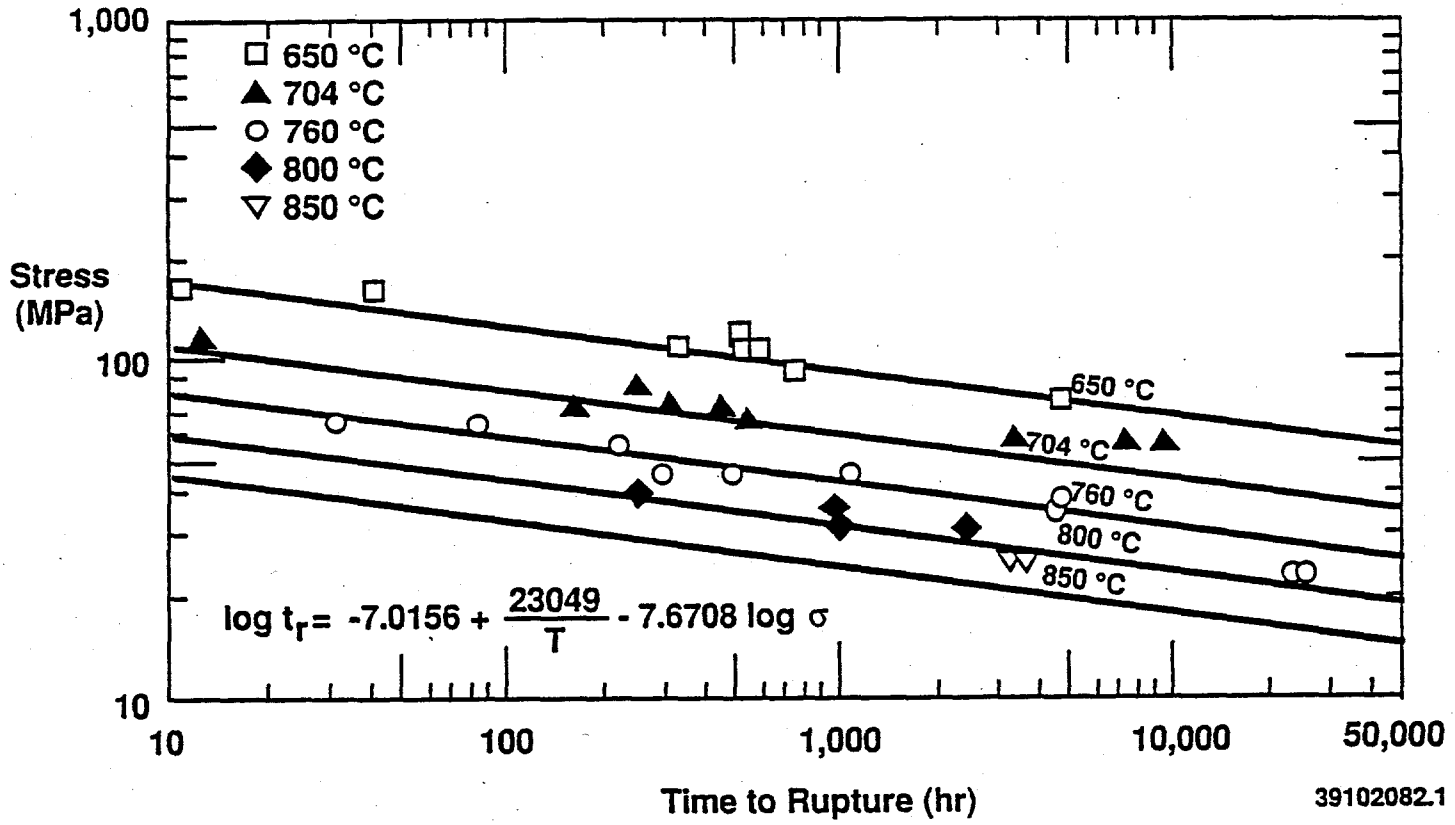

Figure 31. Predictions of Dorn Parameter equation and data on which regression analysis was based.

$$\log_{10} t_r = -7.0156 + 23049/T - 7.6708\log_{10} \sigma$$

where t_r is the time to rupture in hours, T is the test temperature in K and σ is the hoop stress in MPa. The value of r^2 for the regression on this equation was 0.913, with a standard error of the estimate of 0.259. The standard error on the 1/T coefficient was 1580 and the standard error on the $\log_{10} \sigma$ coefficient was 0.430. The correlation and data are shown in the form of a Dorn Parameter plot in Figure 32, where the parameter plotted on the x axis is $\log_{10} t_r$ - 23049/T.

Biaxial stress rupture tests were performed at 650 and 704°C on both 'defected' and 'undefected' sections of the first straightened segment of the production run of tubing at Cartech. 'Defected' specimens were sectioned from tubing at the location of the strongest indications on the ultrasonic traces (see Figure 22). The data are listed in Table 8 and plotted in Figure 33 with

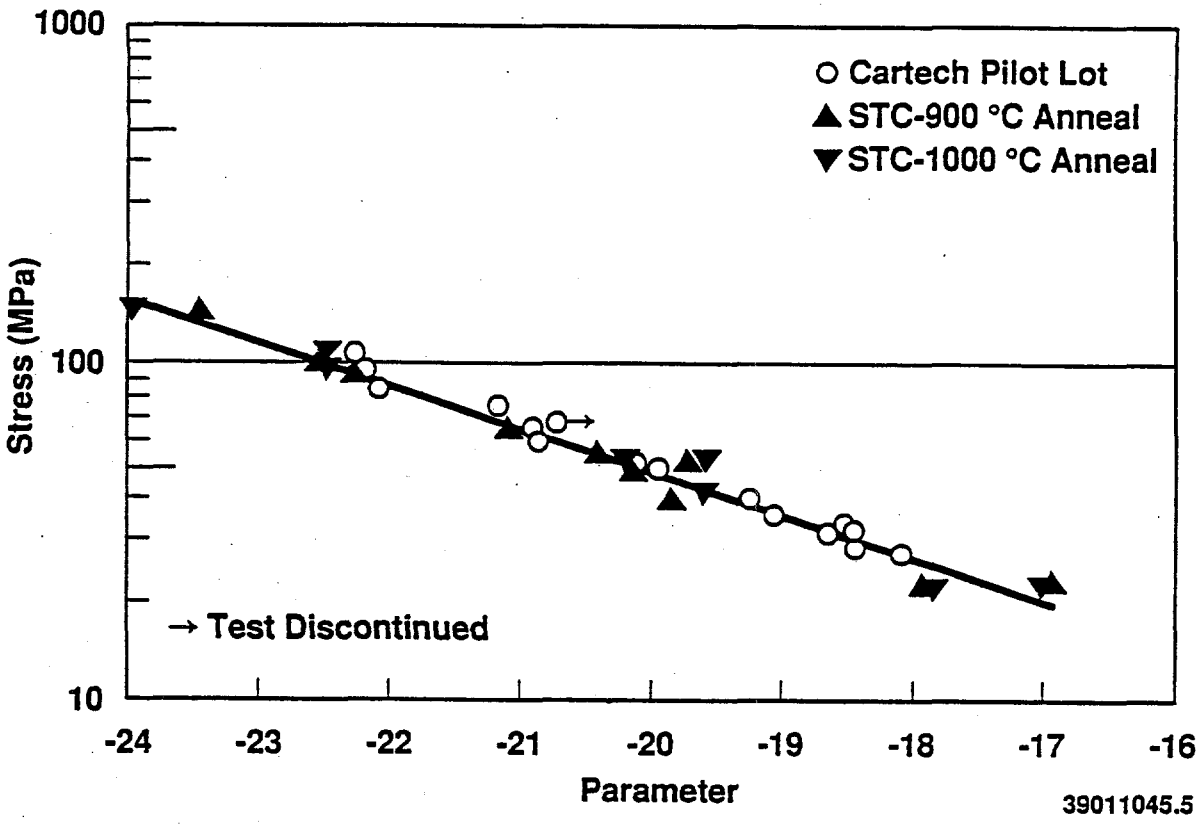

Figure 32. Dorn Parameter plot for MA957 stress rupture data.

the Dorn Parameter equation described earlier. The data on both 'good' and 'defected' specimens of the production lot were consistent with the equation at both test temperatures and there was no apparent difference between the 'good' and the 'defected' tubing. Scanning electron microscopy performed on selected 'defected' ruptured specimens revealed that failure was associated with long cracks on both the inside and outside surfaces. One example of this is given in Figure 34.

Stress rupture data obtained on other types of MA957 tubing are also given in Table 8. These include the production run made by STC for the ORT experiment (referred to as STC ORT), the tubing produced by PNC, and the tubing made by STC using an alternate tube reduction technique (referred to as STC TR). These data are compared to the predictions of the Dorn Parameter equation in Figures 35 and 36, where log σ is plotted as a function of $\log_{10} t_r$ in Figure 35 and as a function of the parameter $\log_{10} t_r$ - 23409/T in Figure 36. It is evident from these figures that the STC ORT tubing is somewhat superior to the equation predictions at longer rupture times or higher temperatures, while the STC TR tubing data coincide a little more closely with the equation predictions. Both forms of STC tubing, however, appear stronger than the PNC tubing, particularly at lower temperatures or shorter rupture lives. Since the slope of the line that would coincide with the PNC data is slightly lower than that of any of the other data sets, the PNC data suggest that for the

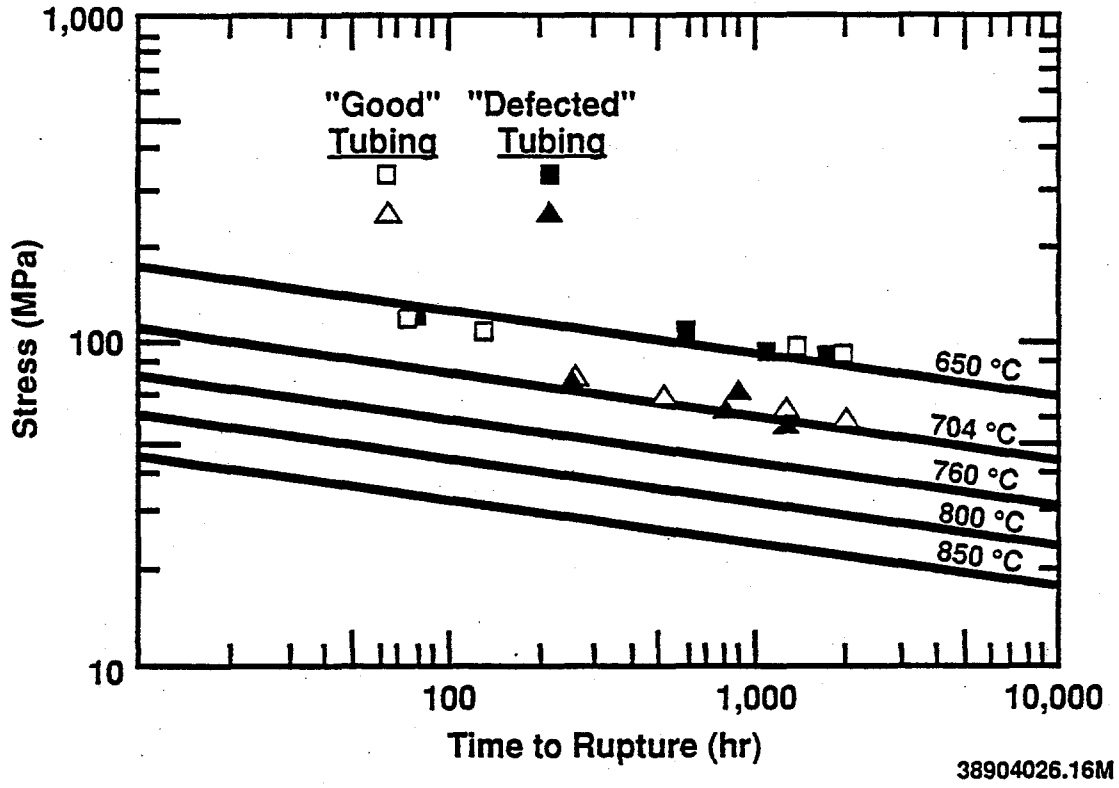

Figure 33. Stress rupture data on 'good' and 'defected' segments of the production run tubing fabricated by Cartech compared to the predictions of the Dorn Parameter regression equation.

longest lifetimes or highest temperatures the PNC tubing might be slightly stronger than the STC tubing. These results are consistent with microscopy observations that the dispersoid in the U.S. product is more stable and more uniformly distributed than that of the Japanese product.

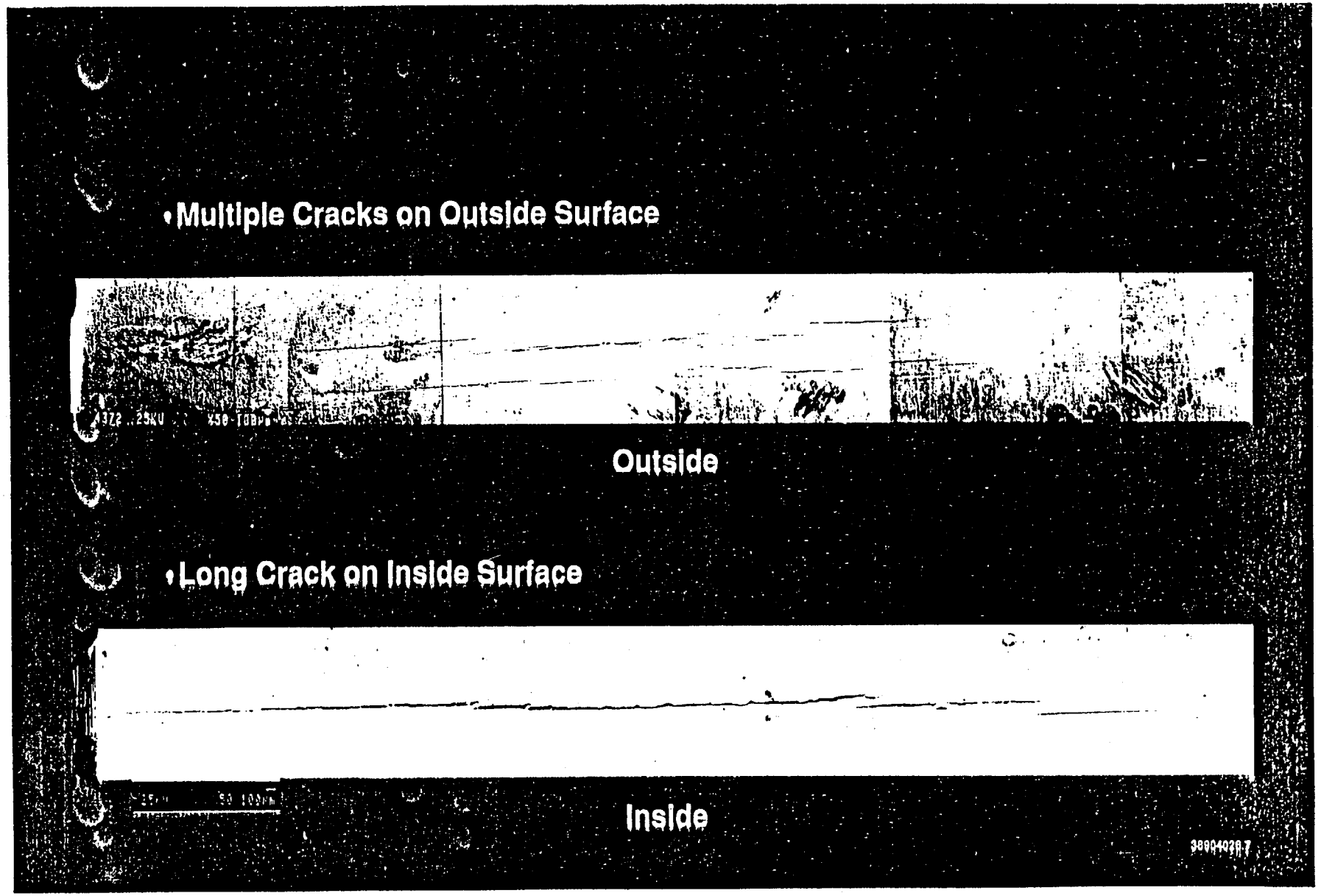

Figure 34. Cracks on inner and outer surfaces of stress rupture sample from production lot of tubing.

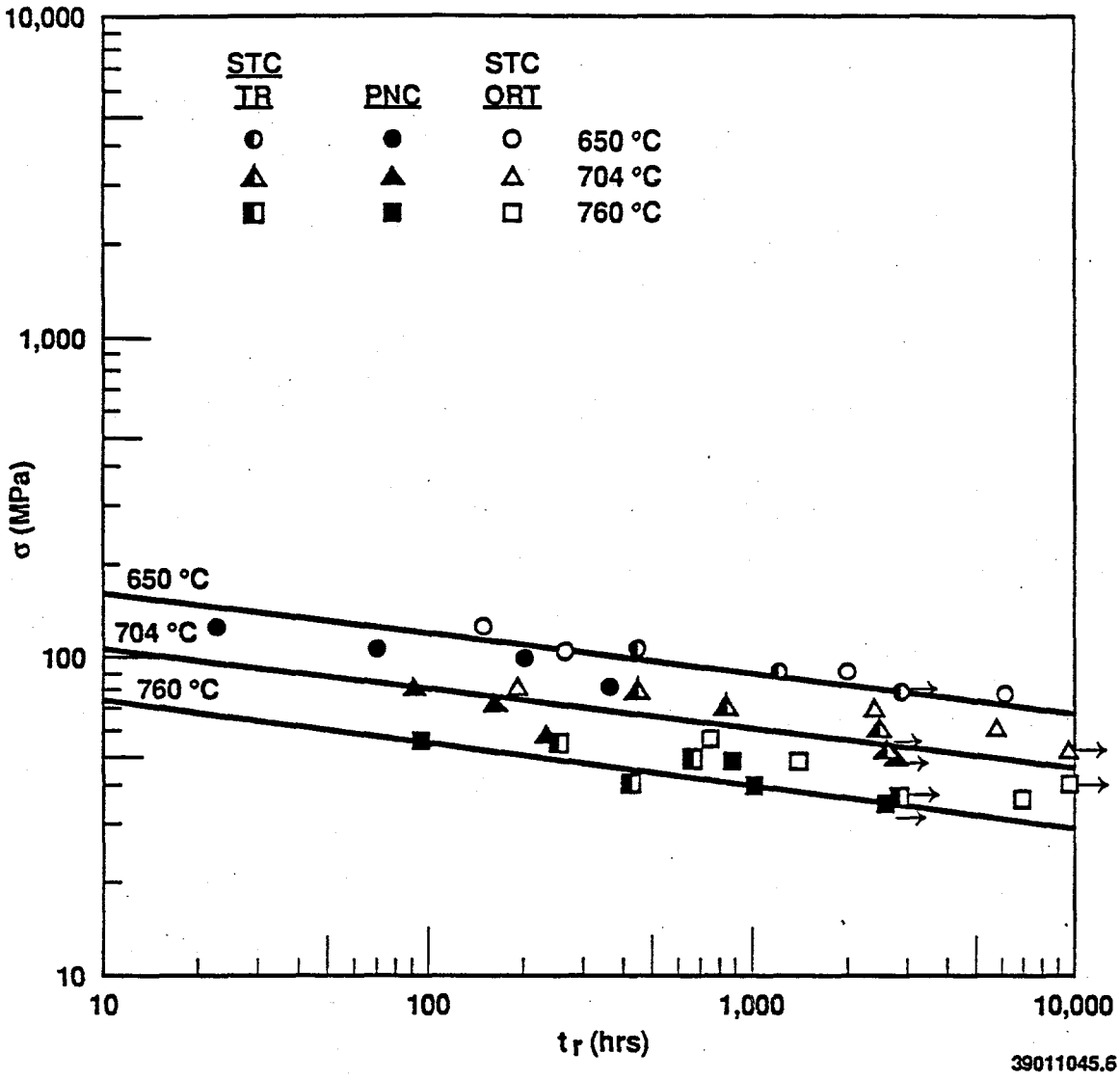

Figure 35. Stress rupture data on PNC, STC ORT and STC TR MA957 tubing.

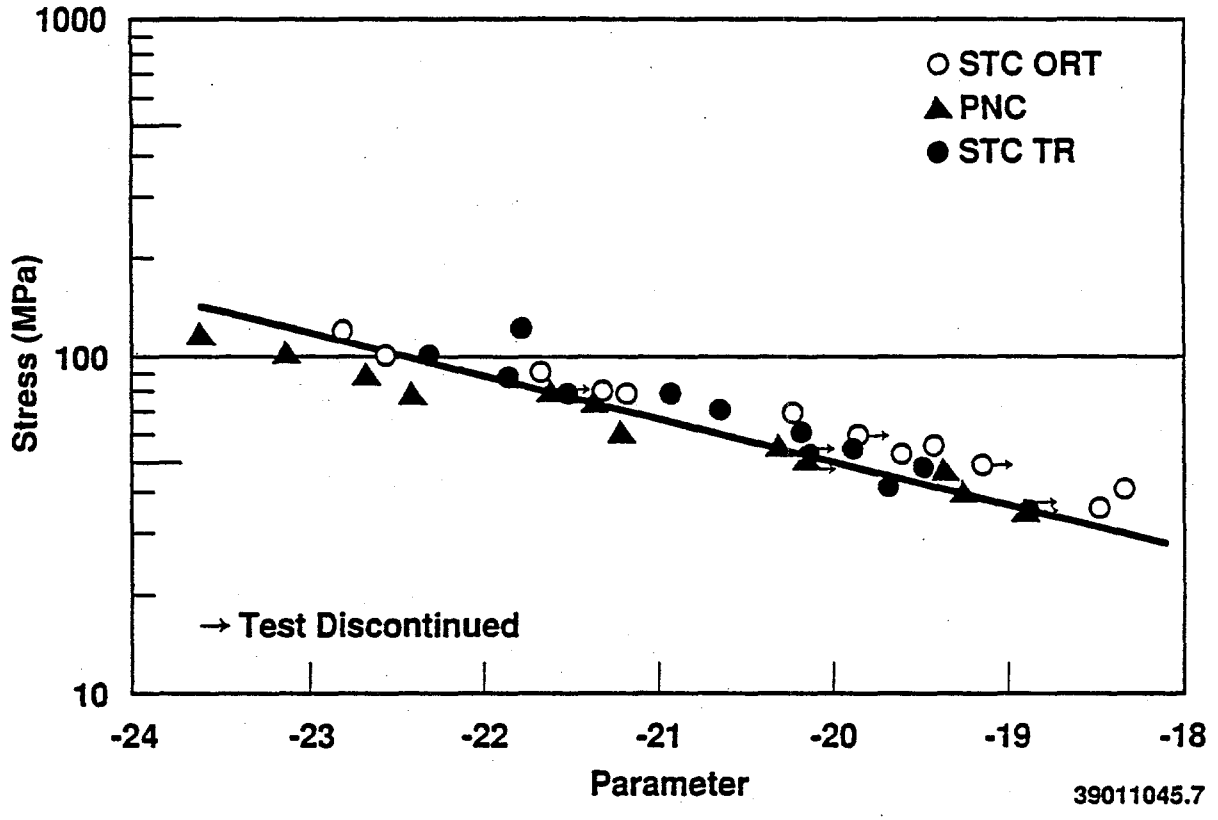

Figure 36. Dorn Parameter representation of PNC, STC ORT and STC TR stress rupture data.

Transient Burst Tests. Transient burst tests were performed on both types of developmental tubing produced by STC (900°C anneal, 1000°C anneal). The data are given in Table 9. The behavior of the two types of tubing was identical and was essentially the same as that of HT9 (Figure 37). This short term similarity in strength is consistent with the similarity observed in short term stress rupture tests. The significant improvement in strength of MA957 over HT9 is only observed at higher temperatures or longer times. Figure 37 also shows that the short term burst tests (done to verify the weld procedures for stress rupture testing) yielded data comparable to the transient data. Failure strains from the transient tests are shown in Figure 38. The failure strains in the specimen center, where all failures occurred, were in excess of about 25%, a result which is also consistent with the results obtained on HT9.

Table 9.
Transient Burst Test Data on Unirradiated MA957 Tubing

SPECIMEN ID	ANNEAL TEMP. (°C)	HEATING RATE (°C/s)	TEST PRESSURE (psi)	HOOP STRESS (MPa)	FAILURE TEMP. (°C)	FAILURE TEMP. (°F)	UNIFORM STR. (%)[a]	PLASTIC STR. (%)[a]	MAX. PROF. STR. (%)[a]
MA9B1.URR	900	5.6	4000	163.5	1530	832	7.4	14.0	37.1
MA9B2.URR	900	5.6	2050	83.8	1814	990	7.8	11.3	29.6
MA9B3.URR	900	5.6	8450	345.4	1310	710	3.7	14.4	42.9
MA9B4.URR	900	5.6	11200	457.9	1232	667	2.6	14.5	35.2
MA9A1.URR	1000	5.6	11350	464.0	1243	673	2.8	14.4	37.0
MA9A2.URR	1000	5.6	8650	353.6	1303	706	4.8	14.3	39.8
MA9A3.URR	1000	5.6	2100	85.9	1833	1001	7.9	10.7	27.8
MA9A4.URR	1000	5.6	4180	170.9	1536	836	6.8	14.3	49.6

[a]Uniform, plastic and maximum profile strains.

Impact Behavior

Impact tests were performed on 1/3 size Charpy samples of unirradiated MA957 in three different orientations. Specimens in the C-R and L-R orientations were fabricated from as-received bar stock. Specimens in the T-S orientation were fabricated from 15% cold worked sheet. All specimens were given a final anneal at 900°C for 15 minutes. The data are listed in Table 10 and plotted in Figure 39. Absorbed energy was normalized to the area of the uncracked ligament.

The ductile brittle transition temperature (DBTT) of the as-received bar in the C-R orientation was on the order of 100°C, with an upper shelf energy (USE) of only ~3 J/cm². In this orientation the long axis of the specimen is parallel to the diameter of the bar and the direction of crack propagation is radially through the bar, with the alumina stringers oriented parallel to the direction of crack propagation. The transition behavior of rolled and heat treated sheet tested in the same orientation (T-S) was similar. As-received bar in the L-R orientation, however, exhibits significantly better transition behavior, with a DBTT no higher than room temperature and a USE on the order of 30 J/cm², comparable to that of HT9. In the L-R orientation the long axis of the specimen is parallel to the long axis of the bar, with crack propagation perpendicular to the alumina stringers.

Fractography on the Charpy specimens in the CR orientation revealed that lower shelf failure was primarily by cleavage but that ductile rupture prevailed on the upper shelf, even though the difference in absorbed energy was only ~2 J/cm². The scale of the structure on the lower shelf is on the order of

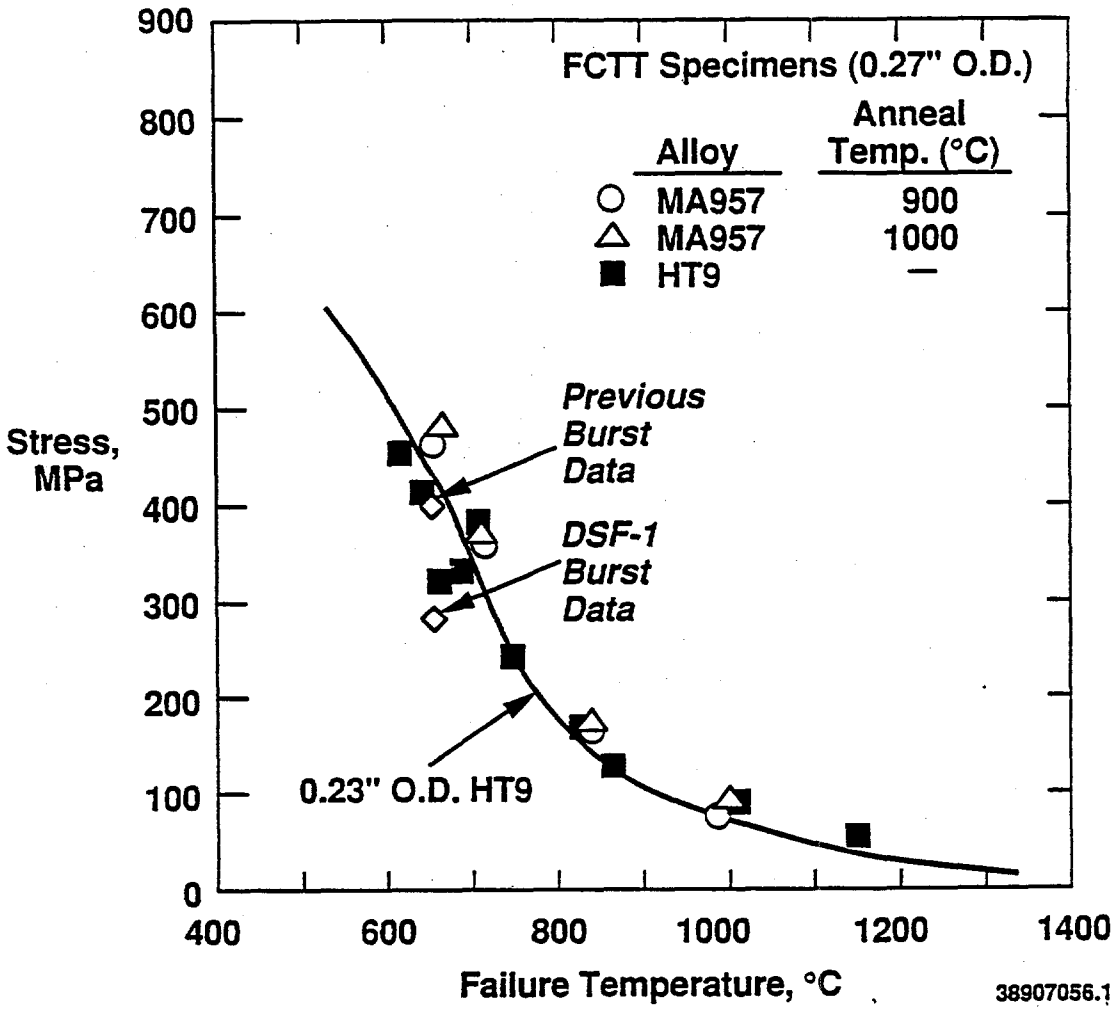

Figure 37. Transient test results on MA957.

10 μm, or 10 to 20 times the size of the subgrain structure. It is therefore believed that the low DBTT and USE are due not to the highly elongated grain structure but to the alumina stringers. Presumably the transition behavior would be improved significantly in the C-R orientation if the stringers were not present.

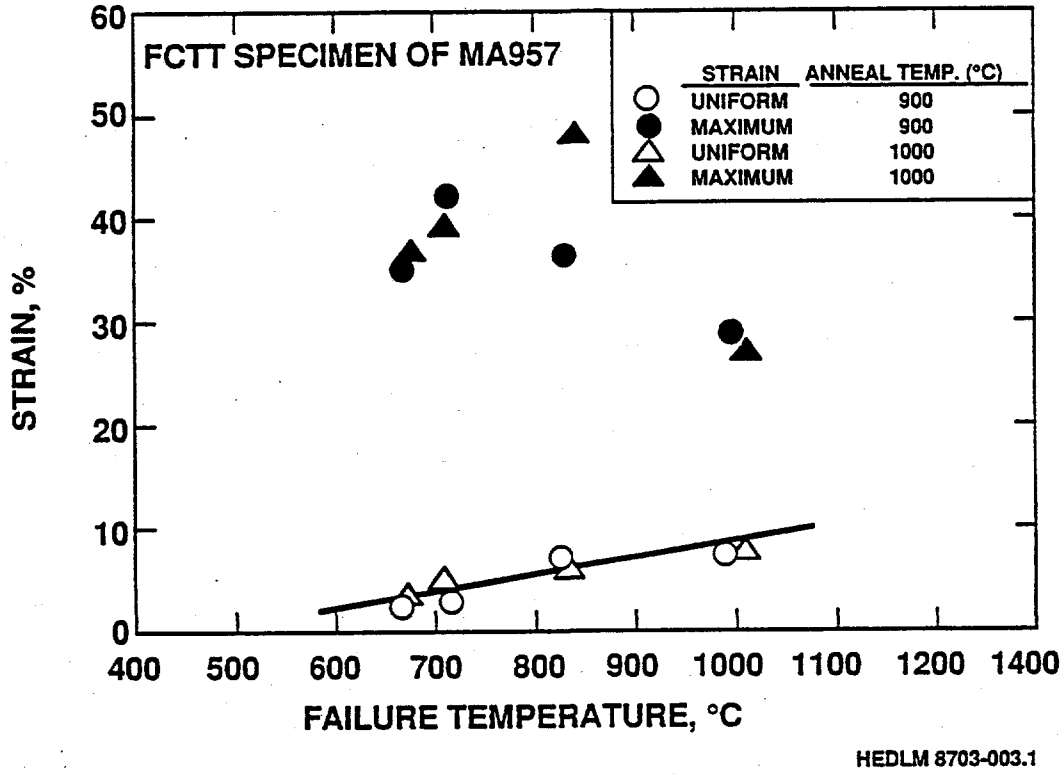

Figure 38. Strain data from transient tests on MA957.

Table 10.
Charpy Impact Data on Unirradiated MA957

ORIENTATION	SPECIMEN ID CODE	TEST TEMPERATURE (°C)	MAXIMUM LOAD (kN)	ENERGY PER UNIT AREA (J/cm²)
C-R	ET10	22	0.3045	0.7910
	ET16	50	0.4396	1.1216
	ET11	100	0.5177	2.4354
	ET12	130	0.5759	2.7079
	ET13	170	0.5698	3.6701
	ET14	220	0.4974	3.4397
	ET15	300	0.4234	3.0675
T-S	EP06	22	0.7142	1.5160
	EP07	200	0.6348	1.6518
L-R	ER02	22	0.8609	NA
	ER04	22	0.8712	32.1724
	ER03	70	0.8132	25.3918

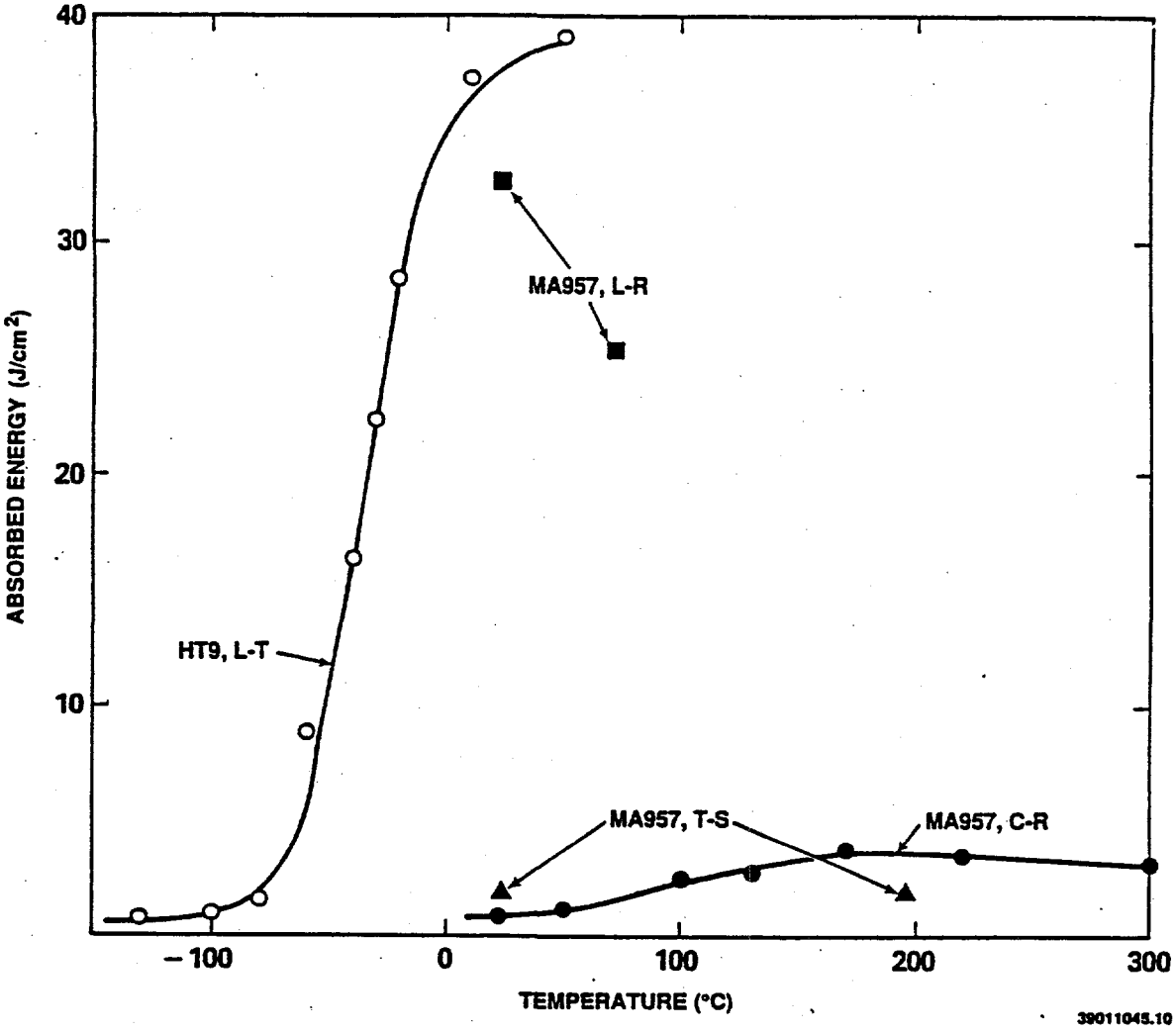

Figure 39. Fracture energy in 1/3 size precracked Charpy impact specimens of MA957.

VII. EFFECT OF IRRADIATION ON MECHANICAL PROPERTIES

Tensile Behavior

Tensile specimens were made from sheet stock in the same condition as the T-S Charpy specimens, annealed at 900°C for 15 minutes after 15% cold work. They were irradiated in MOTA 1E at five temperatures ranging from 410 to 730°C to a fluence ranging from 4.5 - 7.3 x 10^{22} n/cm² (E > 0.1 MeV). The dimensions of the gauge section were 0.060 x 0.030 x 0.8 inches. Tests were performed at an initial strain rate of 4.1 x 10^{-4} /sec at the irradiation temperature, the nominal fuel handling temperature (205°C) or at 110°C above the irradiation temperature. The tensile data are given in Table 11 and plotted in Figures 40 through 42. The figures include data for comparison on specimens annealed at 875°C presented in the previous section.

Table 11.
Tensile Data on Irradiated MA957

$\dot{\varepsilon} = 4.1 \times 10^{-4}$ sec^{-1}

SPEC. ID	IRR. TEMP. (°C)	FAST FLUENCE (10^{22} n/cm^2)	TEST TEMP. (°C)	YIELD STRENGTH (MPa)	ULTIMATE STRENGTH (MPa)	UNIFORM STRAIN (%)	TOTAL STRAIN (%)
CONTROLS							
ET25	-	-	410	945	1016	2.1	4.3
ET26	-	-	650	357	402	4.2	18.7
T_T = 205°C							
ET04	410	7.3	205	1042	1428	0.6	3.0
ET19	650	7.4	205	1116	1188	2.4	4.3
$T_T = T_i$							
ET03	410	7.3	410	1223	1237	0.7	2.7
ET08	470	4.7	470	1053	1058	0.4	3.8
ET13	540	6.8	540	791	820	0.9	9.2
ET18	650	6.8	650	444	468	0.8	10.5
ET22	730	4.5	730	342	362	1.2	5.7
$T_T = T_i$ + 110°C							
ET09	470	4.7	580	800	803	0.4	8.5
ET14	540	7.4	650	553	560	0.8	8.2
ET23[a]	730	4.5	800	267	313	1.6	4.7

[a] $T_T = T_i$ + 70°C.

It is evident from Figures 40 and 42 that the behavior of the material is the same in the unirradiated condition for anneals at 875 and 900°C, as expected. Very little change in yield strength was observed in the irradiated specimens for test or irradiation temperatures above about 500°C. A 20% hardening was observed in low temperature tests performed on specimens irradiated at low temperature (410°C), resulting in a yield strength of 1400 MPa at 205°C. The strength of the material exhibits the same temperature dependence before and after irradiation.

Total elongation, shown in Figure 42, is degraded somewhat by irradiation, ranging from about 3 to 10% at the current exposure as compared to a constant 10% prior to irradiation. The unirradiated sheet specimens (900°C anneal) exhibited much more variability in ductility determinations than the cylindrical specimens (875°C anneal), as might be expected.

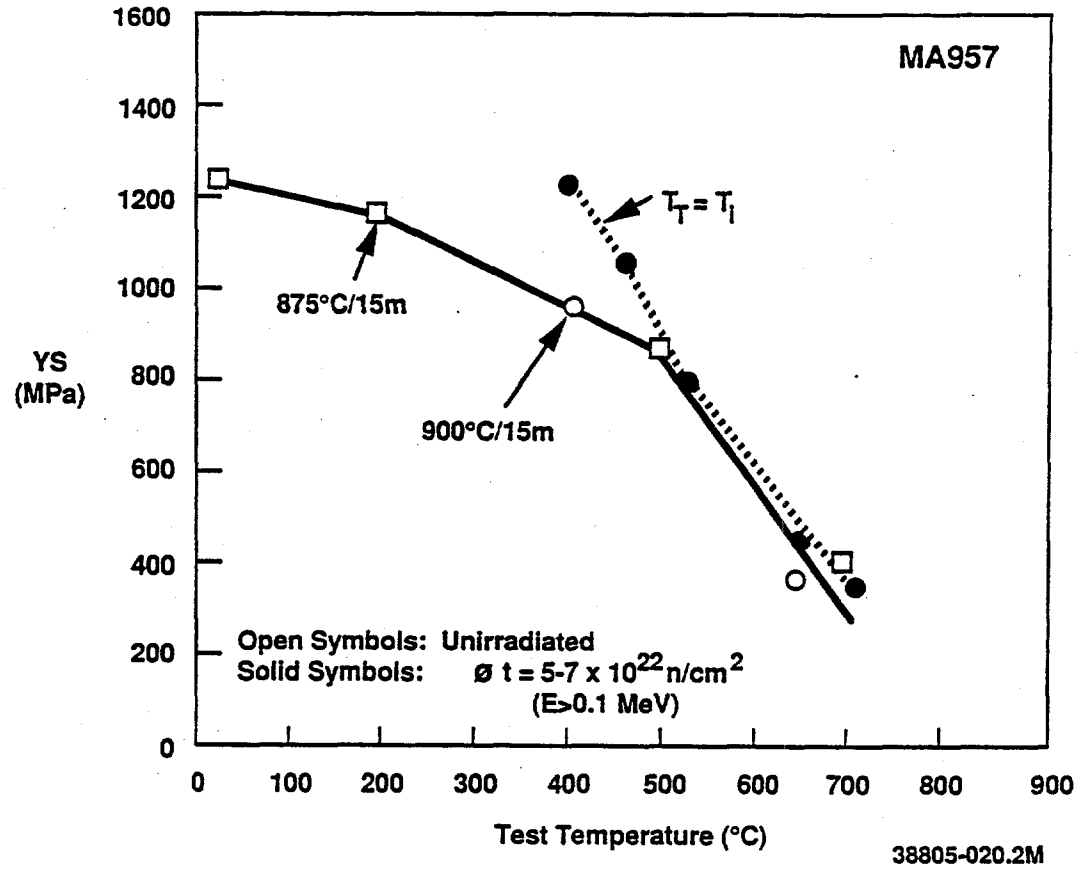

Figure 40. Yield strength of irradiated MA957 tested at the irradiation temperature.

Impact Behavior

Fourteen 1/3 size Charpy specimens were irradiated in MOTA 1E, nine from the as-received bar stock in the C-R orientation and five from the rolled and heat treated sheet stock in the T-S orientation. The C-R specimens were irradiated at 410 and 540°C. The T-S specimens were irradiated only at 410°C. The fluences accumulated at 410 and 540°C were 7.6 - 8.2 x 10^{22} n/cm² and 6.5 - 7.0 x 10^{22} n/cm² (E > 0.1 MeV), respectively. No specimens in the L-R orientation were irradiated. The impact data are given in Table 12 and plotted in Figure 43.

Irradiation at 410°C produced a large increase in DBTT. The data suggest that the DBTT of the C-R specimens was in excess of 350°C, while that of the T-S specimens was on the order of 325°C. Irradiation at 540°C caused a smaller increase in DBTT, to ~200°C, accompanied by an increase in the width (i.e., the temperature range) spanned by the transition region. No change in USE was evident in any of the three irradiation conditions.

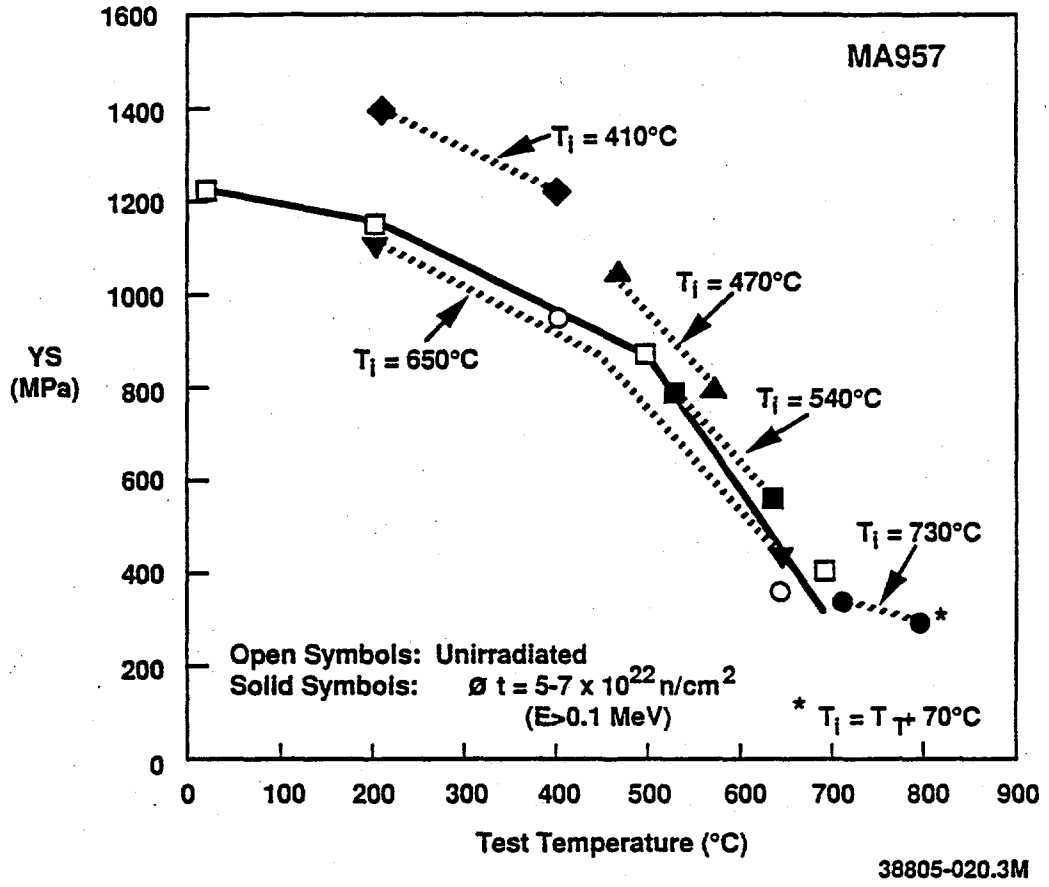

Figure 41. Yield strength of MA957 for tests performed at various temperatures relative to the irradiation temperature.

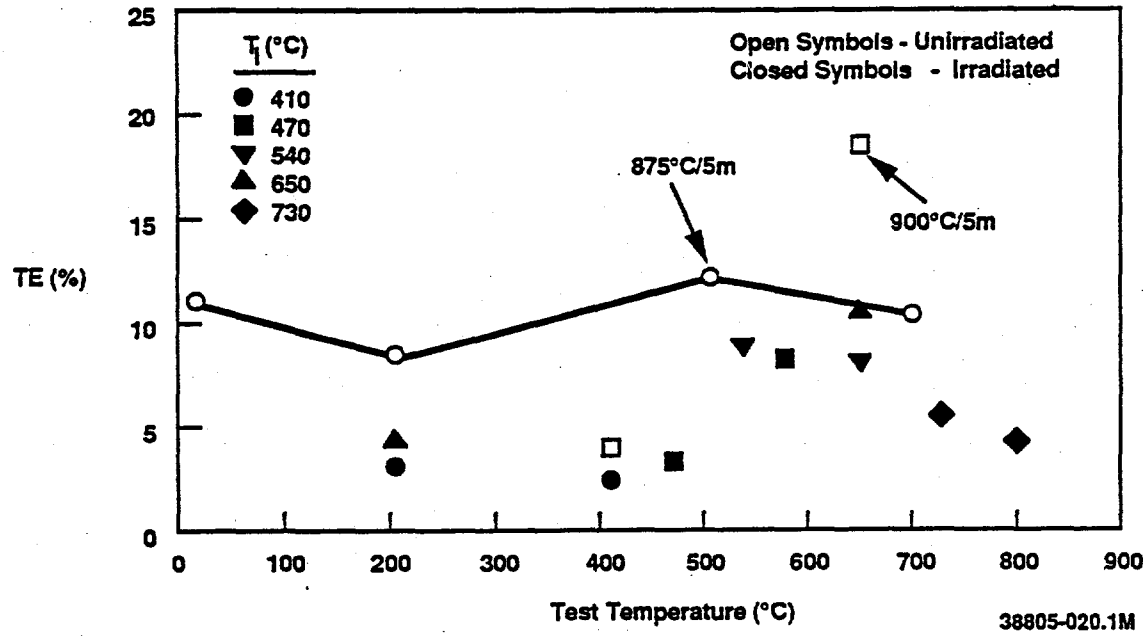

Figure 42. Total elongation in irradiated MA957.

Table 12.
Charpy Impact Data on Irradiated MA957

ORIENTATION	SPECIMEN ID CODE	IRRADIATION TEMPERATURE (°C)	TEST TEMPERATURE (°C)	MAXIMUM LOAD (kN)	ENERGY PER UNIT AREA (J/cm²)
T-S	EP01	410	270	0.0462	0.7363
	EP02	410	300	0.0569	0.9592
	EP03	410	325	0.0631	1.1217
	EP04	410	350	0.1003	1.3446
	EP05	410	395	0.1139	1.4647
C-R	ET01	410	200	LOST DATA	
	ET04	410	300	0.0523	0.7025
	ET02	410	350	0.0992	0.8261
	ET03	410	393	LOST DATA	
	ET05	410	395	0.4433	0.7898
C-R	ET09	540	90	0.0687	0.8691
	ET07	540	150	0.1098	1.3214
	ET06	540	200	0.1647	1.7074
	ET08	540	300	0.2489	2.3630

In-Reactor Creep Behavior

In-reactor creep and stress rupture were determined over a wide range of temperature and irradiation exposure using 1 inch long pressurized tube specimens irradiated in the Materials Open Test Assembly (MOTA). Specimens inserted into MOTA 1E were fabricated by gun drilling lengths of rod reduced at WHC to a diameter of 0.250 inches using interpass anneals of 1050°C, as described in Section IV above. The final annealing treatment for the gun drilled specimens was 760°C/30m/AC. Additional specimens obtained from tubing produced by STC were inserted into MOTA 1F. The final dimensions of the gun drilled specimens were 0.230 inches x 0.200 inches (5.84 mm x 5.08 mm). The final dimensions of the STC cladding specimens were 0.270 inches x 0.226 inches (6.86 mm x 5.74 mm). The desired stress levels were obtained by pressurizing the specimens to a predetermined level based on specimen geometry and the target irradiation temperature. Strain values were calculated from pre- and post-irradiation measurements of specimens diameters.

MOTA 1E was irradiated in the Fast Flux Test Facility (FFTF) during cycles 9A through 9C, accumulating 341.8 effective full power days (EFPD). Based on reactor physics calculations made for cycle 9A, the specimens' peak exposure in MOTA 1E was nominally 8.3 x 10^{22} n/cm² (E > 0.1 MeV). MOTA 1F was irradiated during cycles 10A, 10B and 10C.1, accumulating 335.4 EFPD. Based on reactor physics calculations made for cycle 10A, the specimens' peak exposure in MOTA 1F was nominally 8.15 x 10^{22} n/cm² (E > 0.1 MeV). Specimens that did not fail were reconstituted into MOTA 1G for further irradiation.

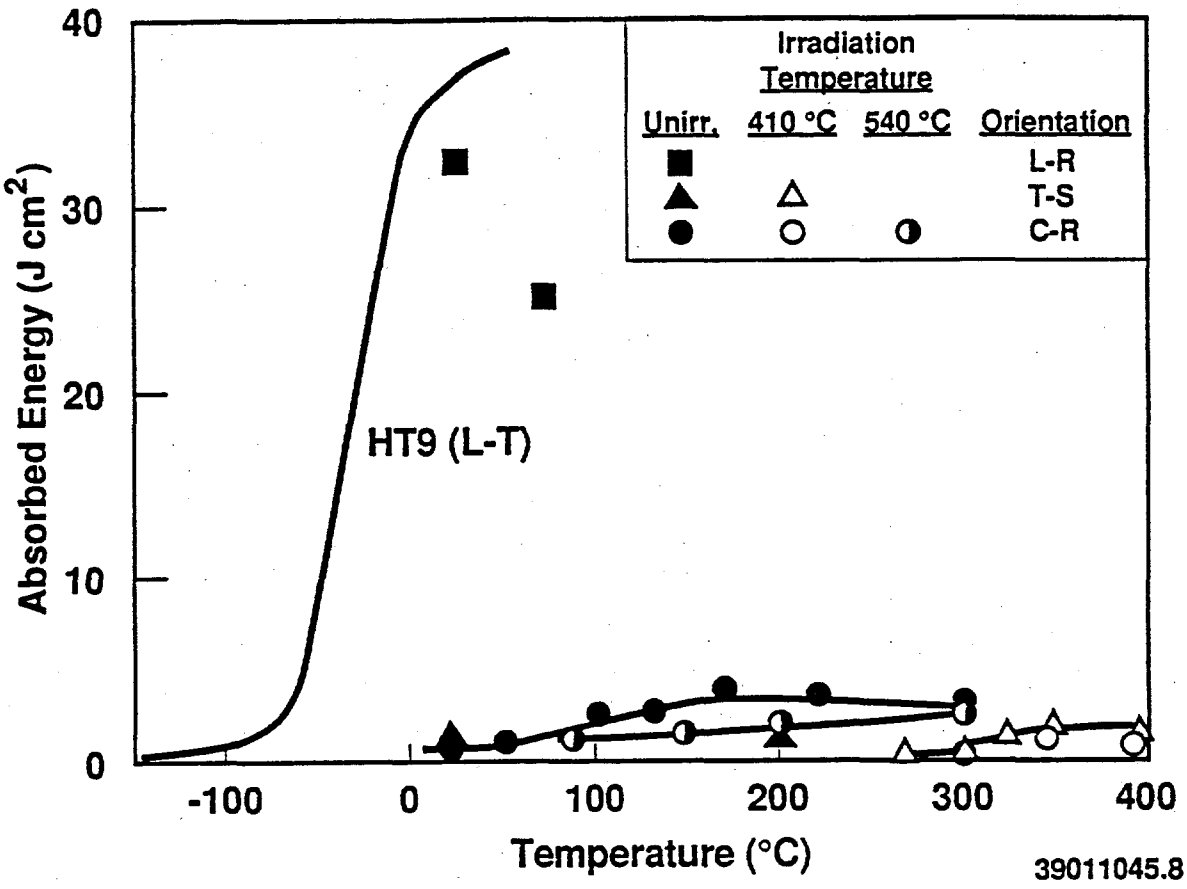

Figure 43. Fracture energy of 1/3 size precracked Charpy impact specimens of MA957 irradiated at 410 and 540°C.

Strain data for all MA957 pressurized tubes are given in Table 13. Gun drilled specimens are identified by EV codes, while STC cladding specimens are identified by TX codes. Following irradiation to a fluence of ~8 x 10^{22} n/cm^2, those gun drilled specimens of MA957 that had failed were removed from the MOTA irradiation vehicle. Effective strain is plotted as a function of effective stress for several temperatures in Figures 44 through 47. Other ferritic alloys are included in the graphs for comparison.

The data in Table 13 demonstrate that negligible diametral change was observed in unstressed specimens at or below 670°C, indicating that void swelling is not significant in this alloy. The diametral change observed in the drawn STC tubing at 760°C was also minimal, but slightly higher values were observed in the gun drilled, unstressed specimens at 760°C. It is not clear what caused the difference between the two types of tubing at 760°C, but since void swelling is not expected to occur at that temperature, it is probably due simply to the relaxation of the dislocation microstructure that typically occurs during the primary stage of thermal creep.

Table 13.
In-Reactor Creep Data for MA957

EVxx = gun drilled
TXxx = STC cladding

SPEC. ID CODE	NOM. IRR. TEMP. (°C)	NOM. HOOP STRESS (MPa)	MOTA 1E ACT. IRR. TEMP. (°C)	MOTA 1E TOTAL ϕT_{FAST} [a] (10^{22} n/cm²)	MOTA 1E TOTAL $\Delta D/D_0$ [b] (%)	MOTA 1F ACT. IRR. TEMP. (°C)	MOTA 1F TOTAL ϕT_{FAST} [a] (10^{22} n/cm²)	MOTA 1F TOTAL $\Delta D/D_0$ [b] (%)
TX12	385	0				385	4.6	-0.04
TX03		30						-0.01
TX04		60						0.05
TX00		100						0.10
TX01		140						0.12
TX02		200						0.19
EV07	419	0	414	7.9	-0.05			
EV46		60			0.04			
EV41		100			0.11			
EV40		140			0.17			
EV01	490	0	490	4.7	0.02	495	8.1	0.01
EV38		60			0.09			0.12
EV36		100		5.1	0.20			0.22
TX15	495	0				495	3.4	0.00
TX05		30						0.04
TX06		60						0.01
TX07		100						0.08
TX09		140						0.14
TX17		200						0.29
EV63	550	0	565	8.3	0.04	550	16.5	0.07
EV34		60			0.45			0.51
EV33		100			1.61			1.87
EV12[c]		140			3.89			
TX16		0				550	8.2	0.06
TX10		30						0.14
TX23		60						0.29
TX24		100						0.68
TX25		140						1.14

Table 13 (cont.)
In-Reactor Creep Data for MA957

EVxx = gun drilled
TXxx = STC cladding

SPEC. ID CODE	NOM. IRR. TEMP. (°C)	NOM. HOOP STRESS (MPa)	MOTA 1E ACT. IRR. TEMP. (°C)	MOTA 1E TOTAL ϕT_{FAST} [a] (10^{22} n/cm²)	MOTA 1E TOTAL $\Delta D/D_o$ [b] (%)	MOTA 1F ACT. IRR. TEMP. (°C)	MOTA 1F TOTAL ϕT_{FAST} [a] (10^{22} n/cm²)	MOTA 1F TOTAL $\Delta D/D_o$ [b] (%)
EV45	605	0	620	8.3	0.09	605	16.4	0.11
EV00		30			0.30			0.38
EV02[c]		60			0.95			
EV03[c]		140			2.84			
TX18		0				605	8.2	-0.01
TX11		15						0.10
TX13		30						0.18
TX26		45						0.34
TX27		60						0.63
TX28		100						2.13
EV31	670	0	660	7.5	0.08	670	15.5	0.17
EV04		15			0.17			0.24
EV05		30			0.30			0.40
EV06		60			0.60			0.77
EV47[c]		100			1.36			
TX19		0				670	8.0	0.09
TX14		5						0.14
TX29		10						0.14
TX30		15						0.20
TX32		30						0.30
TX33[d]		45						0.65

Table 13 (cont.)
In-Reactor Creep Data for MA957

EVxx = gun drilled
TXxx = STC cladding

SPEC. ID CODE	NOM. IRR. TEMP. (°C)	NOM. HOOP STRESS (MPa)	MOTA 1E ACT. IRR. TEMP. (°C)	MOTA 1E TOTAL ϕT_{FAST} [a] (10^{22} n/cm²)	MOTA 1E TOTAL $\Delta D/D_o$ [b] (%)	MOTA 1F ACT. IRR. TEMP. (°C)	MOTA 1F TOTAL ϕT_{FAST} [a] (10^{22} n/cm²)	MOTA 1F TOTAL $\Delta D/D_o$ [b] (%)
EV68	750	0	750	8.5	0.23	750	16.5	0.34
EV09		5			0.30			0.39
EV10		10			0.27			0.36
EV11		15			0.41			0.53
TX20		0				750	8.0	0.14
TX34		5						0.25
TX35		10						0.33
TX36		12.5						0.39
TX37		15						0.42

[a] ϕt_{fast} represents total accumulated incremental neutron fluence (E > 0.1 MeV).
[b] Average total diametral strain based upon center three measurements.
[c] Denotes specimen that ruptured during MOTA 1E.
[d] Denotes specimen that ruptured during MOTA 1G.

Inspection of the data obtained from the gun drilled specimens reveals that doubling the neutron exposure produced only modest increases in strain levels, with further increases ranging from 15 to 40% of the value at the lower fluence. The largest strain after the second irradiation cycle (1.87%, at 565°C and 100 MPa) was less than half the largest (failure) strain observed after the first irradiation cycle (3.89%, at 565°C and 140 MPa), suggesting that gun drilled MA957 can exhibit a large amount of primary creep relative to the secondary creep that develops. Strain data generated after MOTA 1G will provide the third data point needed at each temperature and stress level to define the steady state creep response and to demonstrate that specimen failure has not yet occurred.

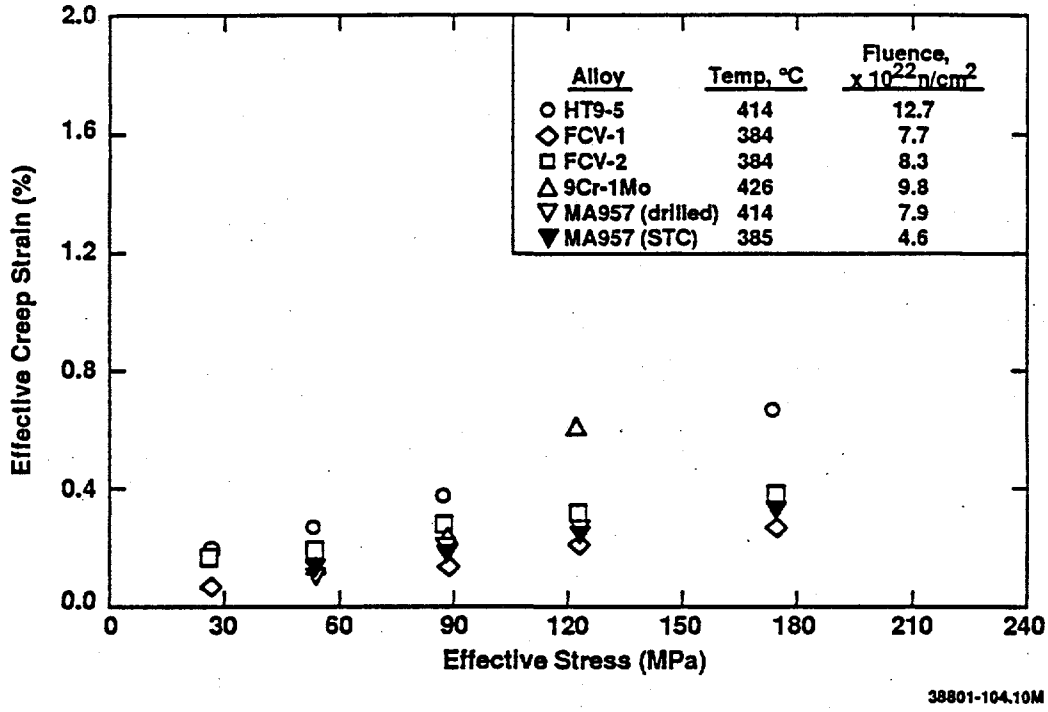

Figure 44. In-reactor creep data for various ferritic alloys at ~400°C.

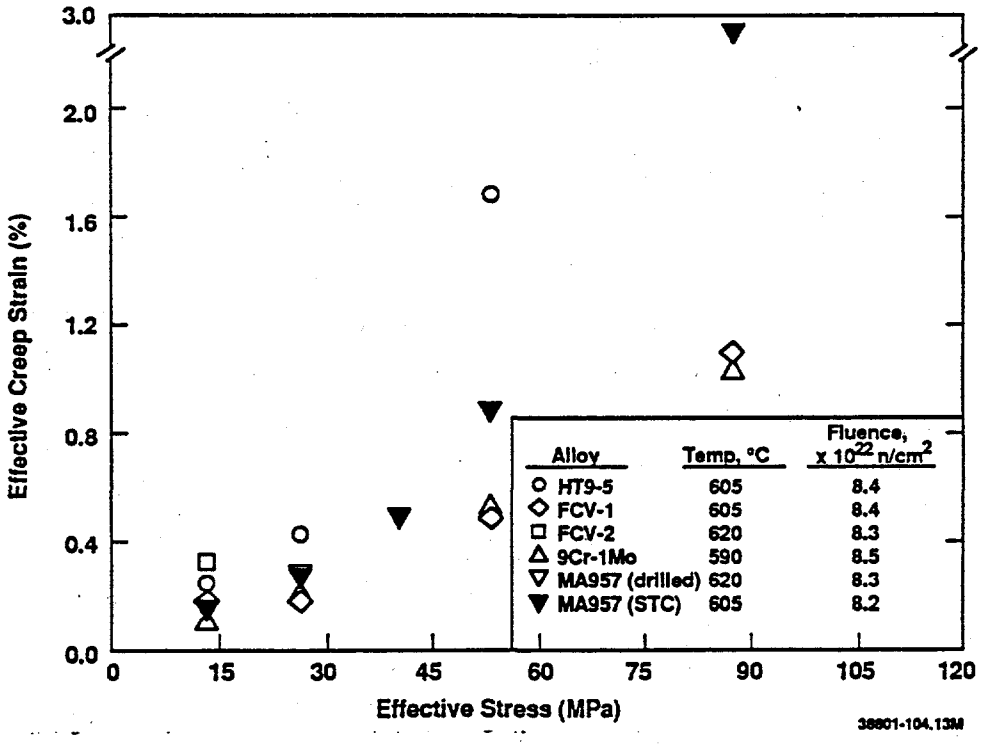

Figure 45. In-reactor creep data for various ferritic alloys at ~600°C.

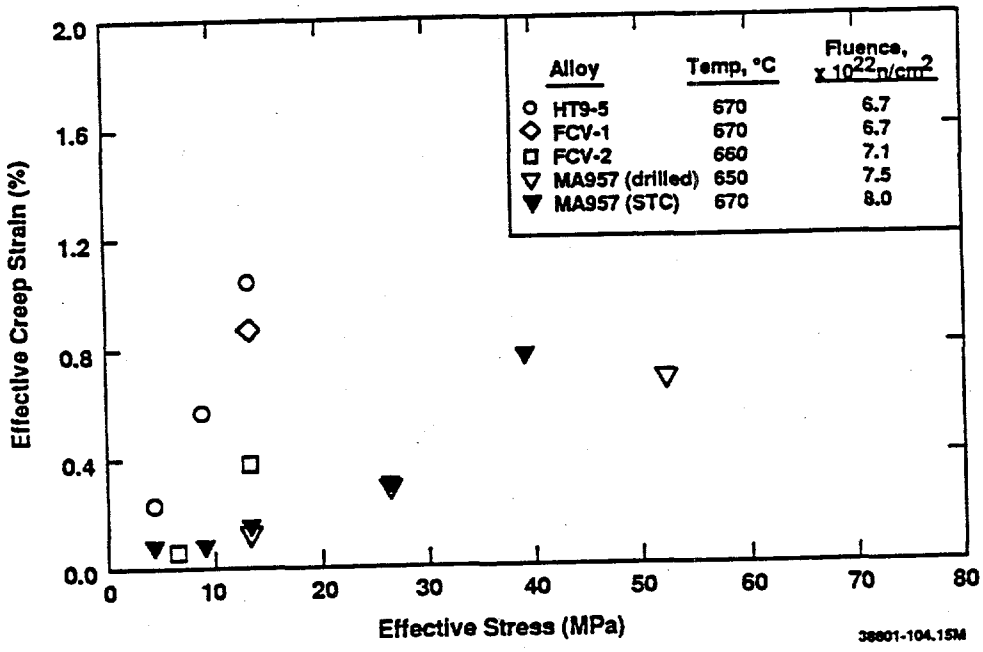

Figure 46. In-reactor creep data for various ferritic alloys at ~660°C.

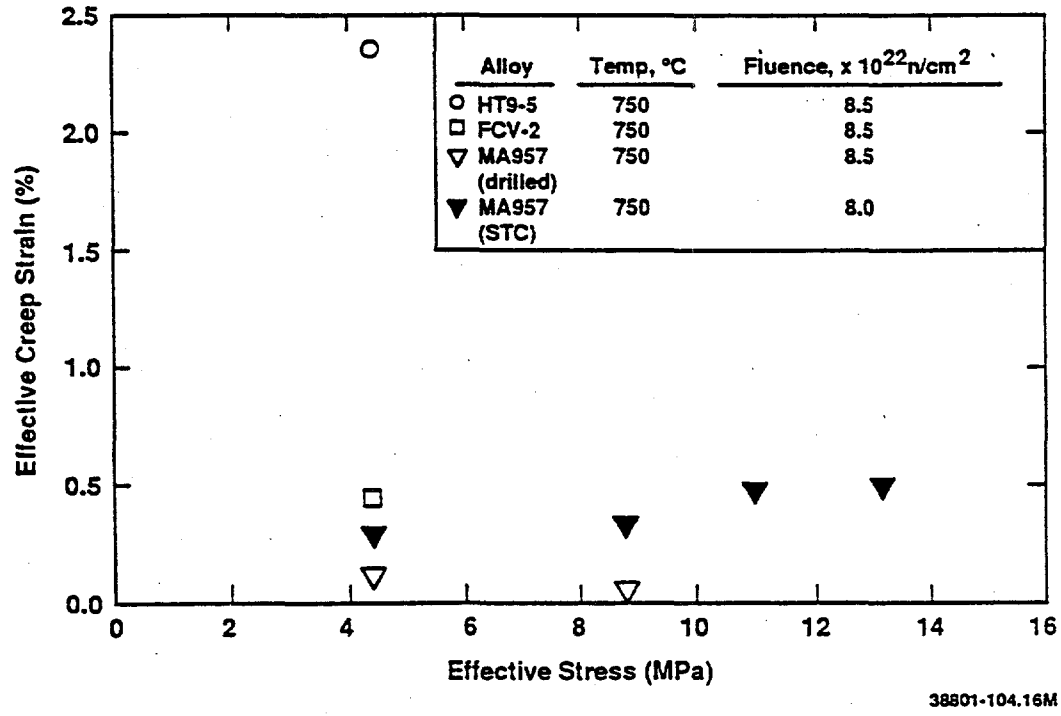

Figure 47. In-reactor creep data for various ferritic alloys at 750°C.

The graphs shown in Figures 44 through 47 and the other data given in Table 13 suggest that the tubing made by STC exhibits similar creep behavior but has a lower secondary creep rate and probably a smaller amount of primary creep than the gun drilled tubing. These differences are presumably due to the differences in processing techniques.

The data demonstrate that the creep response of the MA957 alloy is acceptable at temperatures as high as 750°C. Tubing produced by both fabrication routes strained 0.5% or less for stresses as high as 15 MPa. Figures 44 through 47 demonstrate that the creep behavior of MA957 is similar to that of other ferritic alloys up to temperatures as high as about 620°C. At 670 and 760°C, however, the response of MA957 is clearly superior.

In summary, the in-reactor creep response of MA957 tubing is comparable to other ferritic alloys in the temperature range 385 to 620°C and is clearly superior to other ferritic alloys at 670 and 760°C. Drawn tubing possesses better creep resistance than tubing made by gun drilling drawn rod stock. This difference could be due partially to differences in primary creep response, but data at higher neutron exposures are needed to verify that primary creep is a significant part of the creep response of MA957. The in-reactor creep data base supports the expectation that use of the ODS alloy MA957 will allow higher cladding temperatures and therefore significant improvement in reactor efficiency.

Stress Rupture Behavior

Rupture times are given in Table 14 for pressurized tubes irradiated in MOTA 1E and 1F, and through cycle 11B of MOTA 1G. No ruptures were recorded during MOTA 1F. As is shown in Figure 48, the data are reasonably consistent with the predictions of the Dorn Parameter equation developed using stress rupture data on unirradiated specimens. This is interesting in that the majority of the data on irradiated specimens were obtained on gun drilled drawn rod, whereas the data on which the equation was based were obtained on specimens cut from drawn tubing.

VIII. EFFECT OF IRRADIATION ON MICROSTRUCTURE

Tubing for TEM studies was obtained from the pilot lot produced by Cartech. Curved disks 0.12 inches in diameter were punched from longitudinal sections of 0.270 x 0.226 inch tubing. The disks were ground flat to a thickness of ~0.008 inch. A sufficient number of disks were inserted into MOTA 1F to allow irradiation at five temperatures (nominally 365, 410, 550, 670 and 760°C) to four different fluences. The irradiation history of the specimens discharged from MOTA 1F for microscopy is given in Table 15.

Table 14.
Rupture Life of Irradiated Pressurized MA957 Tubes

SPEC. ID CODE	NOM. IRR. TEMP. (°C)	NOM. HOOP STRESS (MPa)	MOTA 1E ACT. IRR. TEMP. (°C)	MOTA 1E ϕT_{FAST} [a] (10^{22} n/cm²)	MOTA 1E RUPTURE LIFE [b] (hrs)	MOTA 1F ACT. IRR. TEMP. (°C)	MOTA 1F ϕT_{FAST} [a] (10^{22} n/cm²)	MOTA 1F RUPTURE LIFE [b] (hrs)
Gun Drilled Specimens								
EV12	550	140	565	7.6	7137.6			
EV02	605	60	620	5.9	5677.6			
EV03		140		0.1	74.7			
EV47	670	100	660	0.8	755.3			
STC Cladding Specimens								
TX33	670	45				670	-12.7	12499.2

[a] ϕt_{fast} represents accumulated incremental neutron fluence (E > 0.1 MeV) at time of rupture.
[b] Accumulated time within 20°C of actual irradiation temperature.

Table 15.
Irradiation History of TEM Specimens from Pilot Lot

SPECIMEN ID CODE	NOMINAL TEMP. (°C)	ACTUAL TEMP. (°C)	FAST FLUENCE (n/cm²)	DOSE (dpa)
6437	365	370	1.8×10^{22}	8.5
6439	410	406	7.7×10^{22}	37.0
644A	550	550	8.0×10^{22}	38.4
644B	670	670	6.1×10^{22}	29.4
644E	750	750	8.0×10^{22}	38.5

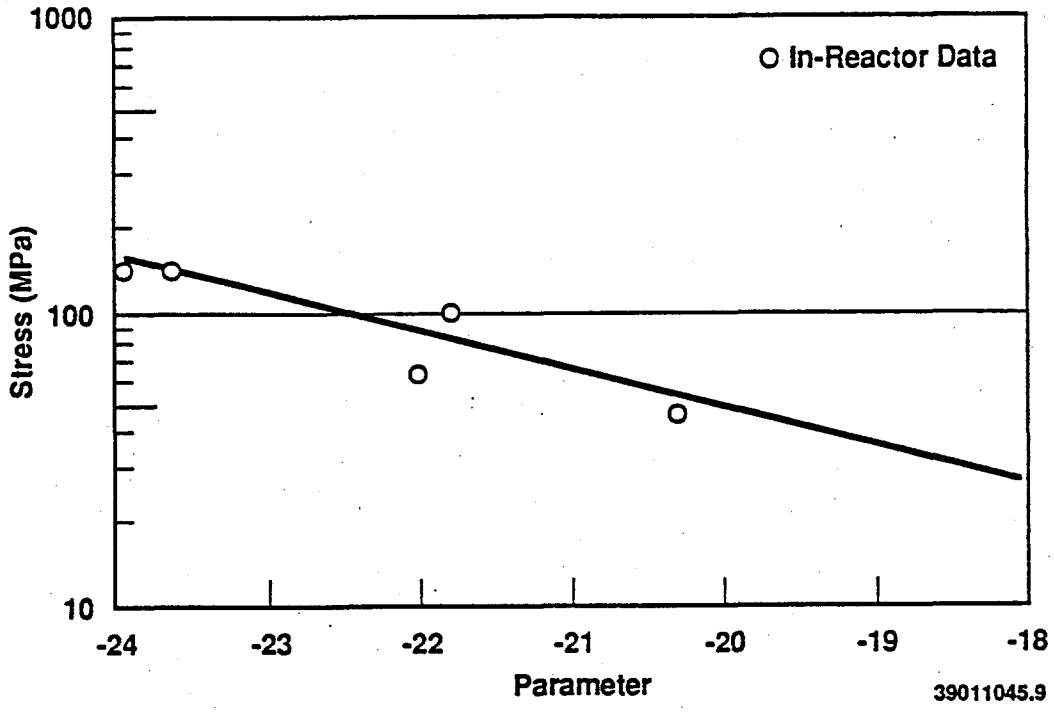

Figure 48. Rupture behavior of pressurized tubes of MA957 tested in-reactor.

Thin Foil Results

Changes in the microstructure of MA957 due to irradiation can be divided into two regimes. Below 550°C, dislocation development, α' precipitation and void evolution in the matrix are found, while above 550°C, damage appears to be restricted to cavity formation within TiO_2 particles. Evidence for very low levels of void swelling was found in the matrix at 370 and 410°C and in TiO_2 particles at 670 and 750°C. The precipitation of α' accompanied dislocation and void evolution below 550°C, while above 550°C radiation damage was restricted to within the 100 nm TiO_2 precipitate particles that were present prior to irradiation at low density throughout the material. The initial subgrain structure and the fine dispersion of Y_2O_3 particles were retained following irradiation at all temperatures.

The observation of void swelling in TEM specimens was surprising, especially at fast fluences as low as 1.8×10^{22} n/cm². The visible voidage remained very low, however, and the nonuniformity of the swelling observed at 370°C may be a consequence of the mechanical alloying process, which can lead to some compositional inhomogeneity. Additional TEM disks are available for density measurements to determine swelling values quantitatively. If swelling does continue in MA957 with irradiation to higher exposures, the swelling rate is expected to be low, no more than the 0.3% per 10^{22} n/cm² found for simple binary Fe-Cr alloys.

Cavitation such as that observed within the TiO_2 particles could be expected to alter the properties of the particles and produce stresses in adjacent regions. The absence of strain effects in the microstructures, however, implies that the irradiation temperatures were sufficiently high to allow these stresses to relax. It was suspected that cracks nucleating at voided TiO_2 particles could lead to failure, although the fact that the in-reactor rupture lives are as good as the unirradiated rupture lives suggests that this does not happen.

The remainder of this section discusses the details of the microstructure at each irradiation temperature.

370°C. The microstructure of MA957 was altered in three ways following irradiation at 370°C to 1.8 x 10^{22} n/cm²: 1)α' precipitation, a common occurrence in Fe-Cr alloys, was formed; 2)dislocation evolution occurred, presumably by loop nucleation, growth and interaction; and 3)cavity formation occurred within wider subgrains, typical of void swelling in the incubation regime. Examples of these phenomena are given in Figure 49.

Figure 49a shows the subgrain structure at low magnification under strain contrast. The structure is similar to that shown in Figure 7a except for changes in the fine detail within the subgrains. A wide subgrain is shown in Figure 49b in both void and dislocation contrast. Many small voids on the order of 7 nm in diameter can be identified in the center and lower left areas of the micrograph. The dislocation structure within the subgrain is visible at the top of the micrograph, comprising a tangle of dislocation segments and loops. There was apparently sufficient dislocation evolution to allow void development, but the accumulated swelling remains very low. A narrower subgrain can be seen in a thin area of Figure 49c revealing dislocation line segments and darker circular features that are larger than the original dispersoid. Figure 49d shows similar features in a still thinner area. Such features revealed under weak contrast conditions such as this are usually ascribed to chromium-rich α' formation. Since the alloy is known to form α' during thermal aging at low temperatures, it is likely that it also forms α' during irradiation at low temperatures. The α' images can obscure the Y_2O_3 dispersoid. No void formation is evident in Figures 49c and d, indicating that void swelling is not uniform.

410°C. Similar dislocation evolution was observed following irradiation at 406°C to a higher fluence of 7.7 x 10^{22} n/cm². Larger voids were identified at lower density, but evidence for α' precipitation was not found. Examples of this microstructure are given in Figure 50.

The elongated subgrain structure (Figure 50a) was retained, but the fine detail appears to be different from both the unirradiated and 370°C examples. At higher magnifications (Figures 50b and c) the dislocation structure comprises dislocation loops and tangles, but the structure is more uniformly distributed and on a finer scale than was observed in Figure 49b. The photograph in Figure 50d was taken under imaging conditions similar to those used for Figure 49c, i.e., weak contrast. Features typical of α' do not appear in Figure 50d, but an example of a solitary void is found at the lower left.

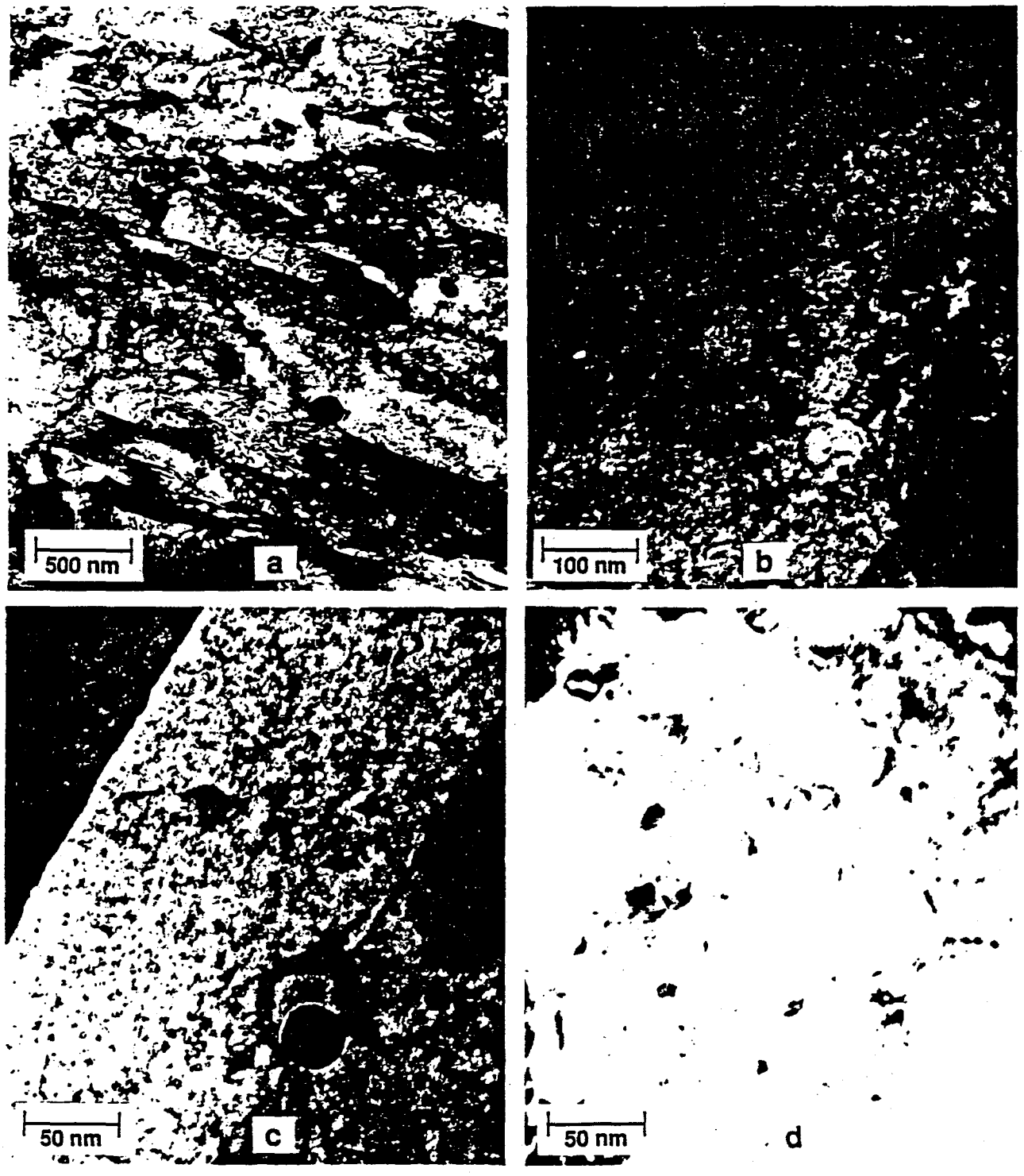

Figure 49. Microstructure of MA957 tubing following irradiation at 370°C to 1.8 x 10^{22} n/cm^2. The subgrain structure is shown in (a) at low magnification, void swelling and dislocation development are shown in (b) at intermediate magnification, and precipitate and dislocation structures are shown in (c) and (d) at higher magnification.

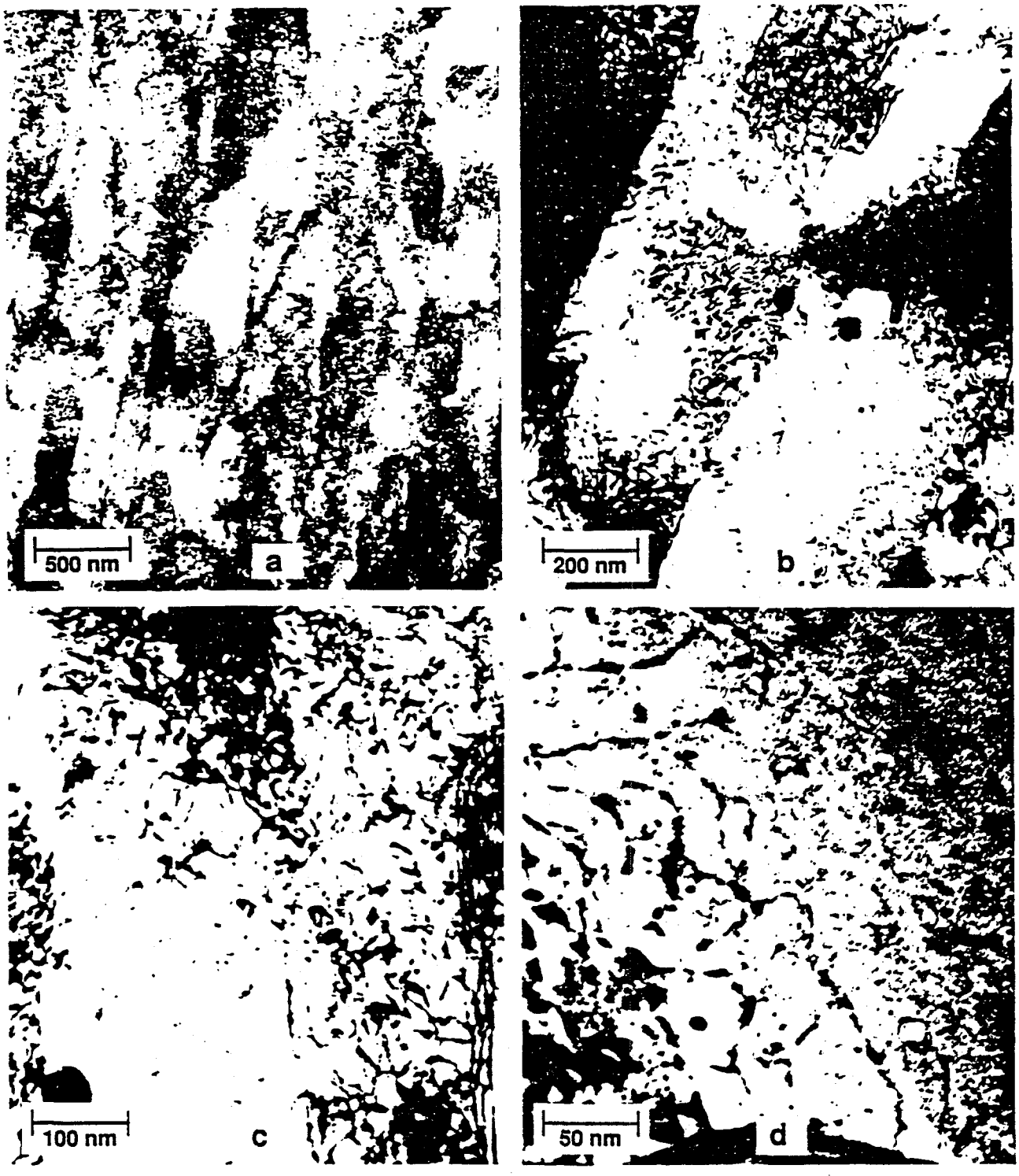

Figure 50. Microstructure of MA957 tubing following irradiation at 406°C to 7.7 x 10^{22} n/cm². The subgrain structure is shown at low magnification in (a) and at higher magnification in (b). Void and dislocation development are shown at higher magnification in (c) and (d).

550°C. Evidence for radiation damage was not found after irradiation at 550°C to 8.0 x 10^{22} n/cm². The elongated subgrain structure was retained, but the dislocation structure appeared more relaxed than in the unirradiated condition. Figure 51 provides examples of the microstructure following irradiation at 550°C.

The subgrain structure is shown at low magnification in Figure 51a, while Figures 51b and c provide examples of the dislocation structure at higher magnifications. The photograph in Figure 51d was taken under the same contrast conditions as were used in Figure 7b so that both the dislocation structure and the Y_2O_3 dispersoid are visible. There was no apparent change in dispersoid size as a result of irradiation.

670°C. Microstructural development was similar during irradiation at 670°C to 6.1 x 10^{22} n/cm² to that at 550°C except that small clusters of cavities were found throughout the material. The cavity clusters were associated with large pre-existing TiO_2 particles. Examples of the microstructure following irradiation at 670°C are given in Figure 52.

The subgrain structure is unchanged after irradiation at 670°C, as is shown in Figure 52a at low magnification. The dislocation structure is similar to that observed after irradiation at 550°C, as shown in Figure 52b at higher magnification. Typical cavity clusters are shown in Figure 52c. The voids have unusual morphologies but are all clearly retained within hexagonal shaped regions believed to be TiO_2 on the basis of extraction replica results.

750°C. The microstructure of MA957 after irradiation at 750°C to 8.0 x 10^{22} n/cm² was similar to that observed after irradiation at 670°C. The subgrain and dislocation structure remained stable, but clusters of cavities were found within large TiO_2 particles. Examples of the microstructure are provided in Figure 53.

The similarities in the subgrain structure with other irradiation conditions and the with the as-received structure are evident in the low magnification photomicrograph Figure 53a. The dislocation structure is shown at higher magnifications in Figures 53b and c. The dispersoid is weakly imaged in Figure 53c. Further examples of cavity formation in TiO_2 particles are given in Figures 53c and d.

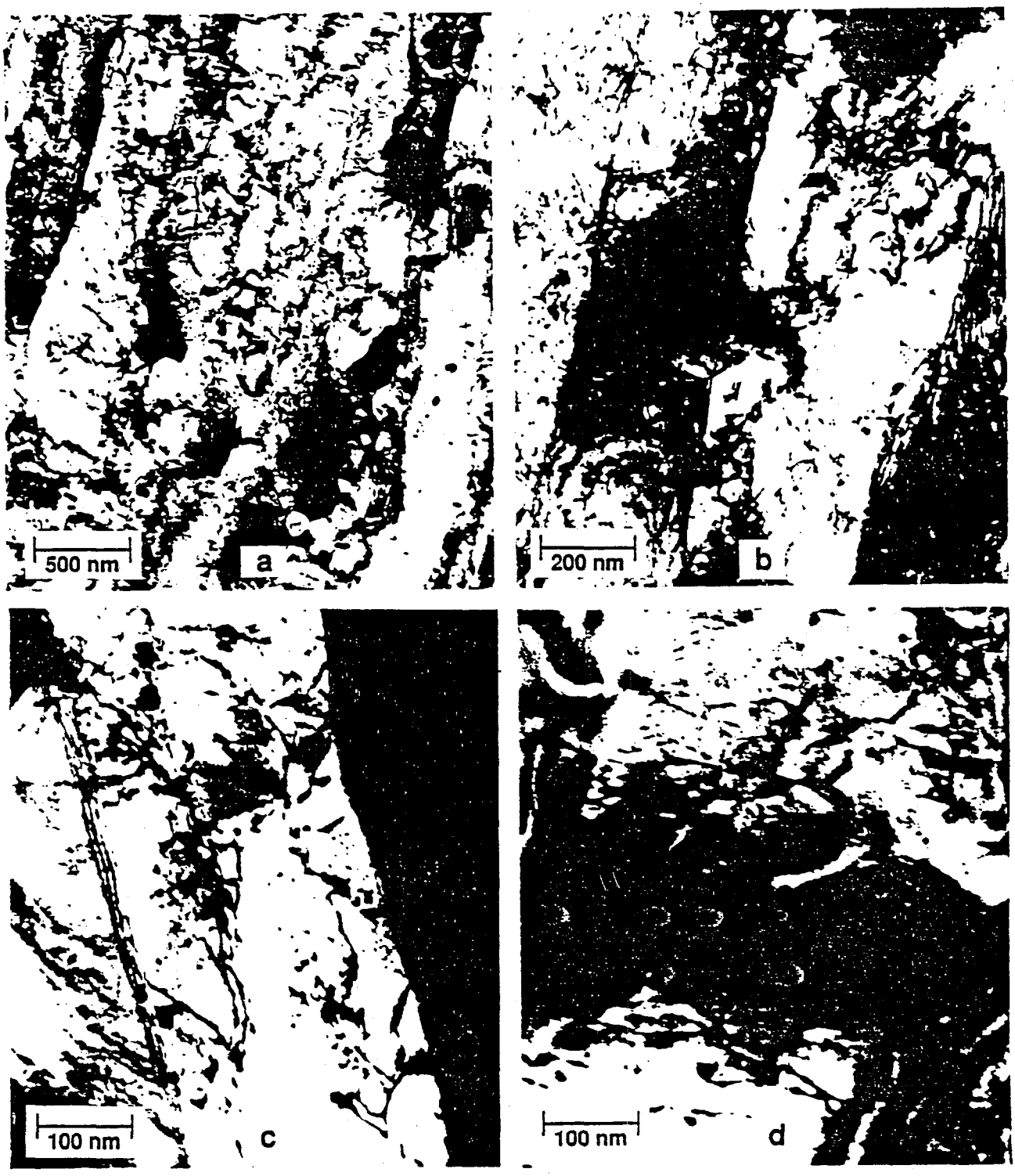

Figure 51. Microstructure of MA957 tubing following irradiation at 550°C to 8.0 x 10^{22} n/cm². The subgrain structure is shown at low magnification in (a), at intermediate magnification in (b) and at higher magnification in (c). The dispersoid is visible at higher magnification in (d).

Figure 52. Microstructure of MA957 tubing following irradiation at 670°C to 6.1 x 10^{22} n/cm^2. The subgrain structure is shown at low magnification in (a) and at intermediate magnification in (b). Cavities within TiO_2 particles are visible in (c) at higher magnification.

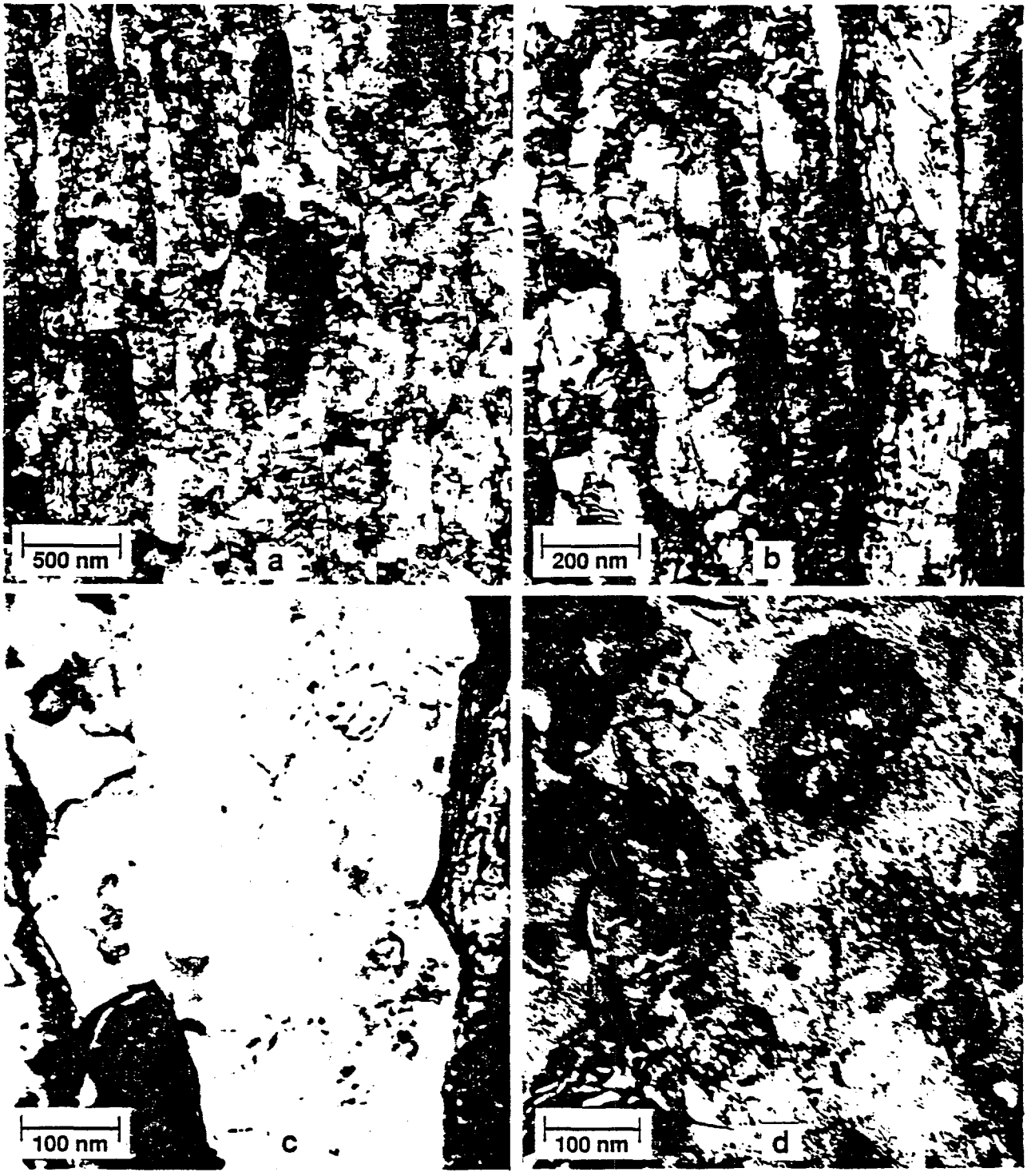

Figure 53. Microstructure of MA957 tubing following irradiation at 750°C to 8.0 x 10^{22} n/cm^2. The subgrain structure is shown at low magnification in (a) and at higher magnifications in (b) and (c). Cavities within TiO_2 particles are visible at higher magnification in (d).

Extraction Replica Results

Extraction replicas were made from the specimens irradiated at 550 and 750°C. Both replicas exhibited primarily precipitate particles rich in titanium. The results of x-ray dispersive analysis are given in Table 16. The 550°C condition contained particles with 72 to 92% Ti, low levels of Fe, Cr and Mo, and 2% or less Y. The 750°C condition yielded similar results except that some precipitates contained Al, and one particle showed equal parts of Ti, Fe and Cr. Since Y_2O_3 normally contains a high fraction of Y, it is evident that the precipitate composition revealed by the extraction replicas is not that of the dispersoid. The particles analyzed were therefore larger precipitates that resulted from the addition of titanium to the alloy, and are probably titanium and aluminum oxides or carbides containing minor amounts of Fe, Cr, and Mo. Note, however, that Fe and Cr would also be measured if the extraction replicas retained some matrix material.

Table 16.
Precipitate Composition in Irradiated MA957

SAMPLE IDENTITY	COMPOSITION (weight percent) Fe	Cr	Ti	Y	Mo	Al	No.	PRECIPITATE IDENTITY
550°C	4-13	3-9	72-92	0-2	0-7	-	3	TiO_2
750°C	8-13	3-9	75-90	0-3	0-9	0-3	15	TiO_2
	7-13	5-6	67-72	0-4	0-4	13-17	4	Garnet
	13	13	63	-	12		1	Chi?
	27	33	41	-	-	-	1	?

IX. DISCUSSION

Comparison to HT9

While the data base for MA957 is much smaller than that for HT9, the ODS alloy appears to provide improved performance relative to HT9 in several areas. The aging data demonstrate that the thermal stability of MA957 is superior to that of HT9 at the higher aging temperatures, suggesting that MA957 will have long term high temperature properties which are significantly better than HT9.

At low temperatures, however, a larger increase in DBTT was induced by irradiation than has been observed in HT9 under similar conditions. This hardening is due in part to the precipitation of α'. Thus any long term use

of the alloy should be preceded or accompanied by further exploration of the effect of neutron exposure at reactor temperatures on mechanical properties to avoid embrittlement during low temperature irradiation. Any embrittlement that occurs due to precipitation induced by irradiation, however, will be exacerbated by the elongated grain structure and the alumina stringers present in the ODS alloy. However, because precipitation in MA957 does not include G phase, as it does in HT9, the hardening that occurs in MA957 due to irradiation-induced precipitation must be due to α'. The level of α' that forms should be higher in MA957, with 14% Cr, than in HT9, with only 12% Cr. Since a similar shift in DBTT is observed in HT9 for similar reason, any changes in the compositional specification of MA957 must be made carefully to prevent, for example, the formation of additional phases like G phase, known to be detrimental to HT9.

Improvement Issues

The major drawbacks to the new ODS alloy are related to the difficulty of fabrication and therefore its cost, and to the poor impact behavior of the alloy. It should be possible, however, to improve both of these to some extent. Compressive tube reduction, or reductions that rely more on radial working than on area reduction, should decrease the number of passes required to produce tubing. An improved composition should lead to improvements in the impact behavior, particularly if this is accompanied by tighter specifications for the starting powders to eliminate the alumina stringers.

One of the most difficult phenomena to quantify in the fabrication of MA957 is the differences in recrystallization behavior that were observed with variations in fabrication technique and vendor. Recrystallization was not completely reproducible, but appears to be very strongly dependent on the imposed stress state. Zones of recrystallization were observed on both the inner and outer diameter, as well as at 45° angles to the wall. Regardless of where a recrystallized zone appeared, it usually degraded further fabrication or welding efforts. Any improvements in fabrication will undoubtedly eliminate as much of this phenomenon as possible.

Comparison to Other ODS Tubing

Microstructural differences between tubing produced in the U.S. and in Japan and Belgium can be expected to produce differences in performance. It is reasonable, for example, that the rupture life of the U.S. tubing is somewhat superior to that of the Japanese tubing, since the dispersoid is eliminated to some extent in the Japanese tubing with the production of Y_2TiO_5 during the hot working process. The differences between MA957 and the Belgian DT2203Y05 are large enough, however, that straightforward predictions are difficult. The increased molybdenum in the DT2203Y05 promotes the formation of chi phase, an alternate source of hardening. The Belgian alloy therefore probably does not rely as strongly on the hardening from the oxide dispersion as does MA957 despite the fact that the volume fraction of the dispersoid is doubled. In

addition, the added complexity of the additional hardening is expected to degrade the irradiation response.

X. CONCLUSIONS

The ODS alloy MA957 has been successfully fabricated into cladding for use in fast breeder reactors. Characterization of the physical and mechanical behavior of the alloy demonstrate that it possesses reasonable potential for such applications. Further testing is necessary, however, to determine the response of the alloy to the high levels of neutron irradiation that would be encountered in a reactor core.

XI. REFERENCES

1. R. W. Powell, G. D. Johnson, M. L. Hamilton and F. A. Garner, "LMR Cladding and Duct Materials Development," Proceedings of International Conference on Reliable Fuels for Liquid Metal Reactors, Tucson, AZ, September 1986.

2. J. J. Fischer, U. S. Patent 4,075,010, "Dispersion Strengthened Ferritic Alloy for use in Liquid Metal Fast Breeder Reactors," issued Feb. 21, 1978.

3. M. L. Hamilton, D. S. Gelles, R. L. Lobsinger, M. M. Paxton, and W. F. Brown, "Fabrication Technology for ODS Alloy MA957," (2000) PNNL-13165.

4. J. J. Huet, L. Coheur, A. De Bremaecker, L. de Wilde, J. Gedopt, W. Hendrix and W. Vandermeulen, "Fabrication and Mechanical Properties of Oxide Dispersion Strengthened Ferritic Alloy Canning Tubes for Fast Reactor Fuel Pins," Nucl. Tech., 70 (1985) 215.

APPENDICES

APPENDIX A

MA957 PATENT

United States Patent [19]
Fischer

[11] 4,075,010
[45] Feb. 21, 1978

[54] DISPERSION STRENGTHENED FERRITIC ALLOY FOR USE IN LIQUID-METAL FAST BREEDER REACTORS (LMFBRS)

[75] Inventor: John Joseph Fischer, Suffern, N.Y.

[73] Assignee: The International Nickel Company, Inc., New York, N.Y.

[21] Appl. No.: 655,463

[22] Filed: Feb. 5, 1976

[51] Int. Cl.[2] B22F 3/00
[52] U.S. Cl. ..... 75/235; 75/126 D
[58] Field of Search ..... 75/226, 206, 126 D; 29/187.5

[56] References Cited

U.S. PATENT DOCUMENTS

3,591,362	7/1971	Benjamin	75/0.5 A
3,837,930	9/1974	Cairns et al.	29/187.5
3,852,063	12/1974	Niimi et al.	75/126 D

OTHER PUBLICATIONS

Snykers & Hunt, *Dispersion-Strengthened Ferritic Alloys for High-Temperature Applications*, pp. 237-241.
Huet et al., Nuclear Technology, vol.24, Nov. 1974, pp. 216-224.

Primary Examiner—Brooks H. Hunt
Attorney, Agent, or Firm—Ewan C. MacQueen; Raymond J. Kenny; Miriam W. Leff

[57] ABSTRACT

A dispersion-strengthened ferritic alloy is provided which has high temperature strength and is readily fabricable at ambient temperatures and which is useful as structural elements of liquid metal fast breeder reactors.

17 Claims, No Drawings

DISPERSION STRENGTHENED FERRITIC ALLOY FOR USE IN LIQUID-METAL FAST BREEDER REACTORS (LMFBRS)

This invention relates to a dispersion-strengthened ferritic alloy which has high strength at elevated temperatures and is readily fabricable at ambient temperatures. More particularly, it concerns a ferritic alloy which is useful for liquid metal fast breeder (LMFB) reactor core assemblies.

BACKGROUND OF THE INVENTION

Certain austenitic stainless steels and ferritic alloys have properties which make them suitable for use as structural materials in LMFB reactors. Neither of the materials have been found entirely satisfactory. The austenitic stainless steels, which are currently preferred as best able to meet the strength requirements, are known to exhibit a property referred to as "swelling" when subjected to fast neutron irradiation. Also, they lose ductility and have a tendency to brittle fracture on exposure to radiation. Ferritic alloys are considerably better than the austenitic stainless steels with respect to their swelling and ductility properties, and they have the advantages of higher thermal conductivity and lower thermal expansion compared to austenitics. However, the overriding drawback to the conventional ferritic alloys is that they do not have sufficient strength in the temperature range of interest for LMFB reactors which is about 600° to 750° C. The strength required at these elevated temperatures should be preferably at least equivalent to that of 316 stainless steel. In addition, a "candidate alloy" must possess a high degree of room temperature fabricability to facilitate the production of thin walled tubing and other reactor core components. One method of strengthening ferritic steels is by precipitation hardening. It is known that titanium addition of more than 2% titanium to ferritic steel results in the precipitation of a new phase (Fe_2Ti) which has a strengthening effect. U.S. Pat. No. 3,719,475, for example, concerns a ferritic Fe-Cr-Ti alloy containing about 2% up to 7% titanium. According to the patent, the processing conditions to produce a suitable alloy include a thermo-mechanical treatment to produce precipitation hardening. The tensile strength shown for this material is considerably less than that for 316 stainless steel.

A number of dispersion strengthened ferritic alloys have also been investigated for LMFB reactors. Where titanium has been employed, it has been added in sufficient amounts to form a precipitation hardenable phase. For example, in ISI Special Report 151, pp. 237–241 (1974) and NUCL. TECHNOL. 24 216–224 (1974) investigations are reported on dispersion-strengthened ferritic alloys including titanium-containing materials. The publications report effects of 3.5% and 5% titanium in dispersion-strengthened ferritic alloys. The data show that with respect to high temperature strength, the dispersion-strengthened alloys containing 5% Ti are better than those containing 3.5%. Only one of the alloys containing 5% Ti exceeded the strength of 316 stainless steel at elevated temperature. Despite the good strength exhibited by this material, higher strength would be even more desirable so long as this could be achieved without undue sacrifice of ductility or fabricability.

In accordance with the present invention a ferritic alloy has been found for use in LMFB reactors which not only has the desirable properties attributable to ferritic alloys but also has high temperature mechanical strength and is readily fabricable at ambient temperatures.

In discussion of the invention below, all percentage compositions are given in weight percent.

THE INVENTION

The alloy of the present invention is a dispersion-strengthened ferritic alloy which consists essentially of, by weight, about 13% to about 25% chromium, about 0.2% to less than about 2% titanium, up to 2% molybdenum and a small but effective amount for sufficient high temperature strength up to less than about 2%, yttria, and the balance, apart from incidental elements and impurities, essentially iron.

The chromium in the alloy gives strength and oxidation resistance to the alloy and it stabilizes the ferritic structure at elevated temperatures. In general, the chromium level is about 13% to about 25%. Alloys having a chromium content of less than about 13% form austenite upon heating to temperatures greater than about 850° C, and those having a chromium level above about 25% tend to lose ductility. Preferred alloys contain about 13% to less than about 20% chromium, and preferably to less than 16%, e.g. about 14% or 15%, chromium.

Titanium and molybdenum when added in small amounts serve to improve the ductility and the oxidation resistance of the alloy. Although the action of titanium and molybdenum are not completely understood, it is believed they combine with small amounts of nitrogen and carbon that might be present, forming carbides and nitrides within the metal matrix, thus preventing grain boundary embrittlement caused by chromium carbide or nitride. In addition, the titanium and molybdenum give solid solution strengthening in iron. It has also been found that titanium helps prevent chromium volatilization during annealing of the alloy, thus preserving the benefits of chromium and/or lowering the cost to achieve the desired chromium level. A further benefit is that titanium appears to suppress the formation of porosity during the annealing stage, which is believed to be related to the volatilization of chromium.

It will be noted that in the present alloy the formation of a titanium-containing precipitation hardenable phase is not relied upon for strength. The maximum titanium content in the present alloy is up to less than 2% titanium, that is below the level at which a precipitation hardenable phase will form. In fact, little or no advantage is gained by the addition of more than about 1% or even 1.5% titanium. To insure oxidation resistance and permit high temperature annealing without occurrence of chromium volatilization and concurrent formation of porosity the minimum titanium content is about 0.2%. Advantageously, the maximum titanium content is about 1.5%. Preferably, the titanium content is about 0.5% to about 1%.

Molybdenum is not an essential component. However, since it gives both high temperature strength and ductility and increased room temperature fabricability, it is preferably present in the alloy. Accordingly, preferred alloys in accordance with the present invention contain molybdenum. A very small amount can be effective for improved high temperature strength. The preferred molybdenum range is a small but effective amount up to less than about 1% or even less than about

0.75%. In a particularly advantageous embodiment of this invention the titanium content is about 0.2% or 0.5% up to about 1.5% e.g. about 0.8 or 1%, and the molybdenum content is less than about 0.75%, e.g. about 0.2% to about 0.5%.

The principal function of the yttria is to retard recrystallization after cold or hot working. To achieve this the yttria is provided as a uniformly distributed, fine dispersion. It has long been known that the ambient and elevated temperature strength of an alloy can be raised by plastic deformation, i.e. hot or cold working. However, in conventional wrought alloys that do not contain a fine dispersion of a second phase, the strengthening provided by the plastic deformation "quickly" anneals out upon exposure to elevated temperature. This occurs principally by the migration of dislocations and subsequent recrystallization of new grains. A uniformly distributed dispersoid will prevent this recrystallization by blocking the dislocation motion. The yttria may combine with other components in the composition, such as titanium or aluminum values, e.g., to form phases such as $Y_2Ti_2O_7$ or $Y_2Al_2O_6$. Very small amounts of yttria have been found effective for improving strength. In general the yttria level may vary from a very small but effective amount up to less than about 2%. Materials containing such low yttria contents can be produced having high strength, e.g. a 100-hour stress-rupture life at 650° C of at least 40 ksi. Because of the low levels of dispersoid at which this strength can be achieved, there is no substantial sacrifice in fabricability. Advantageously, the maximum yttria content is about 1.5%, and preferably it is less than about 0.75% or even less than about 0.5%. In the present alloy system a small amount of Y_2O_3, e.g. about 0.25%, enables a surprisingly high level of strength to be achieved without causing embrittlement. Thus, the alloys can be fabricated readily into the desired structures. For example, they can be cold rolled to more than 70% reduction in area without annealing.

The yttria is particularly useful as a dispersoid because it does not increase the size appreciably upon exposure to high temperature and does not agglomerate. Other refractory oxides and refractory carbides, nitrides, are suitable as dispersoid materials provided they have such high temperature stability. Examples of other suitable dispersoids are thoria, ceria, and rare earth oxides, and carbides or nitrides of titanium, zirconium and hafnium. Among the less desirable materials are alumina, titania and chromium carbides since it is expected that they would increase in particle size upon high temperature exposure and therefore they would be less effective in retarding or preventing recrystallization. The function of the dispersoid as an agent to retard recrystallization at high temperature, which is crucial in the present alloys, is not as important in alloys in which precipitation hardening is relied upon for strength. Thus, in alloys in which the titanium precipitation-hardenable phase is important, the titanium content must be suitably high, but there is much more flexibility in choice of the dispersoid.

As indicated above, the present alloys consist essentially of iron, chromium, titanium and yttria. In preferred alloys molybdenum is also present. However, the alloys may contain small amounts of certain other elements which may be added intentionally or present as contaminants, provided they do not disturb the characteristics of the alloy. For example, the alloys of the present invention may contain up to about 2% each of

zirconium, silicon, tantalum, vanadium, tungsten and niobium. The zirconium and silicon tend to serve a similar function to titanium and therefore zirconium and/or silicon may be substituted, in part, for titanium. Tantalum, vanadium, tungsten and niobium tend to behave similarly to molybdenum and therefore may be substituted in part for molybdenum. However, as noted above, titanium must be present in a small amount and in preferred alloys molybdenum is present. Aluminum is known to increase the oxidation resistance of alloys and it would be advantageous to have it present in amounts of up to about 5%. However, it is believed that aluminum may be vulnerable to attack by liquid sodium and for that reason in preferred alloys it is limited to less than about 2% or even less than 1%. Also, the alloys can tolerate up to about 4% nickel and up to about 2% each of manganese and cobalt. The carbon level is preferably no higher than about 0.2% and preferably it is less than about 0.1%.

To achieve suitable structure for high strength without sacrificing fabricability the alloys of this invention are preferably prepared by a technique utilizing high energy milling such as the mechanical alloying technique, which is described in detail in U.S. Pat. Nos. 3,591,362, 3,660,049 and 3,837,930. For example, Benjamin U.S. Pat. No. 3,591,362, which is incorporated herein by reference, a method is disclosed for producing a wrought composite metal powder comprised of a plurality of consituents mechanically alloyed together, at least one of which is a metal capable of being compressively deformed such that substantially each of the particles is characterized metallographically by an internal structure comprised of the starting constituents intimately united together and identifiably mutually interdispersed. One embodiment of a method for producing the composite powder resides in providing a dry charge attritive elements and a powder mass comprising a plurality of constituents, at least one of which is a metal which is capable of being compressively deformed. The charge is subjected to agitation milling under high energy conditions in which a substantial portion of cross section of the charge is maintained kinetically in a highly activated state of relative motion and the milling continued to produce wrought composite metal powder particles of substantially the same composition as the starting mixture characterized metallographically by an internal structure in which the constituents are identifiable and substantially mutually interdispersed within substantially each of the particles. The internal uniformity of the particles is dependent on the milling time employed. By using suitable milling times, the interparticle spacing of the constituents within the particles can be made very small so that when the particles are heated to an elevated diffusion temperature, interdiffusion of diffusible constituents making up the matrix of the paticle is effected quite rapidly.

The mechanical alloying process may be conducted in a variety of equipment, including a stirred ball mill, shaker mill, vibratory ball mill, planetary ball mill, and even certain ball mills provided attention is had to the ball-to-powder ratio of the charge and size of the mill as taught by the above Benjamin patent. Preferably, the process is effected to an atmosphere which will avoid formation of oxides or nitrides.

One type of stirred ball mill attritor found to be particularly advantageous for carrying out the Benjamin invention comprises an axially vertical stationary cylin-

der or tank having a rotatable agitator shaft located coaxially of the mill with spaced agitator arms extending substantially horizontally from the shaft, such a mill being described in Szegvari U.S. Pat. No. 2,764,359 and in Perry's Chemical Engineer's Handbook, Fourth Edition, 1963, at pages 8 to 26. The mill contains attritive elements, e.g. balls, sufficient to bury at least some of the arms, so that, when the shaft is rotated, the ball charge, by virtue of the agitating arms passing through it, is maintained in continual state of unrest or relative motion throughout the bulk thereof. The mill can be water cooled by means of a jacket about the tank.

The foregoing method enables the production of metal systems in which insoluble non-metallics such as refractory oxides, carbides, nitrides, silicides, and the like, can be uniformly dispersed throughout the metal particle. In addition, it is possible to interdisperse alloying ingredients within the particle, particularly large amounts of alloying ingredients, e.g. such as chromium, which have a propensity to oxidize easily due to their rather high free energy of formation of the metal oxide. In this connection, mechanically alloyed powder particles can be produced by the foregoing method containing any of the metals normally difficult to alloy with another metal.

The ferritic alloy powder which consists essentially of iron-chromium-titanium(= molybdenum)-yttria, produced by the mechanical alloying process is a wrought, dispersion-strengthened heat-resistant alloy product characterized by a highly uniform internal composition and structure.

Generally speaking, in accordance with this invention, the alloy powders are consolidated as follows: the powders are canned (packed in a container which may be mild steel, stainless steel, nickel, etc.), said can then being welded shut, the can containing the powders is then extruded at an elevated temperature preferably in the range of 1700°–2200° F (ca. 926°–1205° C) at an extrusion ratio of about 3:1 to 50:1 or higher. Following extrusion, the canning material is removed by acid leaching or machining. The consolidated powders which are now in the form of a wrought bar are then further consolidated by, e.g., hot rolling between about 1500° and 2200° F (ca. 815° and 1205° C) with 25–90% reduction in area. Following the hot rolling the product is then cold worked (rolled, drawn, swaged, etc.) preferably 25–85% reduction in area to the final shape. The cold worked product is annealed at a temperature below its recrystallization temperature. The recrystallization temperature is generally in the range 1800°–2200° F (ca. 980°–1205° C). Annealing above the recrystallization temperature is not desirable since this leads to a significant loss in stress rupture strength at about 1200° F (ca. 650° C).

The resultant consolidated products possess a combination of strength and fabricability that is superior to ferritic alloys previously proposed for LMFB reactors. The alloy is particularly suitable as fuel cladding, wrapper tubes and other structural components in such reactors.

The invention will be better understood by reference to the following illustrative examples.

EXAMPLE I

To produce a ferritic dispersion-strengthened alloy composed of iron, chromium, titanium, molybdenum, and yttria the following materials are employed: a commercially available atomized iron powder of about minus 80 mesh, a low carbon ferrochrome powder of about minus 80 mesh containing about 75% chromium and the balance essentially iron, a ferrotitanium powder of about minus 40 mesh containing about 70% titanium and the balance essentially iron, a molybdenum powder of about minus 80 mesh and yttria of about 150 Angstroms average size. The powders are used in a proportion to give a nominal composition, by weight, of 14% Cr, 1% Ti, 0.3% Mo, 0.25% yttria and the balance essentially iron.

A 4,500 gram batch proportioned to yield the foregoing composition is placed in a Szegvari 4S attritor mill. The batch is dry milled in an essentially pure argon atmosphere for 24 hours at 288 r.p.m. using a ball-to-powder ratio of 20 to 1. After attrition, the mechanically alloyed powder is sealed in a mild steel can and extruded at 1950° F (ca. 1065° C). An extrusion ratio of 6 to 1 is used at a speed of approximately 2 inches/sec. Following extrusion the alloy is decanned and hot rolled to ½ inch thick plate at 1950° F (ca. 1065° C), which corresponds to approximately 75% reduction in area. The plate is then cold rolled to approximately 0.060 inch thick sheet. Thereafter the sheet is annealed at a temperature of about 2000° F (ca. 1090° C), and the ultimate tensile strength (U.T.S.) and stress rupture properties determined at 1200° F (ca. 650° C). Analysis of the composition and results of the tests are tabulated in TABLE I together, for comparison, with the results of a stress rupture test similarly performed on a typical sample of 316 stainless steel.

TABLE I

	Tests at 650° C		
	U.T.S.	Stress-Rupture Life	
Sample	(KSI)	(KSI)	(hrs.)
Fe-14Cr-0.9Ti-0.3Mo-0.25Y_2O_3	66.3	50	16
		47.5	> 72
316 Stainless Steel	54	32	94

The high 1200° F (650° C) stress rupture life of the ferritic dispersion-strengthened alloy of this invention demonstrates its high level of strength at the operating temperature level of LMFB reactors. TABLE I also shows that the alloy of this invention compares favorably with 316 stainless steel with regard to ultimate tensile strength at 650° C.

The room temperature bend angle of 316 stainless steel is typically about 180° about a diameter equal to twice the sheet thickness. The bend angle of the alloy prepared in accordance with this example is also 180°. This demonstrates the fabricability of the alloy of this invention.

EXAMPLE 2

A series of alloys are prepared in the manner described in Example 1, except that the powders charged to the attritor are proportioned to give the compositions shown below. To provide the aluminum content, ferroaluminum powder is used, to provide silicon, a ferrosilicon powder is used, and to provide molybdenum elemental molybdenum powder is used. The alloys are annealed at 2000° F (ca. 1090° C). The composition, bend fabricability and stress rupture properties of these alloys are given below in TABLE II.

TABLE II

Composition	Room Temperature bend angle (D = 2t)*	Stress Rupture at 65° C Stress (ksi)	Life (hrs)
Fe-14.9Cr-0.2Y_2O_3	48°	20	3
Fe-14.1Cr-0.8Ti-0.2Y_2O_3	115°	44.5	4
Fe-14.2Cr-1.0Si-0.2Y_2O_3	53.5°	37.5	21
Fe-14.4Cr-0.8Al-0.2Y_2O_3	56°	35	0.5

*diameter = twice thickness

The results demonstrate that the addition of 0.8% Ti to an Fe-Cr-Y_2O_3 base composition improves the room temperature bend angle and the stress rupture properties at 650° C. Furthermore, the addition of 0.8% Ti to the Fe-Cr-Y_2O_3 base composition was more effective in improving the bend angle and stress rupture properties than additions of either 1.0% Si or 0.8% Al.

EXAMPLE 3

In order to determine the effect of an increasing titanium content, two additional alloys were prepared. The preparation and processing of these alloys was substantially the same as in Example 1, except the proportion of ferrotitanium was adjusted to give the compositions with higher titanium levels. Compositions and room temperature bend angle and stress rupture properties at 650° C are given in TABLE III.

TABLE III

Composition	Room Temperature Bend Angle (D = 2t)	Stress Rupture at 650° C Stress (ksi)	Life (hrs)
Fe-14.1Cr-0.8Ti-0.20Y_2O_3	115°	44.5	4
Fe-13.7Cr-2.0Ti-0.25Y_2O_3	90°	47.5	19
Fe-13.9Cr-3.3Ti-0.25Y_2O_3	76°	42.5	2

The results show an increase in titanium content leads to a decrease in the room temperature fabricability as measured by the bend angle. Increasing the titanium content from 0.8 to 2.0 percent provides a moderate increase in the stress rupture properties at 650° C. However, the data indicates that further additions of titanium to the 3.3 percent gives a decrease in the stress rupture strength.

EXAMPLE 4

This example demonstrates the effect of increasing molybdenum content in a nominal base composition of Fe-14Cr-1Ti-0.25Y_2O_3 The preparation and processing of the alloys are substantially the same as in Example 1, except the proportion of elemental molybdenum powder is adjusted to give various amounts of molybdenum. Compositions, bend angle and stress rupture tests are reported in TABLE V.

TABLE IV

Composition	Room Temperature Bend Angle (D = 2t)	Stress Rupture at 650° C Stress (ksi)	Life (hrs)
Fe-14.1Cr-0.8Ti-0.20Y_2O_3	115°	44.5	4
Fe-14.0Cr-0.9Ti-0.3Mo-0.25Y_2O_3	180°	50	16
Fe-13.5Cr-1.0Ti-1.2Mo-0.25Y_2O_3	70°	50	2
Fe-13.5Cr-1.1Ti-1.9Mo-0.25Y_2O_3	140°	50	14

The results show an increase in the room temperature bend angle and the 650° C stress rupture properties are obtained by adding 0.3 percent molybdenum. Further additions of molybdenum up to 1.9 percent give essentially the same stress rupture properties as the 0.3 percent molybdenum level. The room temperature bend angle shows an inconsistent behavior for additions of molybdenum above the 0.3 percent level. An additional alloy with a nominal composition of Fe-14Cr-5Ti-2Mo-0.25Y_2O_3 was prepared by attritor processing as in Example 1. Although this alloy was successfully extruded and hot rolled as in Example 1, it could not be cold rolled. Severe cracking occurred during the cold rolling indicating poor ductility.

Although the present invention has been described in conjunction with preferred embodiments, it is to be understood that modifications and variations may be resorted to without departing from the spirit and scope of the invention, as those skilled in the art will readily understand. Such modifications and variations are considered to be within the purview and scope of the invention and appended claims.

What is claimed is:

1. As a powder metallurgy article of manufacture, a structural element of a LMFB reactor comprising a wrought dispersion-strengthened, heat resistant ferritic alloy having a composition consisting essentially of, by weight, about 13% to about 25% chromium, about 0.2% to less than 2% titanium, up to about 2% molybdenum, up to about 2% aluminum, a small but effective amount for improved strength up to about 1.5% yttria and the balance, except for incidental elements and impurities, essentially iron, said wrought ferritic element being characterized substantially throughout by composition uniformity and by a high degree of dispersion uniformity.

2. An article of manufacture according to claim 1, wherein molybdenum is present in a small but effective amount for improved strength up to less than about 1%.

3. An article of manufacture according to claim 1, wherein the chromium content is about 13% up to about 20%.

4. An article of manufacture according to claim 2, wherein the maximum titanium content is about 1.5%.

5. An article of manufacture according to claim 2, wherein the chromium is about 13% up to less than about 16% and the titanium content is about 0.5% to about 1%.

6. An article of manufacture according to claim 5, wherein the yttria content is less than about 0.75%.

7. An article of manufacture according to claim 1, wherein the alloy is characterized by a 100 hour stress rupture life of at least 40 ksi at 650° C.

8. An article of manufacture according to claim 1, wherein the alloy contains less than 1% aluminum.

9. A structural element of a nuclear reactor comprising a wrought dispersion-strengthened, heat resistant ferritic alloy having a composition consisting essentially of, by weight, about 13% up to less than about 16% chromium, about 0.2% to about 1.5% titanium, up to

about 1% Mo, a small but effective amount for improved strength up to about 0.75% of a refractory stable compound selected from the group metal oxide, metal nitride and metal carbide, and the balance, except for incidental elements and impurities, essentially iron, said element being prepared as a powder metallurgy product by the steps comprising a) mechanically alloying a mixture of fine powder containing components of said alloy in amounts proportional to give said composition, b) consolidating the resultant mechanically alloyed powder and effecting at least 25% reduction in area; thereby producing a dispersion-strengthened heat resistant ferritic alloy having a 100-hour stress-rupture life at 650° C of at least 40 ksi.

10. A structural element of a nuclear reactor according to claim 9, wherein the consolidated product is annealed at a temperature below the recrystallization temperature of the alloy.

11. A structural element of a nuclear reactor according to claim 9, wherein the dispersoid is selected from the group consisting of yttria, thoria, ceria, and rare earth oxides.

12. A structural element of a nuclear reactor according to claim 11, wherein the titanium content is less than about 1%, and wherein the dispersoid comprises yttria, the yttria content being less than about 0.5%.

13. A structural element of a nuclear reactor according to claim 12, wherein the molybdenum content is about 0.1% to about 0.5%.

14. A mechanically alloyed ferritic dispersion-strengthened heat resistant alloy used as a structural element of a LMFB reactor consisting essentially of, by weight, about 13% to about 25% chromium, about 0.2% up to less than 2% titanium, up to about 2% molybdenum, less than about 1% aluminum, a small but effective amount for improved strength up to about 1.5% yttria and the balance, except for incidental elements and impurities, essentially iron, said wrought ferritic element being characterized substantially throughout by composition uniformity and by a high degree of dispersion uniformity.

15. A mechanically alloyed ferritic dispersion-strengthened heat resistant alloy used as a structural element of a LMFB reactor according to claim 14, wherein the chromium content is about 13% up to less than about 16%, the titanium content is about 0.5% up to about 1%, the molybdenum content is up to about 1%, and the yttria content is less than about 0.5%.

16. As a powder metallurgy article of manufacture, a structural element of a LMFB reactor comprising a wrought dispersion-strengthened, heat resistant ferritic alloy having a composition consisting essentially of, by weight, about 13% to about 25% chromium, about 0.2% to less than 2% titanium, up to about 2% molybdenum, up to about 2% aluminum, up to about 2% each of zirconium, silicon, vanadium, tungsten, niobium, and manganese, and up to about 4% nickel, provided that the level of the elements zirconium, silicon, vanadium, tungsten, niobium, manganese and nickel is such that it is below that which in combination with the titanium level will effect a precipitation hardening phase in the alloy, a small but effective amount for improved strength up to about 1.5% yttria and the balance, except for incidental elements and impurities, essentially iron, said wrought ferritic element being characterized substantially throughout by composition uniformity and by a high degree of dispersion uniformity.

17. An article of manufacture according to claim 1, wherein the alloy is characterized in that it is in a non-recrystallized, hot-worked, cold-worked condition.

* * * * *

APPENDIX B

COMPOSITION OF MA957

Overcheck analyses were performed at Koon-Hall and at Cartech on the four heats of the alloy available. A complete summary of the results of the chemical overcheck analyses is given in Table B.1.

Table B1.
Composition of MA957
(weight percent)

	Wiggin Certifications				Carpenter Technology Overcheck Certifications						Koon-Hall Overcheck Certifications							
Cast No:	DBB0111	DBB0114	DBB0120	DBB0122	DBB0111	DBB0111	DBB0111	DBB0114	DBB0120	DBB0122	DBB0111	DBB0111	DBB0111	DBB0111	DBB0111	DBB0114	DBB0122	DBB0122
WHC Bar No.:	---	---	---	---	1[a]	2[b]	3[b]	---[b]	---[b]	---[b]	---[b]	1[a]	1[a]	2[b]	3[b]	---[b]	---[b]	---[b]
Cr	14.17	13.59	14.10	14.16	13.84	13.93	13.84	13.49	14.01	14.19	13.95	14.03	13.54	13.57	13.57	13.62	14.07	14.23
Ti	0.99	0.95	1.01	1.02	1.08	0.99	1.00	0.96	1.03	1.03	1.38	1.10	1.04	1.07	1.07	1.03	1.11	1.11
Mo	0.30	0.29	0.31	0.31	0.31	0.29	0.28	0.30	0.31	0.31	0.30	0.31	0.32	0.31	0.31	0.3	0.31	0.31
$Y(Y_2O_3)$	0.27	0.28	0.27	0.27	NA[c]	0.22	0.22	0.22	0.22	0.22	0.26	(d)	20.19	0.22	0.20	0.29	0.28	0.28
O	0.22	0.24	0.21	0.02	0.006	0.019	0.014	0.22	0.22	0.22	0.12	0.22	0.22	0.22	0.22	0.059	139 pm	0.062
C	0.017	0.015	0.013	0.014	0.014	0.016	0.012	0.013	0.016	0.013	0.014	0.015	0.015	0.014	0.015	0.02	0.02	0.02
Mn	NA	NA	NA	NA	0.05	0.05	0.05	0.06	0.06	0.06	NA	NA	0.12	0.11	0.11	0.07	0.08	0.07
Si	NA	NA	NA	NA	0.05	0.05	0.05	0.03	0.03	0.03	0.02	0.04	0.07	0.05	0.05	0.03	0.02	0.02
P	NA	NA	NA	NA	<0.005	<0.005	<0.005	<0.005	<0.005	<0.005	0.030	0.004	0.011	0.011	0.011	0.004	0.005	0.004
Ni	NA	NA	NA	NA	0.13	0.13	0.13	0.10	0.10	0.10	0.15	0.12	0.14	0.15	0.15	0.09	0.10	0.11
B	NA	NA	NA	NA	NA	NA	NA	NA	NA	NA	NA	<0.005	NA	NA	NA	NA	NA	NA
Al	NA	NA	NA	NA	0.07	0.06	0.06	0.09	0.08	0.07	0.055	0.10	0.16	0.17	0.17	NA	NA	NA
Sn	NA	NA	NA	NA	0.005	0.005	0.005	<0.005	<0.005	<0.005	0.002	<20 ppm	26 ppm	26 ppm	24 ppm	NA	NA	NA
N	0.045	0.045	0.038	0.033	0.039	0.045	0.039	0.051	0.047	0.040	0.046	0.049	0.048	0.048	0.048	0.046	0.042	0.038
Ce	NA	NA	NA	NA	NA	0.02	0.02	0.02	0.02	0.02	NA	NA	NA	NA	NA	NA	NA	NA
S	NA	NA	NA	NA	0.006	0.006	0.006	0.004	0.006	0.004	NA	NA	0.006	0.006	0.006	0.009	0.010	0.010
Cu	NA	NA	NA	NA	NA	NA	NA	NA	NA	NA	NA	NA	0.03	0.02	0.03	0.01	0.01	0.01
Nb + Ta	NA	NA	NA	NA	NA	NA	NA	NA	NA	NA	NA	NA	0.009	0.009	0.009	NA	NA	NA
As	NA	NA	NA	NA	NA	NA	NA	NA	NA	NA	<0.0001	<70 ppm	5 ppm	3 ppm	2 ppm	NA	NA	NA
Fe	Bal	Bal	Bal	Bal	Bal	Bal	Bal	Bal	Bal	Bal	Bal	Bal	Bal	Bal	Bal	Bal	Bal	Bal

(a) Quarter-inch diameter rod stock.
(b) One-inch diameter bar stock.
(c) Not analyzed.
(d) Certification read 0.017 wt% but probably a typographical error meant to read 0.20 wt%.

APPENDIX C

WHC REDUCTION SEQUENCES

The following tables document some of the reduction sequences used at WHC to produce both rod and tubing. The first table documents the successful reduction of rod stock to roughly a quarter inch in diameter from 1 inch diameter bar stock. The second table documents the unsuccessful reduction of tubing from the same bar due to the cracking which occurred. The third and fourth tables summarize the production of additional rod and tubing.

Table C1.
MA957 Reduction Sequence by Swaging

INITIAL OD (inches)	FINAL OD (inches)	REDUCTION IN AREA (%)	SWAGED HARDNESS (R_C)	SUBSEQUENT INTERPASS ANNEAL (°C/minutes)	ANNEALED HARDNESS (R_C)
1.00	0.865	25.0	36.4	1050/13	36.4
0.865	0.754	24.0	36.0	1050/13	35.9
0.754	0.633	29.5	37.8	1050/13	34.5
0.633	0.504	36.7	36.9	1050/13	33.9
0.504	0.438	24.5	35.9	1050/13	31.6
0.438	0.370	28.7	35.2	1050/13	30.5
0.364	0.327	21.9	32.8	1050/13	30.8
0.327	0.295	18.7	33.6	1050/13	---
0.295	0.260	22.3	---	1050/13	---

Table C2.
MA957 Tube Reduction

INITIAL SIZE OD X ID (inches)	FINAL SIZE OD X ID (inches)	REDUCTION IN AREA (%)	SWAGED HARDNESS (R_C)	SUBSEQUENT INTERPASS ANNEAL (°C/minutes)	ANNEALED HARDNESS (R_C)
0.913 x 0.579	0.875 x 0.563	10.0	36.0	1012/13	32.9
0.875 x 0.553[a]	0.800 x 0.525	18.8	36.2	1050/15	33.2
0.800 x 0.525[a]	0.760 x 0.500	10.1	35.9	1050/15	35.0
0.760 x 0.500[a]	0.700 x 0.475	19.3	36.1	800/60	35.4
0.700 x 0.475[a]	0.650 x 0.450	16.8	35.0	800/15	34.1
0.650 x 0.450[a]	0.600 x 0.425	18.5	35.0	800/15	[b]
0.600 x 0.425[a]	0.550 x 0.400	20.6		[c]	

(a) Swaged on mandrel.
(b) Cracks appeared on ID.
(c) Swaged 1/2 tube, stopped due to OD cracks.

Table C3.
Reduction Sequence of Second Rod

INITIAL SIZE (inches)	FINAL SIZE (inches)	REDUCTION IN AREA (%)	INTERPASS ANNEAL (°C/minutes)
1.000	0.930	13.5	825/15
0.930	0.870	12.5	825/15
0.870	0.820	11.2	825/15
0.820	0.770	11.8	875/15
0.770	0.720	12.6	875/15
0.720	0.661	15.7	875/15
0.661	0.615	13.4	875/15
0.615	0.593	7.0	875/15
0.593	0.565	9.2	875/15
0.565	0.540	8.7	875/15
0.540	0.515	9.0	875/15
0.515	0.480	13.1	875/15
0.480	0.437	17.1	875/15
0.437	0.412	11.1	875/15
0.412	0.387	11.3	875/15
0.387	0.361	12.9	875/15
0.361	0.334	14.5	875/15
0.334	0.310	13.8	875/15
0.310	0.297	8.2	875/15
0.297	0.281	10.5	875/15
0.281	0.265	11.0	875/15

Table C4.
Successful Reduction of MA957 Tubing

INITIAL SIZE OD X ID (inches)	FINAL SIZE OD X ID (inches)	REDUCTION IN AREA (%)	INTERPASS ANNEAL (°C/minutes)	ANNEALED HARDNESS (DPH)
0.902 x 0.485	0.875 x 0.476	6.8	1000/15	---
0.875 x 0.476	0.821 x 0.479	16.2	1000/15	---
0.821 x 0.470	0.800 x 0.450	3.5	---	---
Machined to 0.800 x 0.460			---	---
0.800 x 0.460	0.752 x 0.450	15.3	1000/15	---
0.752 x 0.450	0.700 x 0.430	16.0	1000/15	369
0.700 x 0.430	0.662 x 0.420	14.2	1000/15	368
0.662 x 0.420	0.615 x 0.410	19.8	1900/21	369
0.615 x 0.410	0.587 x 0.395	10.2	1000/17.5	344
0.587 x 0.395	0.550 x 0.380	16.1	1000/15	363
0.550 x 0.380	0.525 x 0.370	12.2	1000/12.5	363
0.525 x 0.370	0.500 x 0.360	13.2	1900/16.5	364
0.500 x 0.360	0.475 x 0.350	14.4	1000/10	367
0.475 x 0.350	0.450 x 0.340	15.7	1000/11	360
0.450 x 0.340	0.425 x 0.325	13.8	1000/12	346
0.425 x 0.325	0.400 x 0.310	14.8	1000/12	364
0.400 x 0.310	0.385 x 0.305	13.6	1000/15	375
0.385 x 0.305	0.364 x 0.290	12.4	1000/15	360
0.364 x 0.290	0.345 x 0.280	16.1	990/12	348
0.345 x 0.280	0.330 x 0.272	14.1	1000/24	357
0.330 x 0.272	0.314 x 0.263	15.7	1000/12	364
0.314 x 0.263	0.295 x 0.250	16.5	1900/12	352
0.295 x 0.250	0.285 x 0.242	7.8	1000/12	350
0.285 x 0.242	0.269 x 0.233	20.2	1000/12	358
0.269 x 0.233	0.250 x 0.218	22.5	1000/12	359
0.250 x 0.218	0.230 x 0.200	8.2	1000/12	364, 346[a]

(a) For unrecrystallized and recrystallized areas, respectively, that appeared after the last anneal.

APPENDIX D

PULSE MAGNETIC WELDING

The feasibility of using pulse magnetic welding on ODS alloys was demonstrated on both MA956 and MA957 tubing. The MA956 cladding samples were machined from 0.490 inch bar stock provided by INCO. The MA957 cladding samples were obtained from the developmental tubing fabricated by Superior Tube Company using interpass anneals at 900 or 1000°C. The results from these tests are summarized in Tables D.1 and D.2.

Table D1.
Results from Pulsed Magnetic Welding Feasibility Tests

MATERIAL (PRIOR HEAT TREATMENT)	SAMPLE NUMBER	KILO-VOLTS	HE LEAK TEST	AXIAL BOND LENGTH (MILS)	CIRCUM. BOND LENGTH (°)	METALLOGRAPHY
MA956(none)	16307	35.0	---	40 to 70	360	Solid state weld No cracks
MA956(none)	16308	35.0	---	0 to 50	220	Solid state weld No cracks
MA957(1000°C)	16586	35.0	---	none	none	---
MA957(1000°C)	16592	35.0	Leaker	20 to 40	150	---
MA957(1000°C)	16603	36.0	No leak	20 to 100	360	Solid state weld No cracks
MA957(900°C)	16614	36.0	No leak	20 to 50	360	Solid state weld No cracks
MA957(900°C)	16615	36.5	No leak	50 to 100	360	Solid state weld No cracks

Table D2.
Average Hardness in Welded PMW Samples

MATERIAL (PRIOR HEAT TREATMENT)	SAMPLE NUMBER	MICROHARDNESS (DPH) [500 gm load] HT9 END CAP	CLAD APPROX. 0.3 INCH FROM WELD REGION	CLAD ADJACENT TO WELD	CLAD/HT9 WELD INTERFACE
MA956(none)	16308	272	327	358	348[a]
MA957(1000°C)	16603	284	407	407	323
MA957(900°C)	16615	274	429	428	359

(a) Single hardness value; others are average of two and three values.